12-14-2015

Intercode Advanced Fuels and Cladding Comparison Using BISON, FRAPCON, and FEMAXI Fuel Performance Codes

Aaren Rice
University of South Carolina - Columbia

Intercode Advanced Fuels and Cladding Comparison Using BISON, FRAPCON, and FEMAXI Fuel Performance Codes

by

Aaren Rice

Bachelor of Science
University of Tennessee 2012

Submitted in Partial Fulfillment of the Requirements

for the Degree of Master of Science in

Nuclear Engineering

College of Engineering and Computing

University of South Carolina

2015

Accepted by:

Travis Knight, Director of Thesis

Elwyn Roberts, Reader

Lacy Ford, Senior Vice Provost and Dean of Graduate Studies

Acknowledgments

Coffee

Abstract

The high density uranium-based fuels are regaining popularity as the current fleet of LWR's are showing interest in uprating plants to increase accident tolerance and performance. Fuels such as U_3Si_2, UN, and UC all contain a higher uranium loading and thermal conductivity than that of UO_2 making them attractive in combination with an advanced cladding type such as the ceramic SiC cladding. In addition to adding more mass uranium to the core without surpassing current enrichment limits, these advanced fuels and claddings are designed with increased accident tolerance performance in a LOCA type scenario in mind.

One of the possible concerns that comes with this combination of advanced fuels and cladding type is that PCMI should be avoided almost all together. From past experiments, the advanced fuels, U_3Si_2, UN, and UC, all show higher swelling rates than what UO_2 experiences. In addition to higher swelling rates in the fuel, the SiC cladding is unyielding in nature and will crack before creeping outward with the fuel like current generation Zr based claddings will do. The combination of a fuel with higher swelling rate plus an unyielding cladding is concerning in terms of accident mitigation. Modeling the fuel and cladding based on properties found in literature can be accomplished with codes such as FRAPCON and BISON. Earlier work done on FRAPCON at USC has shown that UC with a creep model will allow the SiC cladding to remain under the suggested maximum allowable hoop stress for up to 30 MWd/kgU. This was essentially the time until contact was made with the cladding. A similar implementation of UC and UN fuels into BISON has been done with comprable results.

With the BISON code, a much more detailed analysis can be performed as it is a fully-coupled, transient solution which can be solved in 1, 2, and 3 dimensions. This allows for more detailed results to be drawn. This study will compare results from identical models that are implemented in both BISON and FRAPCON based on semi-realistic PWR test conditions. This intercode comparison allows for further conclusions to how these advanced fuels interact mechanically with the SiC type cladding. Work has also been accomplished in the Japanese FEMAXI fuel performance code. A modified executable has been made which allows for the SiC cladding to be modeled with UO_2 fuel. With all of these modified codes, PWR type simulations were run to examine how these codes modeled these advanced fuels and claddings.

Table of Contents

List of Tables

List of Figures

List of Abbreviations

ATF	Accident Tolerant Fuel
DOE	Department of Energy
FCC	Face Centered Cubic
FRL	Fuels Research Laboratory
HTGR	High Temperature Gas Reactor
INL	Idaho National Laboratory
LANL	Los Alamos National Laboratory
LFA	Laser Flash Analysis
LHGR	Linear Heat Generation Rate
LOCA	Loss of Coolant Accident
SiC	Silicon Carbide
TD	Theoretical Density
UC	Uranium Carbide
UN	Uranium Nitride
UO_2	Uranium Dioxide
U_3Si_2	Uranium Silicide

Chapter 1

Introduction

1.1 Motivation

Since the Fukishima accident in 2011, the DOE has implemented an Accident Tolerant Fuels (ATF) campaign that has sparked research in the area of advanced fuels for the intermediate stage between Gen-III and Gen-IV reactors. These fuels will be designed to keep the plants safer under normal operating conditions as well as accident conditions. They will also be designed to uprate existing plants to help them become more fuel efficient, burning fuel longer and leaving fewer long-lived actinides per unit mass of fuel.

Among these intermediate fuels is the uranium silicides, uranium nitride and uranium carbides. U_3Si_2, in particular, has recently re-gained recognition as a promising fuel in this new ATF campaign. It shows promise with its high uranium density, increased thermal conductivity, and compatibility with water. This makes it a desirable choice as a new fuel option in combination with an advanced cladding. However, there is very little data collected on the properties of the U_3Si_2 fuel since the 1960's and even less on monolithic U_3Si_2.

From the data that is available, it is seen that U_3Si_2 is expected to have a higher swelling rate and lower melting point than that of UO_2. To consider this as a viable option for use in current LWR's, modeling the U_3Si_2's creep will need to be done in order to get an accurate representation of what will really happen when PCMI occurs.

The UC and UN fuels haven't gained as much popularity as U_3Si_2 fuel for LWR

applications due to their poor stability with water. The nitride fuel is currently being researched as a candidate for coated UN-U_3Si_5 hybrid fuel where the nitride is coated with a layer of U_3Si_5 to help protect against water corrosion in the case of a clad breach [24]. There is very little to no data on the irradaiation properties of this new hybrid nitride-silicide fuel complex making modeling difficult if not impossible due to the complex nature of fuel performance.

Since an in-reactor experiment is an expensive and long-term process, modeling the fuel in a state of the art fuel performance code such as BISON is a good way to estimate what to expect in an experimental test. BISON allows users to easily code in new materials with their own specific properties so that a detailed analysis can be performed.

To help further validate this study, the results from the BISON code will be compared against those of FRAPCON. Since the FRAPCON code has already been modified to allow for advanced fuels to be coded in, this will be a study to show the differences in how the similar models can calculate different results due to the way the code formulates results.

1.2 Objectives

An analysis in BISON to examine the effects of creep on UC, UN, and U_3Si_2 fuels in combination with the SiC type cladding was performed in order to compare cladding stress results against other codes such as FRAPCON and FEMAXI. Work at the University of South Carolina has already compared UC and UO_2 type fuel in FRAPCON and FEMAXI. An extension of adding the BISON code to the assessment bank plus the UN and U_3Si_2 type fuels in the mix will give greater insight to how these advanced fuels compare with each other.

Using the advanced fuels in combination with the SiC type cladding model will give more insight into the viability of commercial use of this cladding from a stress

standpoint. Modeling fuel creep is integral to this study as the advanced fuels all contain a much higher swelling rate than that of UO_2. This high swelling rate could cause Pellet Cladding Mechanical Interaction (PCMI) to occur which gives a means for the fuel to creep due to the interfacial pressure between the pellet and cladding. Currently the UO_2 fuel creep is not considered in the assessment of the BISON code due to the fact that for an LWR simulation with Zr-4 type cladding, there is very little to no fuel creep occuring once PCMI occurs. The Zr-4 cladding will creep much greater than UO_2 fuel and will have negligable effects in the overall results of how much net displacement the UO_2 fuel will experience. With the SiC type cladding, the cladding walls will be much thicker and much more unyielding. This will cause an immediate stress buildup once PCMI occurs and ultimately cladding failure. From work done with FRAPCON, adding in fuel creep for UC and UO_2 allowed the cladding to stay under failure criteria for a much longer time than without modeling fuel creep [7].

The novelty of this is that no study done with BISON on the advanced fuels UN and UC have been done. Furthermore, no research comparing these fuels to FRAPCON results with the SiC type cladding increases the novelty of this study. Researching literature to find the models that will be needed has been be done firstly. After the models had been chosen, implementation into the BISON code while verifying that the input models are giving correct values has be done. Once all of the material models and physics have been implemented correctly, the setting up models to run and compare against similar FRAPCON models has been done. To increase the valididity of this study, sample cases consisting of the UO_2 and Zry based claddings have been included. Since the codes have all been validated independently with this fuel/cladding combination, this will be a benchmark for how then initially comparte against each other.

Chapter 2

Literature Review

2.1 U_3SI_2

Silicide fuels have been studied for quite some time now, but are getting renewed recognition as part of DOE's Accident Tolerant Fuel (ATF) Program for the intermediate step between Gen-III and Gen-IV reactors. Currently, the bulk of the data that is available on the silicide fuels comes from experiments run over 50 years ago. Some of the properties show that this might be a good alternative to currently used UO_2. There is, however, still much research data that needs to be collected so that more accurate computational modeling can be done.

Some of the notable properties of the silicide fuel is its higher thermal conductivity, higher metal density compared with traditional UO_2, and stability with water. Table 2.1 shows various fuel types and someof their properties of interest. The higher conductivity of U_3Si_2 creates a lower temperature gradient throughout the pellet moving from the center toward the surface. This reduces the thermal stresses on the pellet and the amount of energy stored inside the pellet. With a higher uranium density in the pellet, current LWR's can up-rate their plants to run longer and produce more power for the same volume of fuel. Using this fuel with advanced cladding alternatives may also help compensate for the cladding's neutronic inefficiencies without increasing the current enrichment limits.

The uranium-silicon system contains two different stoichiometric ratios that have past been studied for the use of possibly becoming reactor fuel: U_3Si and U_3Si_2. While

Table 2.1: Comparison of various fuel properties

	UO_2	**UN**	**UC**	**U_3Si_2**
Melting Point (°C)	2840	2850	2507	1665
Density/U Density (g/cm^3)	10.96/9.6	14.3/13.5	13.63/12.97	12.2/11.3
Thermal Conductivity @ 500°C (W/mK)	4.6	20.9	20.0	16.3
Irradiation Induced Swelling (Relative)	Low	Medium	High	Medium
Stability With Water (Relative)	Good	Poor	Poor	Good
Ease of Manufacture (Relative)	Easy	Difficult	Medium	Medium

the U_3Si compound has a higher U/Si ratio, its irradiation stability and melting point are both lower than that of the U_3Si_2 compound [10]. The U_3Si_2 compound has been considered as the more feasible option with its theoretical density of 12.2 g/cm^3, uranium density at 11.31 g/cm^3, and melting point at 1665° C.

The U_3Si_2 is a primitive tetragonal structure with lattice parameters $a_0 = 7.3299 \pm 4$ Å and $c_0 = 3.9004 \pm 5$ Å. At perfect stoichiometric form, it undergoes no transformations until it melts at 1665° C. A phase diagram of the uranium-silicon system can be seen in Figure 2.1 shown below.

Upon making sample compounds to test, Shimizu notes that it would be beneficial to add an excess of silicon before heating to suppress the formation of the U_3Si phase present due to losses of silicon during arc melting [36]. He notes that all of his samples became hypo-stoichiometric after arc melting, causing a U solid solution and U_3Si phase to be present. The U_3Si phase is to be avoided due to its extreme silicon mobility near the phase transformation temperature of 930°C and poor irradiation properties of the compound [36][10].

Currently U_3Si_2 is only available for lab scale production due to the lack of methodology on how to convert UF_6 to U_3Si_2 similar to the industrial process for UO_2 fabrication. A lab production requires the uranium metal and silicon are arc melted together several times to ensure homogeneity and that solid U solutions and secondary phases are kept to a minimum (<10% for RETR standards). It is also noted that

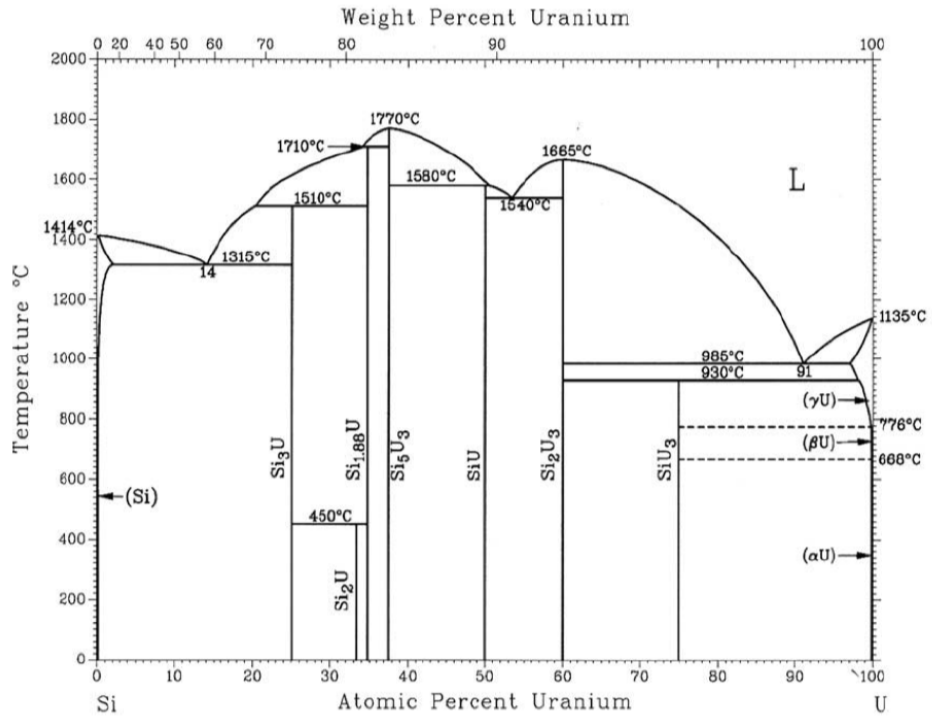

Figure 2.1: Uranium-Silicon phase diagram [42]

there should be an excess amount of initial silicon before arc melting, around 7.5 wt%, to account for the loss of silicon during the arc melting process and ensure that the mixture ends up at the desired stoichiometric weight of 7.3 wt% Si [36]. The U_3Si_2 fabricated at the INL facility under the ATF program yielded U_3Si_2 that was 1.5% volume fraction U_3Si making it well within the margins of acceptability set by RETR.

The process for making sintered pellets continues by crushing the arc melted ingots to a fine powder ranging in particle sizes from 1 μm to 10 μm. Pellets are then pressed under around 138 MPa using a double-ended floating die system to around 55% to 65% theoretical density (TD) using binders to help hold the pellet together after it has been pressed. The diameter of the die is 0.9525 cm with a charge mass of 4.0 grams is designed to produce a pellet with a length to diameter ratio of 0.5 if sintered to TD [16]. The pellet is then sintered for around 4 hours at 1500°C under an argon gas to produce a pellet that is at 95.5% TD and is consistent enough to get within

a density of 11.5±0.1 g/cm^3. Centerless grinding of the pellets then aids in getting the pellets within a diameter tolerance of ±2.54μm for use in ATR test rodlets [17]. A photograph of the finished product that has been fabricated at INL for use in the ATF-1W irradiation test capsule can be shown in Figure 2.2

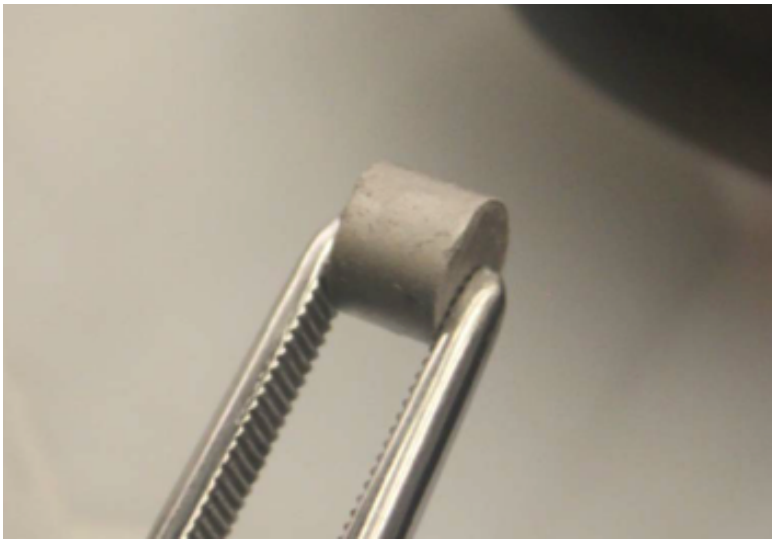

Figure 2.2: U_3Si_2 sintered pellet for ATF test [16]

The process Shimizu (1965) uses differs after the arc melting takes place for the production of cast pellets. Shimizu notes his method for the production of the pellets. Instead of crushing the arc melted ingot, the voltage and amperage on the arc melting device was increased from 200 amp, 20 v to 600 amp, 28 v allowing the melted section to drop through the bottom and into a mold of given specifications. This casting process creates a very different microstructured pellet with increased fractional density, 98% to 99%, and larger grain sizes compared with those of sintered pellets.

To implement a model of U_3Si_2 into FRAPCON, certain thermophysical properties are needed to examine how the fuel performs in the code. Primary thermal properties of interest are the thermal conductivity of the material and a coefficient of thermal expansion. These models differ between test to test due to variances in sample fabrication methods, measurement techniques, and testing conditions.

The physical properties of the silicide fuels have been investigated more than its irradiation properties. One of the biggest assets to the U_3Si_2 fuel is that it has a much higher thermal conductivity than that of UO_2. The arc cast samples of Shimizu were sent out to three separate laboratories for thermal conductivity measurements. One was sent to the National Bureau of Standards for measurements at low temperatures, 100°C to 200°C, another was sent to Battelle Memorial Institute for measurements up to 1200°C, and two measurements were made at Atomics International where one was terminated prematurely at 500°C due to defective vacuum conditions. All of these results showed good agreement that for cast samples of U_3Si_2 the thermal conductivity increases with temperature. The work of Taylor and McMurtry examined sintered pellets, but shows a strong negative correlation with temperature. Shimizu explains that this is most likely erroneous given the method of testing. From all of this data, Shimizu suggests a conservative value:

$$\lambda(T) = 7.98 + 0.0051 \cdot T \tag{2.1}$$

Where T is temperature in °C and holds valid from 20°C to 1200°C [36].

A much more recent study on U_3Si_2 themrophysical properties has been done through Los Alamos National Laboratory (LANL) in 2013. In specific, the tests observed the thermal expansion and the thermal conductivity of U_3Si and U_3Si_2. Because of the difficulty in making large samples of sintered U_3Si_2, a laser flash analysis method was used to determine the thermal diffusivity of the sample. The LFA does not require large samples and provides flexibility in terms of the atmosphere that can be provided to the sample at high temperatures, making it the choice for the study [42]. It is noted that the thermal diffusivity of a material measured by LFA can be related to the thermal conductivity of a sample by the equation:

$$\lambda(T) = D(T) \cdot C_p(T) \cdot \rho(T) \tag{2.2}$$

Where λ is the thermal conductivity in W/m K, D is the measured thermal diffusivity

in m^2/s, C_p is the specific heat in J/kg K, and ρ is the density in kg/m^3. After measurements were taken an equation was formed using a least squares minimization:

$$\lambda(T) = 0.0183 \cdot T + 2.16 \tag{2.3}$$

This new measurement confirms the positive correlation between temperature and thermal conductivity for U_3Si_2. A comparison between this new measurement taken at LANL and previous experimental data taken at AI and Taylor and McMurtry can be seen in Figure 2.3.

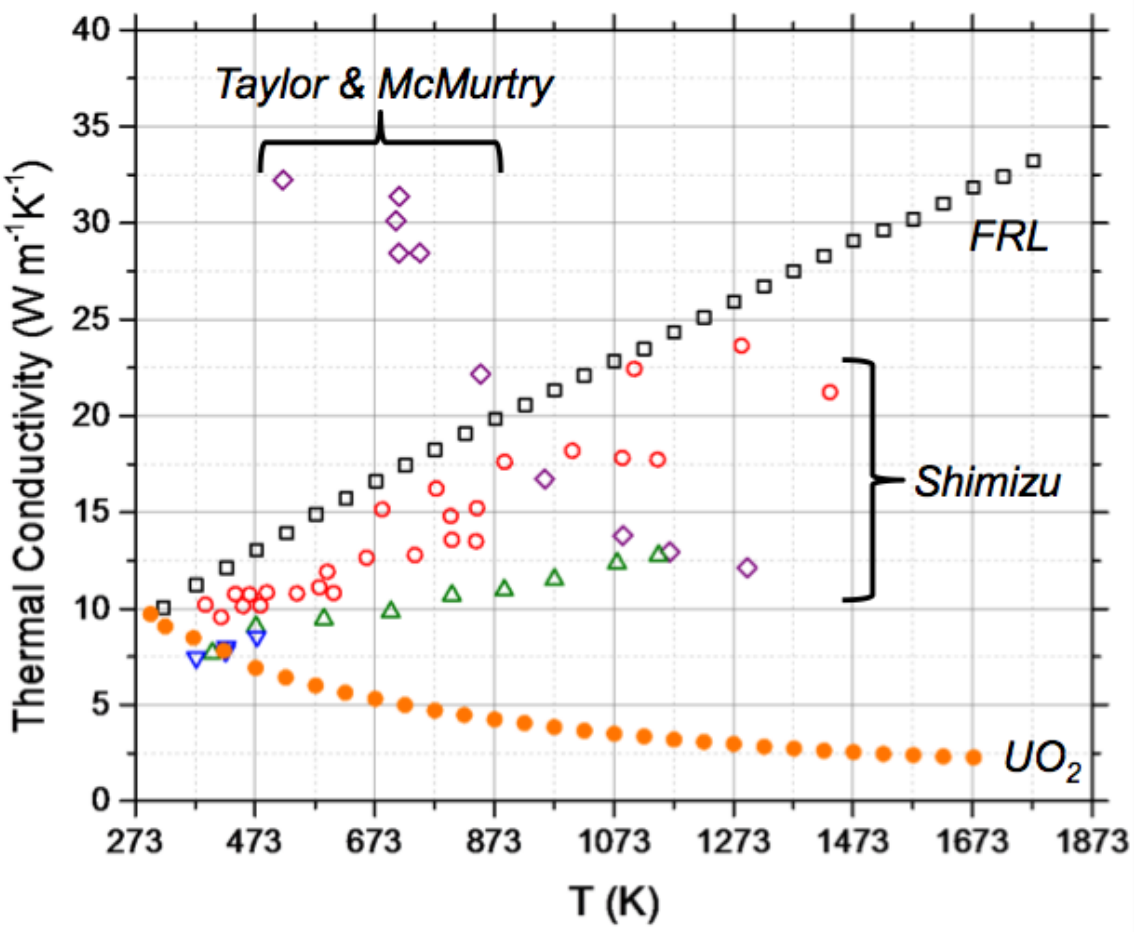

Figure 2.3: New thermal conductivity measurement of U_3Si_2 [42]

One of the biggest differences that can be seen from UO_2's thermal conductivity, is that with U_3Si_2, a positive correlation with temperature throughout operating temperatures is present. This higher thermal conductivity allows the pellet to maintain

a lower temperature gradient throughout the material. Shimizu notes that original expectations were that the fuel would be severely cracked or pulverized during irradiation testing, but notes that it had remained relatively intact throughout the test despite the extreme brittleness of the material. Expectations were that the fuel will not exhibit nearly as much cracking as what occurs in UO_2 at the same power due to the lowered temperature gradient.

In addition to thermal conductivity measurements taken by LANL, a confirmation of the thermal expansion of U_3Si_2 was obtained. Thermal expansion strain data for the U_3Si_2 material was taken up to temperatures of 1273 K under an 10ppm O_2 argon gas stream. An observed increase from the linearity of the slope was noticed after 650 K which can be attributed to the heavy oxidation of the sample from the oxygen in the gas. It is proposed that the the dL/L_0 for U_3Si_2 without the presence of oxygen will follow the equation:

$$\frac{dL}{L_0} = 1.518x10^{-5}T - 4.054x10^{-4} \tag{2.4}$$

Taking the derivative with respect to T, in K, will give the thermal expansion coefficient, 1.518x10^{-5}. This number agrees well with other works.

The work of A.G. Samoilov (1965) offers one of the more complete sets of thermal expansion coefficients for the U_3Si_2 material. In this work an average thermal expansion coefficient is given over a set of temperature ranges as shown in Table 2.2.

To get an expression of the coefficient of thermal expansion as a function of temperature, A line was fit that runs through the midpoint of each given range and came up with the function:

$$\alpha = (15.7 - 0.002 \times T) \times 10^{-6} \tag{2.5}$$

Where T is in °C and is valid from 20°C to 950°C.

Shimizu's findings from Atomics International, Carborundum Co., and Battelle Memorial Institute also agree well with these values as shown in Table 2.3. However

Table 2.2: Thermal expansion of U_3Si_2, Samoilov [34]

Temperature Range, °C	**Coefficient of linear expansion, x10^{-6} C^{-1}**
20–200	15.5
20–300	15.9
20–400	15.2
20–500	15.3
20–600	15.2
20–700	15.1
20–800	15.0
20–900	14.7
20–950	14.6

it is noted in Shimizu's work that the results taken from Atomics International may be misleading due to poor vacuum conditions during testing which caused a severe volumetric increase in the specimen before reaching 500°C.

Table 2.3: Thermal expansion of U_3Si_2, Shimizu [36]

Data Source	**α, x10^{-6} °C**	**Temperature Range, °C**	**Method of Manufacture**
AI	17.3	100–880	arc cast
Carborundum Co.	15.0	25–1200	sintered, 92% theoretical density
BMI	15.0	25–800	sintered
BMI	14.6	25–950	sintered

A number of tests have been done looking at U_3Si_2 as plate fuel or dispersal fuel in an aluminum matrix, but very little irradiation testing of monolithic U_3Si_2 has been done. One of the best resources for irradiation testing of monolithic U_3Si_2, is the work done by Shimizu in 1965 [36]. Shimizu tested some of the irradiation properties of the U_3Si_2 fuel by inserting a specially designed fuel capsule into the GE Test Reactor (AKA Vallecitos BWR, light water moderated and cooled, enriched uranium reactor, using stainless steel plate-type fuel). The silicide fuel was arc cast and shaped into six pieces of 0.350-inch diameter and various lengths that were enriched to 10% ^{235}U.

These were then placed in a specially designed, sodium fill gas rod that was inside of another capsule to provide a heat barrier to the water. The capsule was designed to be run up to a linear power of 15.5 kW/ft for a duration of eight months. The design of the capsule used for this experiment is shown in Figure 2.4.

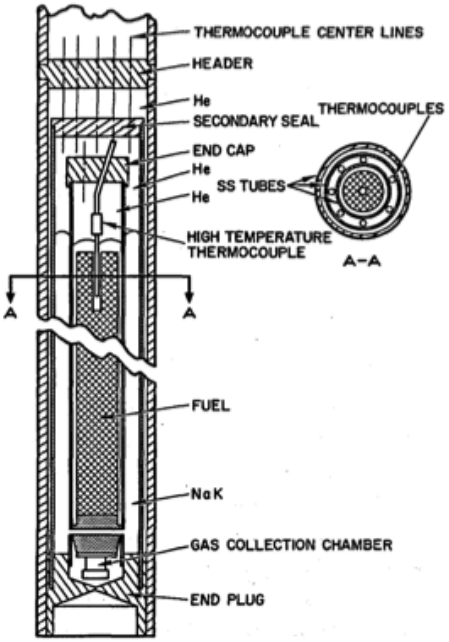

Figure 2.4: Capsule design for irradiation testing of monolithic U_3Si_2 pellets [36]

This irradiation experiment ultimately proved to be somewhat inconclusive due to poor fuel stoichiometry control (hypo-stoichiometric U_3Si_{2-x}), which is detrimental for irradiation stability. All of the pellets were meant to be completely stoichiometric at 7.30wt% Si, but due to the vaporization of Si during arc melting and casting, ended up ranging from 7.08wt%-7.17wt% Si before irradiation and 5.18wt%-7.17wt% after irradiation. This hypo-stoichiometric U_3Si_2 made for erratic results in the length and diameter changes so change in density is the best measure for pellet swelling. He goes on to note that fission gas release in the silicide fuel is a single magnitude higher than what would be expected from that of UC and the swelling is a factor of three higher than that of UC.

One of the more recent irradiation testings of the U_3Si_2 fuel, is the study of athermal irradiation induced swelling done by Finlay. For Finlay's irradiation experiments, 35 U_3Si_2 miniplates were fashioned and placed in the Oak Ridge Research Reactor with many other fuel plates for various lengths of time and at temperatures below 100°C. From the results, a new understanding of athermal swelling in silicide fuels was derived. He showed that at high burnup conditions, the silicide fuels will exhibit a breakaway swelling. Using the relationship between fission density and burnup in terms of MWd/kgU:

$$\left(\frac{10^{21} fissions}{cm^3}\right)\left(\frac{183 MeV}{fission}\right)\left(\frac{cm^3}{11.31g}\right)\left(\frac{10^3 g}{kg}\right)\left(\frac{1.602^{-13} Joules}{MeV}\right)\left(\frac{10^{-6} MW}{W}\right)\left(\frac{day}{86400 sec}\right) \cong \left(\frac{30.0 MWd}{kgU}\right)$$

Figure 2.5 shows that although U_3Si_2 exhibits the most favorable swelling rates of the materials tested, buts it is still about twice as high as what UO_2 shows.

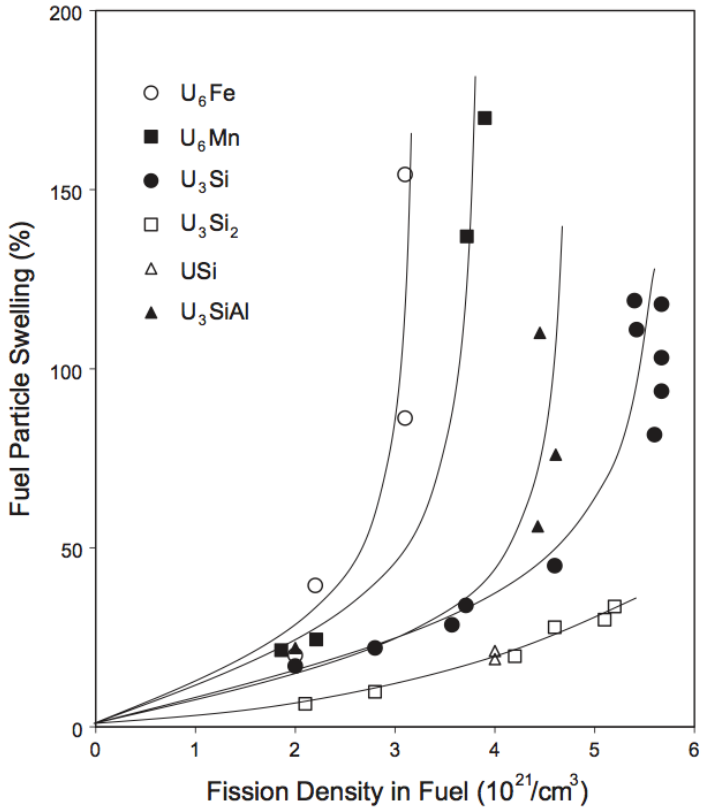

Figure 2.5: Athermal irradiation induced swelling of U_3Si_2 [10]

To get a swelling rate that is usable for BISON, only the first data point taken on Figure 2.5 was used. Creating an exponential best fit between 0 burnup and 0 swelling and the first point on Figure 2.5 gave a total rate of swelling:

$$\frac{V}{V_0} = 3.88008 \cdot Bu^2 + 0.79811 \cdot Bu \tag{2.6}$$

Where $\frac{V}{V_0}$ is in % and Bu is the burnup in atomic %.

Using this model, at 60 GWd/MTU, we would expect swelling to account for around 6.2 % V/V_0 strain. This is roughly double that of UO_2 at similar burnups.

2.2 Uranium Nitride

Uranium mononitride, UN, isn't currently being considered as a top candidate for a new monolithic fuel choice for LWR's, but it contains a very high uranium density, which is great for uprating existing plants, but fails under accident conditions when exposed to water. This fuel may be considered as a possible candidate for a hybrid coated pellet with U_3Si_5 serving as the 'protective coating' [24].

Uranium nitride has a NaCl-type fcc structure with a lattice parameter length of 0.4889 nm. It has a very high density and uranium density at 14.32 g/cm^3 and 13.53 g/cm^3 respectively [12]. This makes them attractive for the additional heavy metal loading that the fuel can bring. UN, however, is lacking in terms of chemical stability. The binary phase can be seen in Figure 2.6 showing a high melting point, at perfect stoichiometry UN, of 2850°C, but any deviation of the 1:1 stoichiometry at high temperatures will lead to a decomposition of the UN to uranuim and nitrogen. In addition to the stoichiometry control issues that are associated with the manufacture of UN, it is also noted that an enrichment in N^{15} is needed to reduce the absorption cross section ($\sigma_a^{N^{14}} \approx 10^5 \sigma_a^{N^{15}}$ in the thermal spectrum), to avoid C^{14} and H generation through the reaction: ^{14}N + n -> ^{14}C + p, which embrittles the fuel [23]. This extra effort just adds to the difficulty of manufacturing and using the UN fuel.

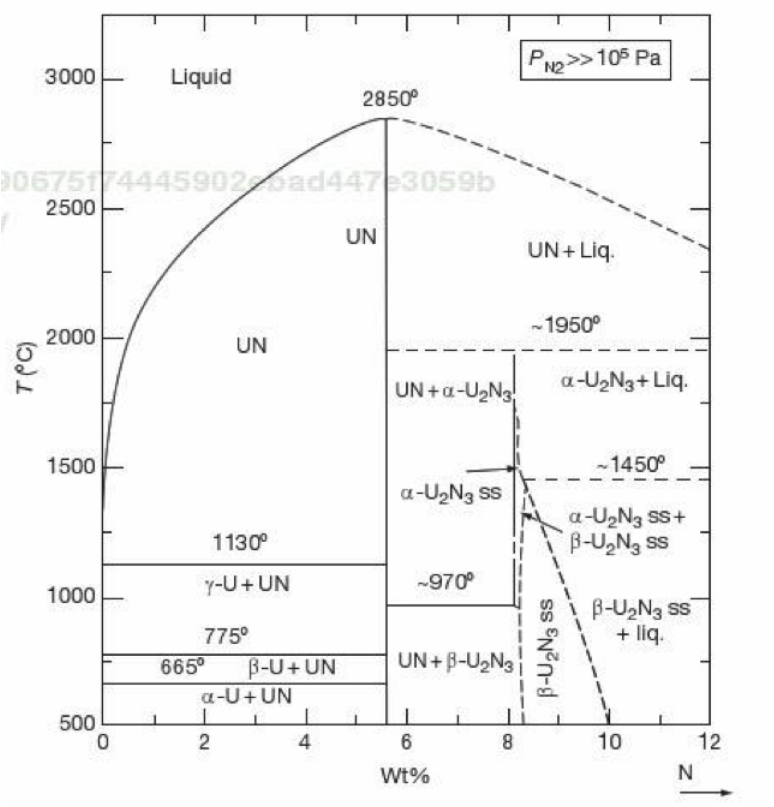

Figure 2.6: Phase diagram of UN [40]

The thermophysical properties of UN are similar to those of U_3Si_2 in that it contains a high thermal conductivity that increases with temperature. The thermal conductivity model that was chosen for use in FRAPCON and BISON fuel performance codes was one taken from Ross et al. given by:

$$\lambda(p,T) = 1.37T^{0.41} \times \frac{1-p}{1+p} \tag{2.7}$$

Where p is the as-fabricated porosity, T is in K, λ is in W/m K, and is valid for $0 \leq p \leq 0.1$ and $T \leq 1700$ K [12]. Hayes et al. gives another model for the thermal conductivity as:

$$\lambda(p,T) = 1.864T^{0.361}e^{-2.14p} \tag{2.8}$$

Where p is porosity, T in K, λ is in W/m K, and is valid for $0 \leq p \leq 0.2$ [12]. Frost notes that the two above porosity factors will give practically identical results in the range $0 \leq p \leq 0.1$. Arai et al. assessed the thermal diffusivity of UN via laser flash method

to get the temperature and porosity dependent term for thermal conductivity. The thermal conductivity relation gives the equation:

$$\lambda(p,T) = (-17.75 + 0.08808T - 6.161 \times 10^{-5}T^2 + 1.447 \times 10^{-8}T^3) \times \frac{1-p}{1+p} \quad (2.9)$$

Where p is the as-fabricated porosity, T is in K, λ is in W/m K, and is valid for $0 \leq p \leq 0.1$ and 680 K$\leq$T$\leq$1600 [40]. The thermal conductivity that Ross et al. gives was chosen for use in our models for its validity in the lower end of the temperature range, where as Arai's is valid from 680 K and above. A quick comparison of the models using a porosity factor of $p = 0.05$, over a temperature range of 500-2500 K can be seen in Figure 2.7.

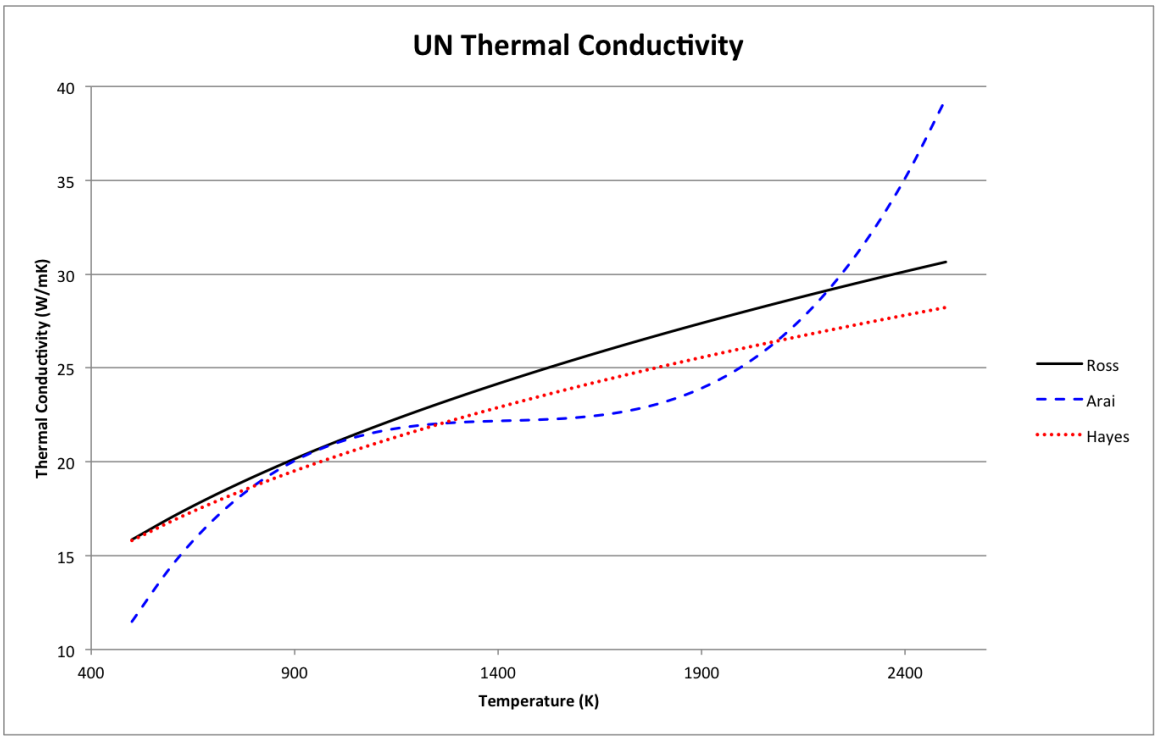

Figure 2.7: Comparison of UN thermal conductivity models [12, 40]

The specific heat of UN used for the fuel performance codes was taken from the equation given from Matzke:

$$C_p(T) = \left(\frac{1}{0.252}\right)(54.1 + 2.28 \times 10^{-3}T + 4.37 \times 10^{-6}T^2 - 6.81 \times 10^{5}T^{-2}) \quad (2.10)$$

Where C_p is in J/kg K, T is in K and valid between 20°C and 2700°C [23]. Hayes et al. gives another relation for UN which possesses 5 fitting parameters and is related to the physics of the lattice vibrations:

$$C_p(T) = 54.14\left(\frac{\Theta}{T}\right)^2 \frac{exp\left(\frac{\Theta}{T}\right)}{[exp\left(\frac{\Theta}{T}\right)-1]^2} + 9.491\times10^{-3}T + \frac{2.642\times10^{11}}{T^2}exp\left(-\frac{18081}{T}\right) \tag{2.11}$$

Where, C_p in J/mol K, T in K, Θ is the empirically determined Einstein temperature of UN, 365.7 K and is valid between 298 K and 2628 K [12]. The equation taken from Matzke was taken for its ease to be implemented into the code.

The irradiation properties of monolithic UN are more researched than those of U_3Si_2 and have limited FGR, irradiation swelling, and irradiation creep models available in literature. Currently, the irradiation swelling and creep are modeled in FRAPCON.

A volumetric swelling correlation for UN fuel in the temperatures range of 1200 K$\leq$ T$\leq$1600 K was found to be:

$$\frac{\Delta V}{V_0} = 4.7\times10^{-11}T_{avg}^{3.12}Bu^{0.83}\rho^{0.5} \tag{2.12}$$

Where T_{avg} is the average fuel temperature in K, Bu is the fuel burnup in at% and ρ is the as-fabricated fuel density (% of theoretical) [33]. This is probably not applicable for fuel temperatures in a typical LWR due to the fuel's excellent thermal conductivity, but is implemented into BISON and FRAPCON over that temperature regime nonetheless.

For temperatures closer to the LWR operational range, a suggested value of 0.9%/atomic% burnup is most accepted [9]. It is also noted that until T$\approx$ 0.5T$_{melt}$, this is approximation is valid. Above this temperature, the UN fuel swelling behavior is highly temperature-dependent. The value that is solely based on burnup is the one that is used in the FRAPCON and BISON codes for the fuel at the lower temperatures. This model agrees well with other lower temperature swelling studies which range anywhere from 0.53% to 1.8% per %Bu [9, 19, 32, 39].

A plot of the different swelling rates at different temperatures can be seen in Figure 2.8. The invalid Ross line shows the amount of swelling his model would show if it were applied to temperatures seen in a LWR simulation.

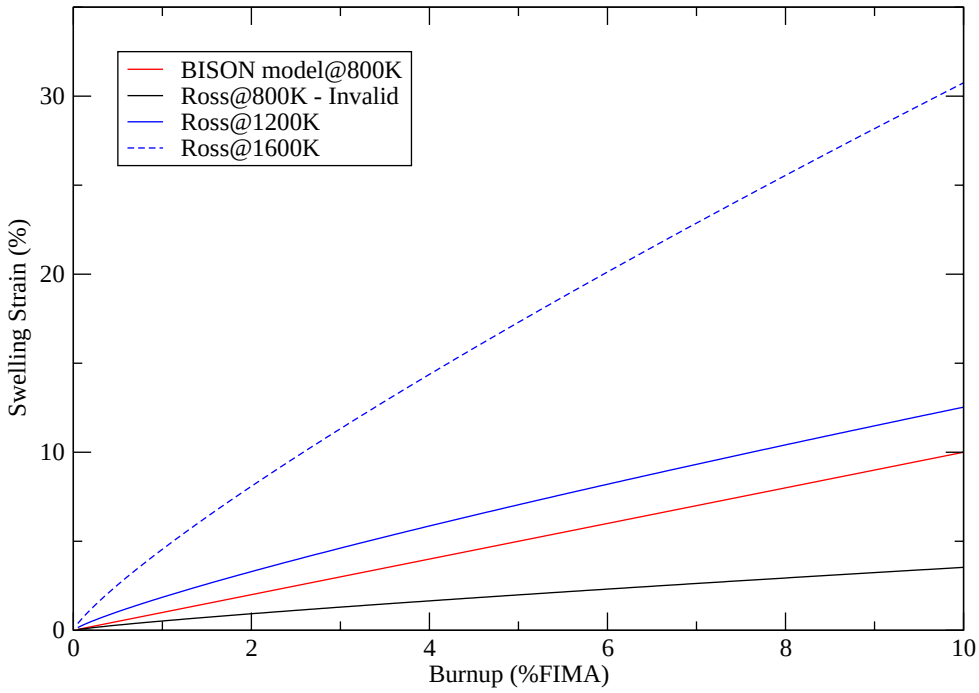

Figure 2.8: Swelling strain for UN type fuel [9, 33]

Thermal and irradiation creep rates were given respectively for monolithic UN as:

$$\dot{\epsilon}_T = 2.054 \times 10^{-3} \sigma^{4.5} e^{\frac{39369.5}{T}} \frac{0.987 e^{-8.65P}}{(1-P)^{27.6}} \tag{2.13}$$

and

$$\dot{\epsilon}_I = 10.8 \times 10^{-26} (1 + 1250P^2) \sigma \dot{F} \tag{2.14}$$

Where σ is the gap pressure in MPa, T is the temperature in K, P is the fractional porosity, $\dot{F}$ is the fission density in fissions/cm^{3}s, and $\dot{\epsilon}$ is in sec^{-1} [9]. Under LWR condiitons, the irradiation creep will dominate due to the relatively low temperatures

in comparison with UN's melting point. Figure 2.9 illustrates the creep rates of both thermal and irradiative creep rates for UN under PWR conditions.

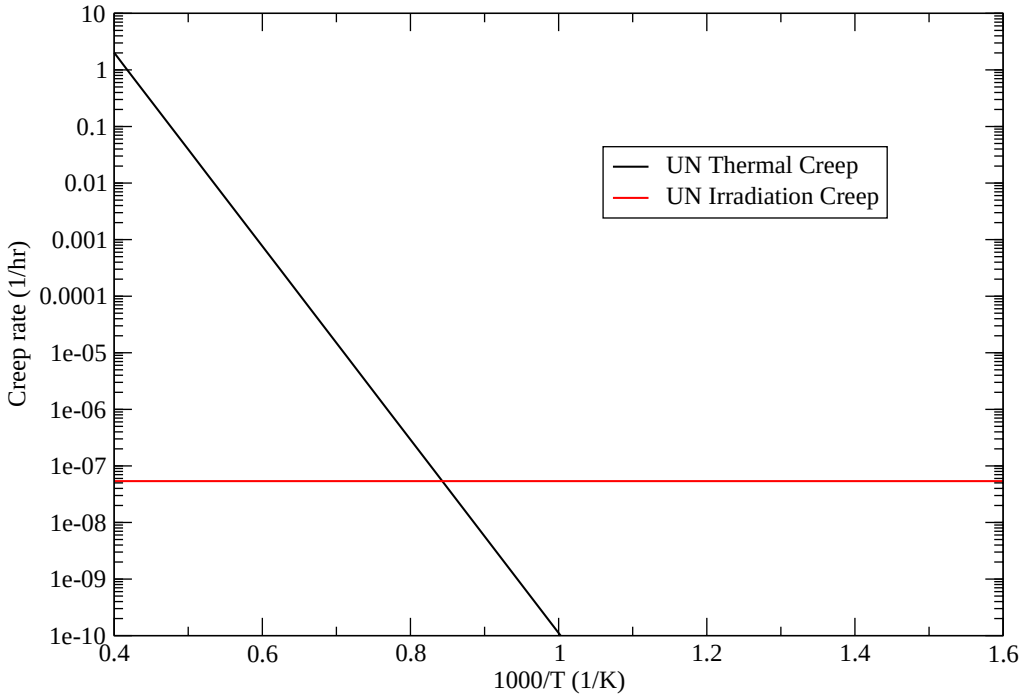

Figure 2.9: Thermal and Irradiative creep rates for UN under gap pressure of 20 MPa, 0.05 porosity, and 10^{13} fissions/cm^{3}s.

Bo Feng of MIT implemented a fission gas release model for UN into FRAPCON-EP that uses the Forsberg-Massih diffusional release model but with a diffusion coefficient for UN that is given by Weinstein as:

$$D = A \cdot F_P \cdot \left[8.22 \times 10^{-31} \cdot F_B \cdot f + 2.37 \times 10^{-10} \cdot e^{\frac{-18800}{T}} + 10^{-18} \cdot \frac{f}{K^2 T^2} \cdot e^{\frac{-18400}{T}} \right] \tag{2.15}$$

where F_P is a porosity dependent exponential factor given by:

$$F_P = e^{-\frac{\rho - 80}{3.4}} \tag{2.16}$$

and a burnup fitting factor, F_B given by:

$$F_B = 30 + Bu \tag{2.17}$$

with Bu in MWd/kgU, $A = 0.0021$, f is the fission rate density in fissions/cm^{3}s, K is the thermal conductivity in W/m K, T is the temperature in K, and D is the fission gas diffusion coefficient for UN fuel in cm^2/s [41]. It is suggested that fission gas release should be comprable to that of UO_2 depending on the power history with values for a typical three cycle PWR power history totalling 3.5% FGR [9]. This model has now been implemented into BISON fuel performance code using the same methodology as done with the FRAPCON-EP. A statistical correlation taken from data recorded from 95 UN and 39 (U,Pu)N fuel experimental results Storms proposed an empirical equation for fission gas release rate as a function of fuel temperature, burnup, and density was statistically derived [2].

$$R = 100/\left(exp[0.0025(90D^{0.77}/Bu^{0.09} - T)] + 1\right) \tag{2.18}$$

Where R is the FP gas release rate in %, D the fuel pellets density in % TD, Bu the burnup in % FIMA, and T the temperature of the fuel in K. This will be used to help assess the validity of the model implemented into the BISON code.

2.3 Uranium Carbide

The 1:1 Uranium Carbide fuel, UC, had been previously implemented into the FRAPCON code as part of South Carolina's work with HTGR fuel performance analysis. Thermophysical and irradiation properties have been collected from various sources and are now being utilized in both the FRAPCON and BISON fuel performance codes. The work collected by Preusser in his article, "Modeling of Carbide Fuel Rods" contains a variety of information used to model UC fuel and is where most of the equations that Luke Hallman uses in FRAPCON come from.

The UC fuel, trending with the UN and U_3Si_2 fuels, has a higher thermal conductivity and higher uranium density than that of the traditional LWR fuel, UO_2. It was primarily researched as a fast reactor fuel due to its instability with water, but has gained renewed interest as a candidate for the new generation of gas cooled reactors.

The crystal structure of UC is NaCl-type FCC, has a density of 13.63 g/cm^3, and does not experience any lattice transformation in stable conditions [31]. UC also has the advantage of having a high melting point at the 1:1 stoichometry at 2780 K [22].

The UC compound keeps with the advanced fuel trend of having a high thermal conductivity compared with that of UO_2. UC thermal conductivity along with most other materials, decreases with increasing porosity. A porosity and temperature dependent model that is used in the URANUS, FRAPCON and BISON fuel performance code is given as:

$$\lambda_P = 20 \cdot \frac{1-P}{1+P} \tag{2.19}$$

for temperatures T $\leq$ 500°C and

$$\lambda_P = (20 + 1.3 \times 10^{-3} \cdot (T - 500)) \cdot \frac{1-P}{1+P} \tag{2.20}$$

for T $>$ 500°C, where T is in °C, P is the fractional porosity and λ_P is in W/m K [31]. Comparing with UO_2, the UC's thermal conductivity at 0.95TD is around six times greater at operational temperature. This increased thermal conductivity again lowers the temperature gradient throughout the pellet, decreasing the chance that pellet fracture will occur due to the lowered thermal stresses.

A thermal expansion coefficient that corresponds with multiple other results very well was given as:

$$\alpha\left(\frac{1}{^\circ C}\right) = 1.007 \times 10^{-5} + 1.17 \times 10^{-9} \cdot T \tag{2.21}$$

Where α is in $^\circ C^{-1}$ and T is in °C [31]. This model is again used in the URANUS, FRAPCON and BISON codes for monolithic UC.

A specific heat model is given as:

$$C_p(T) = 217.8 + 0.03852 \cdot T \tag{2.22}$$

Where T is in K and C_p is in J/kg K where the model is valid from 273 K≤T≤ T_{melt}. Since FRAPCON is a steady-state analysis only, the specific heat function is not called.

A limited look at the irradiation properties of UC is also available in the work of Preusser. Values for swelling, thermal and irradiation creep, and fission gas release models are all available with limited dependencies. Since swelling is the combination of solid and gaseous fission products that accumulates within the fuel matrix, it is important to notice that there is a strong temperature and material structure dependence associated with the fuel swelling. Preusser notes that up to 40% of the fission gas produced can be stored in the fuel, contributing to heightened swelling rates. A temperature dependent model used in URANUS was implemented and given as:

$$\frac{\Delta V}{V} = 0.4667 + 1.711 \cdot f(P, pc) \tag{2.23}$$

for temperatures up to 700°C. For temperatures greater than 700°C a rate was given as:

$$\frac{\Delta V}{V} = 0.4667 + 1.711 \cdot f(P, pc) + [(6.412 - 0.0198 \cdot T + 0.152 \times 10^{-4} \cdot T^2) \cdot f(BU) \cdot f(P, pc)] \tag{2.24}$$

Where:

$$f(BU) = \left(\frac{BU}{BU_0} - a\right), f(BU) \geq 0 \tag{2.25}$$

is a burnup correction factor and:

$$f(P, pc) = e^{[-(P-0.04)]} \cdot e^{\left[-\left(\frac{pc}{pc_0} \cdot b\right)\right]}, (P - 0.04) \geq 0 \tag{2.26}$$

is a porosity correction factor, T is in °C, BU is in MWd/kgU, P is fractional porosity, pc is contact pressure in MPa, a and b are modeling parameters with suggested values

2 and 0.1 respectively, BU_0 is 10 MWd/kgU constant, pc_0 is 1 MPa constant, and $\frac{\Delta V}{V}$ in vol%/10 MWd/kgU. An upper limit on the $\frac{\Delta V}{V}$ is set at 4.558%/10 MWd/kgu. This is one of the more encompassing models for UC swelling. Other, more simplistic models give a rate of $\frac{\Delta V}{V} = 1.5 vol\%/\%Bu$ as the most accepted burnup dependent only model [8].

In Preusser's article, a multitude of creep rates can be found and examined for validity. For the thermal creep portion of the model, three separate models from Freund, Caligara, and Tokar were given respectively.

$$\dot{\epsilon}_{cr}^{th}\left(\frac{1}{h}\right) = 1.45 \cdot 10^{10} \cdot \sigma_v^{2.44} \cdot e^{(-63000/T)} \tag{2.27}$$

where σ_v is the effective stress in MPa and T is temperature in K [11].

$$\dot{\epsilon}_{cr}^{th}\left(\frac{1}{h}\right) = 3.07 \cdot 10^{-9} \cdot \sigma_v^{1.79} \cdot e^{(-3465/T)} \tag{2.28}$$

where σ_v is the effective stress in MPa and T is temperature in K [5].

$$\dot{\epsilon}_{cr}^{th}\left(\frac{1}{h}\right) = 1.49 \cdot 10^{10} \cdot \sigma_v^{2.44} \cdot e^{(-63200/T)} \tag{2.29}$$

where σ_v is the effective stress in MPa and T is temperature in K [38].

Since the UC type fuel has a high thermal conductivity and will be tested under LWR conditions, it is important to note that the fuel will probably not experience much thermal creep, but will be mostly dominated by the irradiation creep regime. Models from Steiner/Matthews, Caligara, and Freund are available for the irradiation induced creep of monolithic UC and are shown respectively below.

$$\dot{\epsilon}_{cr}^{irr}\left(\frac{1}{h}\right) = 3.6 \cdot 10^{-22} \cdot \sigma_v \cdot F \tag{2.30}$$

where σ_v is the effective stress in MPa and F is fission rate density in fissions/cm^{3}s [38].

$$\dot{\epsilon}_{cr}^{irr}\left(\frac{1}{h}\right) = 4.97 \cdot 10^{-29} \cdot \sigma_v \cdot F \tag{2.31}$$

where σ_v is the effective stress in kp/cm^2 and F is fission rate density in fissions/cm^{3}s [5].

$$\dot{\epsilon}_{cr}^{irr}\left(\frac{1}{h}\right) = 3.47 \cdot 10^{-12} \cdot \sigma_v \cdot \frac{\chi}{r_a^2 - r_i^2} \tag{2.32}$$

where σ_v is the effective stress in MPa, χ is the linear rod power in W/cm, and r_a, r_i are the fuel radii in mm [11].

Preusser notes, however, that the irradiation data taken from Freund [11] lies three orders of magnitude below that from Steiner. This is taken to be a transcription error. Caligara's[5] data shows results that are so low that for low temperatures, creep is negligable which also indicates an error is also present. It is suggested that the equations from Matthews and Tokar and Steiner should be used for correctness. A comparison of the Matthews and Tokar and Steiner with the Caligara data can be seen in Figure 2.10. A fission rate density of 1.5×10^{13} fiss/cm^{3}s is typical in BISON runs for LHGR's of 20kW/m and therefore is used for this comparison.

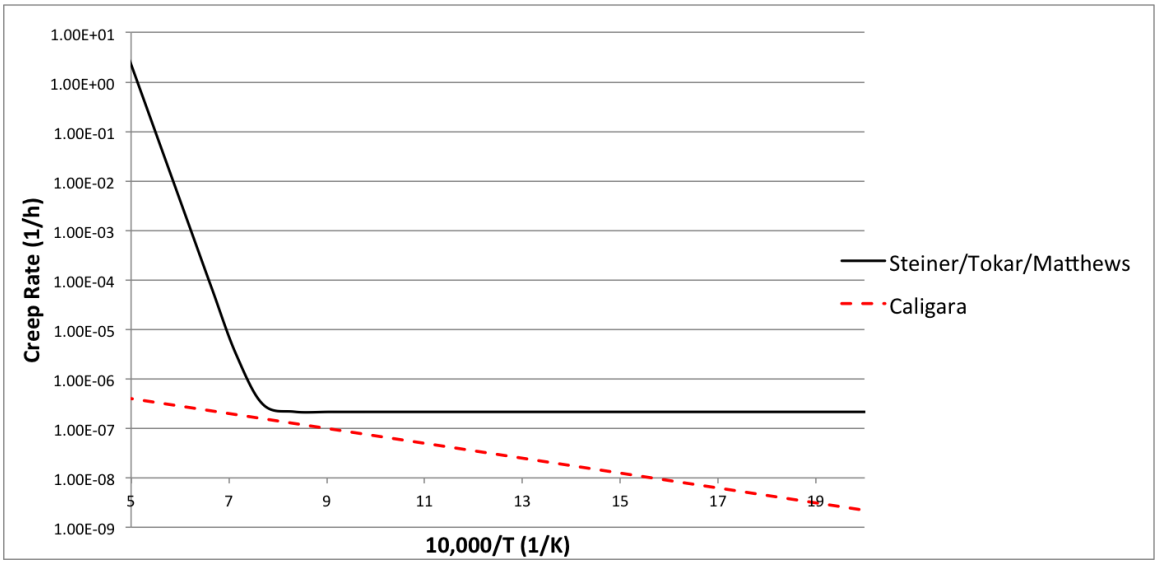

Figure 2.10: Creep model comparison for UC fuel with effective stress = 40 MPa

2.4 Silicon Carbide Cladding

In addition to using the advanced fuels with the ATF program, advanced cladding types are also being looked at. In specific, SiC type cladding. SiC cladding has the major benefit that in the case of a LOCA type accident, the cladding is designed to remain stable even at high temperatures and in the presence of steam. This provides a major benefit over the current Zr based claddings in that at high temperatures and in the presence of steam, Zr undergoes the exotheric redox reaction: $Zr + 2H_2O \rightarrow ZrO_2 + 2H_2$. The recent events at Fukishima Diachii units 1, 2, and 3 were made worse by this reaction, causing hydrogen explosions and dispersal of radioactive material within each plant.

To implement the SiC cladding into a fuel performance code requires that certain properties be implemented. For the FRAPCON code, the SiC has been previously implemented by Bo-Shiaun Li and Ian Porter at the University of South Carolina [21, 30]. The properties needed to correctly model the SiC cladding in FRAPCON include the thermal expansion coefficient, thermal conductivity, elastic modulus, shear modulus, Meyer's hardness, and emissitivity of the cladding. All of these material properties originate from Lance Snead's "Handbook of SiC properties for fuel performance modeling" [37]. Table 2.4 contains a summarized version of the models used to calculate each of these above noted cladding properties.

For the BISON code, the SiC cladding was modeled such that it did not deform plastically as with the FRAPCON code. With the BISON code, the models used are input by the user in the input file directly by changing default flags to match the desired value. Required cladding values for use with the BISON code are thermal conductivity, specific heat, Young's modulus, Poisson's ratio, thermal expansion coefficient, and density. Table 2.5 gives a list of the values used for user input in the BISON code for use of the SiC clad type. Future work will include making a

Table 2.4: FRAPCON SiC cladding properties

Cladding Property	**Validity Range**	**Value**	**Units**
Thermal Expansion	T_{clad}(K)<550	2.08 + 4.51*10^{-3}T - 1.68*$10^{-6}$$T^2$	10^{-6}/K
	550<T_{clad}<1273	-1.8276 + 0.0178T - 1.5544*$10^{-5}$$T^2$ + 4.5246*$10^{-9}$$T^3$	10^{-6}/K
	T_{clad}>1273	5.0	10^{-6}/K
Thermal Conductivity	DPA<1	3.6*([DPA+(-0.00108 + 1.05*$10^{-5}$$T_{clad}$)$^{2.5}$]$^{-0.4}$)	W/m-K
Thermal Conductivity	DPA>1	3.6	W/m-K
Poisson's Ratio		0.21	-
Elastic Modulus		(4.6*10^{11} - [4*$10^{7}$$T_{clad}e^{-962/T_{clad}}$])*(1 - [0.4*(1 - e$^{-0.15*DPA}$)])	Pa
Shear Modulus		Elastic Modulus/(2*(1 + Poisson's Ratio))	Pa
Meyer's Hardness		2.77*10^{10}e$^{(-5.4*Porosity_{clad})}$	N/m^2
Emissivity		0.8	-

mechaincal model for all necessary values based on temperature and fluence.

Table 2.5: BISON SiC cladding properties

Cladding Property	**Value**	**Units**
Thermal Conductivity	3.6	W/m-K
Specific Heat	1100	J/kg-K
Young's Modulus	3.84*10^{11}	Pa
Poisson's Ratio	0.21	-
Thermal Expansion Coefficient	3.0*10^{-6}	1/K
Density	2600	kg/m^3

For the FEMAXI code, implementing the SiC cladding into the code was done in a way where a separate executable was built. In the SiC version of FEMAXI, the Zry based cladding model was removed and the properties of the SiC cladding were added in.

2.5 Fuel Creep

Fuel creep needs to be considered with the advanced fuels as swelling is predicted to be more prominent than with UO_2. The ATF program is ultimately looking to insert the U_3Si_2 fuel into the SiC cladding to help uprate and increase safety in our current generation of reactors. It is noted from many sources to keep away from mechanical contact with SiC cladding due to its inability to plastically deform. In order to represent the advanced fuels most accurately, a fuel creep model will need to be implemented into the codes to allow for a more accurate representation of how long before the onset of PCMI occurs.

Creep is the time dependent, plastic deformation of a material which is under stress and most often higher temperatures. This process can be driven by holding the material at high temperatures, introducing it to a neutron flux, or, in the case of in-core materials, a combination of both heat and irradiation. Plotting the creep strain, ϵ_{creep}, against time for a given material can be broken into three separate creep regimes [27]. A typical creep strain-time graph for a given material would most often follow a general creep regime segmentation similar the one given in Figure 2.11.

Most fuel performance codes do not take into account primary or tertiary fuel creep rates as they are either not available for the material or insignificant. Secondary, or steady state creep occurs after the material has been work-hardened by the primary creep regime and is classified that when the material as a whole has the same amount of dislocations climb away from obstacles as dislocations are blocked on obstacles. When looking at the secondary or steady state creep regime, $\dot{\epsilon} = (d\epsilon/dt)_{ss}$, it most often follows an Arrhenius-type relation which reads:

$$\dot{\epsilon} = A\sigma^n e^{\left(\frac{-Q}{k_B T}\right)} \tag{2.33}$$

Where A is the creep constant, σ is the stress, n is the creep exponent which varies between 3 and 8, and Q is the activation energy (having about the value of that for

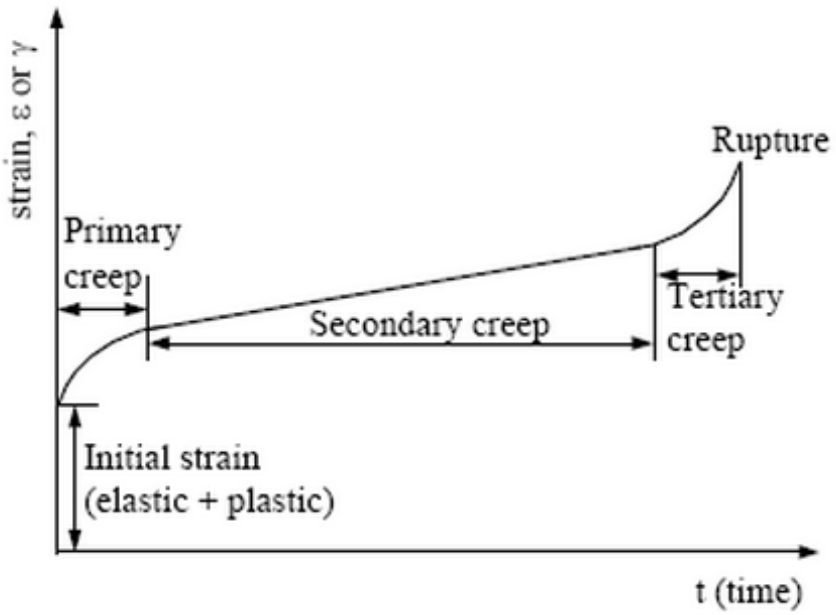

Figure 2.11: Schematic representation of a typical creep curve

self-diffusion) [18].

At lower stress levels, a linear relationship between $\dot{\epsilon}$ and σ occurs and is diffusion controlled. Under low-stress and very-high temperatures, bulk diffusion creep occurs. This type of creep is most commonly known as Nabarro-Herring creep and takes the equation:

$$\dot{\epsilon}_{bulk} = B_{vol}\left(\frac{\sigma}{d^2}\right)e^{\left(\frac{-Q_{vol}}{k_B T}\right)} \tag{2.34}$$

Where B_{vol} is a constant, Q_{vol} is the activation energy of atom self-diffusion in the solid, and d is the grain size [27]. For somewhat lower temperatures and low-stress conditions, grain boundary diffusion is thought to be dominant. This type of creep is known as Coble creep and takes the equation:

$$\dot{\epsilon}_{gb} = B_{gb}\left(\frac{\sigma}{d^3}\right)e^{\left(\frac{-Q_{gb}}{k_B T}\right)} \tag{2.35}$$

Where B_{gb} is a slowly varying function of the ratio of the grain-boundary thickness to the grain diameter and Q_{gb} is the activation energy for grain-boundary diffusion [27]. A visual representation of the two mechanisms of linear stress-dependent creep can be seen below in Figure 2.12.

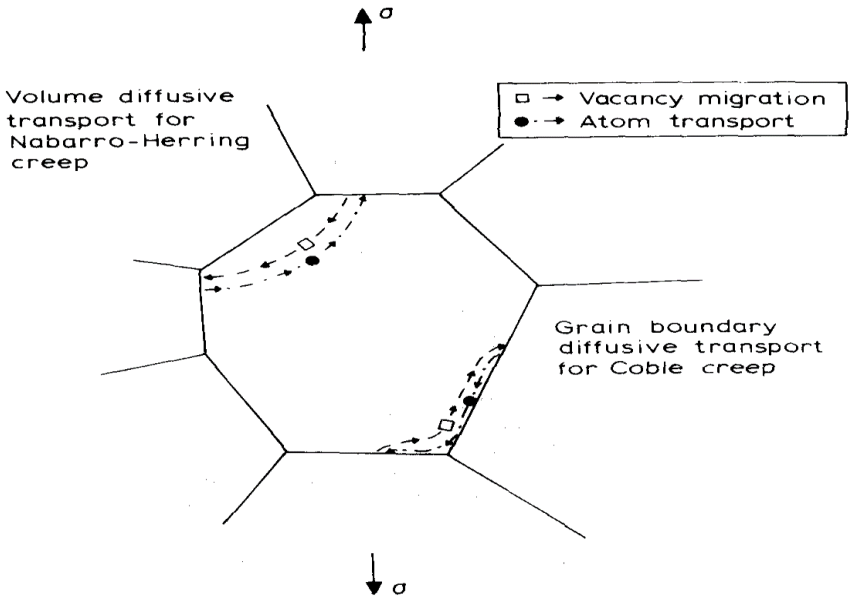

Figure 2.12: Coble and Nabarro-Herring creep mechanisms

For creep occurring under irradiation, the mechanisms for which creep occurs are still valid, but enhanced with the addition of the neutron flux. The neutron flux provides an additional creation of defects, specifically vacancies and interstitial, which then contribute to the diffusion of the defects throughout the material. It is suggested that in-reactor creep of UO_2 is comprised of an elevated temperature regime in which normal thermal creep is enhanced and a low temperature regime in which the fission process induces athermal creep [12]. As a general rule of thumb for ceramics, thermal creep will start occurring around $0.4 - 0.5T_{melt}$ [18], with UO_2 following this rule as well. Figure 2.13 shows the creep rate for UO_2, $\dot{\epsilon}$ in units of hr^{-1}, against inverse temperature $10^{4\circ}K^{-1}$ and how the thermal creep starts to dominate after about 1100°C. Comparing that to $0.4T_{meltUO_2}$ with 2865°C being the accepted melting point of UO_2, we get 1146°C. One can also see the relationship between the thermal and irradiation creep when plotted in this way. At $0.4T_{meltUO_2}$, the curve trends sharply upward suggesting that thermal creep effects are dominant at that temperature. Below that temperature, irradiative effects can be attributed as the

driving force for creep, allowing the irradiation creep term to be approximated by that constant rate.

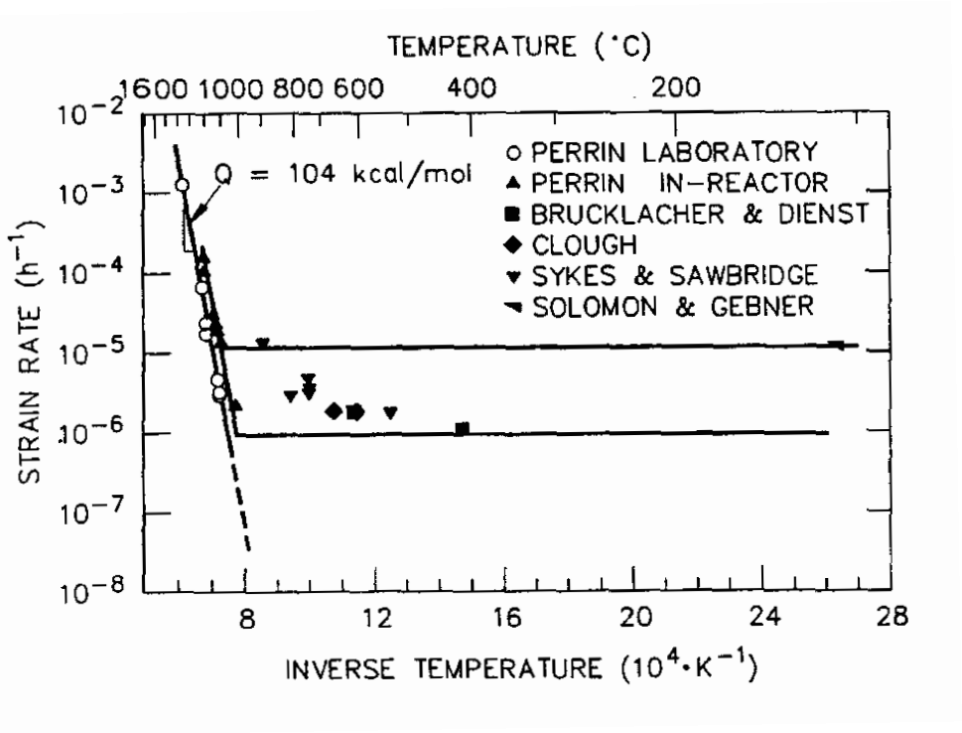

Figure 2.13: In-reactor creep results for UO_2 normalized to 24 MPa and fission rate of 1.2^{13} f/cm^3 s [12]

Currently there is no literature on the creep of silicide fuels. It may be helpful to know or at least get an idea of what to expect how much this fuel will creep due to thermal and irradiative effects. Going by the rule of thumb formula above for thermal creep of ceramics, we could expect thermal creep to begin from 666°C-833°C with 1665°C being used as T_{melt}. This falls well within the temperatures this fuel is expected to run at [36], making it an important phenomenon to study.

2.6 MOOSE/BISON finite-element modeling system

MOOSE is INL's 'Multiphysics Object-Oriented Simulation Environment' finite-element platform that solves fully-coupled PDE's simultaneously in 1,2 or 3D. MOOSE

is inherently parallel and can be coupled with a multitude of other codes specifically developed to run off of the MOOSE platform.

BISON is the engineering scale fuel performance code that is coupled with MOOSE. The code is designed for steady and transient analysis of fuel and is applicable to a variety of fuel forms [29] including traditional LWR fuel rods, TRISO-coated particle fuel, and metallic fuels in both rod and plate geometries. It handles the complex nature of fuel performance, solving the equations that govern heat transfer, irradiation induced changes in the fuel and cladding, interaction with the cladding, and plenum gas composition and temperature changes all simultaneously. Because BISON is a MOOSE based application, it can be run on a desktop or on a massively parallel high-performance cluster.

BISON does take into account fuel creep using the MATPRO model that is implemented in the FEMAXI code. The fuel creep model implemented is a function of effective von Mises stress, temperature, fuel density, grain size, volumetric fission rate and stoichiometry. The models currently implemented in BISON are only valid for the UO_2 and MOX fuels. The MATPRO equation for UO_2 is shown below:

$$\dot{\epsilon} = \frac{A_1 + A_2\dot{F}}{(A_3 + D)G^2}\sigma e^{(\frac{-Q_1}{RT})} + \frac{A_4}{(A_6 + D)}\sigma^{4.5}e^{(\frac{-Q_2}{RT})} + A_7\dot{F}\sigma e^{(\frac{-Q_3}{RT})} \tag{2.36}$$

where $\dot{\epsilon}$ is the creep rate (1/s), σ is the effective (von Mises) stress (Pa), T is the temperature (K), D is the fuel density (percent of theoretical), G is the grain size (μm), $\dot{F}$ is the volumetric fission rate (fissions/m^3-s), Q_i are the activation energies (J/mol), R is the universal gas constant (8.3143 J/mol-K) and A_{1-7} are material constants given as $A_1 = 0.3919$, $A_2 = 1.3100x10^{-19}$, $A_3 = -87.7$, $A_4 = 2.0391x10^{-25}$, $A_6 = -90.5$, and $A_7 = 3.7226x10^{-35}$. The first term represents diffusional thermal creep and is applicable to low stress and low temperature conditions. The second term represents thermal dislocation or power-law creep and is applicable to high stress and high temperature conditions. Note that irradiation effects are included in both the first and third terms.

The activation energies for the thermal creep terms (Q_1 and Q_2) are strongly dependent upon the fuel oxygen to metal ratio x and, in MATPRO, are defined using the Arrhenius type relations

$$Q_1 = 74,829 f(x) + 301,762 \tag{2.37}$$

$$Q_2 = 83,143 f(x) + 469,191 \tag{2.38}$$

where the energies are given in J/mole and

$$f(x) = \frac{1}{e^{\left(\frac{-20}{log(x-2)} - 8\right)} + 1} \tag{2.39}$$

The activation energy for the irradiation term (Q_3) is given in MATPRO as 21,759 J/mole [14].

Using these already built models as templates for the UC and UN materials should allow for easier implementation of a fuel creep model for the advanced fuels. The advantage to using the BISON code for this study with fuel creep is that it will allow for the use of discrete pellet modeling which is able to show the pressure points on the cladding at the pellet's ends and how creep will help relieve some of those stresses.

To account for fuel fracture during operation, BISON gives two means of accomplishing this. The first of these methods is by using a completely empirical equation for UO_2 fuel relocation. Fuel relocation is the process of applying a radial strain on the fuel so that the gap closes slightly simulating the effects of fuel cracking. The model used to apply this strain is the ESCORE relocation model [20]:

$$\left(\frac{\Delta D}{D_o}\right)_{REL} = 0.80 Q \left(\frac{G_o}{D_o}\right)\left(0.005 Bu^{0.3} - 0.20 D_o + 0.3\right) \tag{2.40}$$

Where Q is a function of the LHGR, D_o is the as-fabricated cold diameter of the pellet, G_o is the as-fabricated cold diametral gap, and Bu is the pellet average burnup. The common belief for the activation LHGR for UO_2 to start showing cracking is at a LHGR of 5 kW/m [26] and that a maximum of 4% radial strain be attainable

depending on initial conditions. The equation has been made to fit actual data taken from real experiments so fuel relocation for UO_2 and doesn't give an accurate representation for any other materials besides UO_2. This is a very limiting in that in order to add another material, an accurate representation of fuel cracking can't be obtained until actual experiments are made and an equation is fit to the data.

The second method BISON uses to model fuel cracking is smeared cracking. BISON's smeared cracking model is more mechanistic in the way that it works. The model examines the fuel's principal stresses and compares them to a user given critical stress. If the material stress exceeds the critical stress, the material point is considered cracked in that direction and the stress is reduced to zero. The material point will have no strength unless the strain becomes compressive [14]. It is also important to note that this differs from their discrete cracking model, which is a work in progress, in that no topographical changes are made to the mesh during smeared cracking.

A quick look at the differences between some of the physical phenomena that can be modeled with the BISON and FRAPCON codes can be seen in Table 2.6. This is a quick summary of the models that are described throughout Chapter 2 of this paper.

2.7 FRAPCON steady-state fuel performance code

FRAPCON is the NRC licensing fuel performance code that has been validated for use with UO_2 type fuel with Zr based claddings. Until the recent work done by Porter (2014), all of the properties for UO_2 were hard-coded in making it difficult to add in new materials. The code was reorganized so that adding in a new material is as simple as making a new module and calling it in. This expediated the work done in FRAPCON exponentially.

Other work done at the University of South Carolina included adding in the UN and UC type fuels so making a new model for those materials won't be necessary [7,15]. This helped put focus on making and implementing the BISON material models.

Since the FRAPCON code doesn't take into account axial communication between nodes, creep in FRAPCON is more 'hard-coded' in than what creep is in BISON. The creep model in FRAPCON modifies the fuel's volumetric swelling based on pressure and temperature instead of being its own module. This will get an accurate representation if not looking at the axial component of the fuel, but is not the most accurate way of representing fuel creep. But given the limited time constraints on this study, this gives a result that is very similar to what we should expect from if real results are compared with FRAPCON runs.

Table 2.6: Summary of models available in BISON and FRAPCON

Model (fuel)	**FRAPCON**	**BISON**
Swelling	Fuel changes volumetrically at an isotropic rate according to the fuel's given swelling rate, this is dependent on the type of fuel, burnup, density, and temperature.	Same as FRAPCON.
Creep	Is an adjustment to the swelling model. If the fuel creeps inward radially, it creeps downward axially as well. This is an approximanted method to including creep to the 1.5D FRAPCON code without major code re-write.	A redistribution of material is employed for the most part.
Relocation	FRACAS-I. Fuel is given a radial strain and once contact with the cladding is made, 50% of the initial strain is recovered before entering a 'hard contact' regime.	ESCORE by EPRI. A radial strain is added to the fuel given initial conditions of the fuel and run characteristics.
Cracking	No cracking model available	Smeared cracking is the available model where no topographicical changes in the mesh are made. Adjustments to the fuel's elastic contstants at a determined crack direction and location in the mesh are made. At that point, the stress is reduced to zero, and there is no strength unless the strain becomes compressive. This is a slightly more mechanistic way to model fuel relocation than the empirical relocation model. Using discrete cracking allows for the mesh to show topographic changes and to adjust contastants at the crack location. This is currently under development at INL and will not be available until after my study is complete.
Pellet options	Smeaered pellet stack solvable in axial slices, 1.5D.	Smeared or discrete pellet stacks solvable in 1D, 2D, or 3D

Chapter 3

Implementation

3.1 Thermal Model

BISON fuel performance code is built so that new modules and physics could easily be implemented by users who have access. This makes the addition of UC and UN to the code much more manageable. As mentioned in Chapter 2, the thermal properties of greatest interest in modeling fuel are the thermal conductivity, thermal expansion, and specific heat. For FRAPCON, specific heat is unimportant as it is a steady-state only code. BISON has the ability to solve for transient solutions so the specific heat of a material is included in the solution. For the UN and UC fuels, a material file was implemented containing the given material's specific heat and thermal conductivity. The thermal expansion is a user supplied input which can be changed in the input file.

For the carbide fuel, Steiner's porosity and temperature dependent equation taken from [31] for the thermal conductivity was chosen to implement due to its use in other codes such as URANUS and FRAPCON. The porosity correction factor relates up to 10% porosity fuel with a simplified Maxwell-Eucken relation,

$$\lambda(p,T) = \lambda_0(T)\frac{1-P}{1+\beta P} \tag{3.1}$$

where β is taken as 1 [12]. Thus, the porosity and temperature dependent equation for UC would result in:

$$\lambda_P = 20 \cdot \frac{1-P}{1+P} \tag{3.2}$$

for temperatures T $\leq$ 500°C and

$$\lambda_{P,T} = (20 + 1.3 \times 10^{-3} \cdot (T - 500)) \cdot \frac{1-P}{1+P} \tag{3.3}$$

for temperatures T > 500°C, where T is in °C, P is the fractional porosity and $\lambda_{p,T}$ is in W/m K [31].

For the nitride fuel, a thermal conductivity model for uranium mononitride with a porosity correction factor was used [12].

$$\lambda_{P,T} = 1.37T^{0.41}\frac{1-P}{1+P} \tag{3.4}$$

Where P is the fractional porosity, T in K, λ is in W/m K, and is valid for 0≤P≤0.1 and T≤1700 K [12].

Values used for the thermal expansion coefficient are user supplied in the input file. For 95% dense UC and UN, coefficient values of 1.12e-5 K^{-1} and 8.00e-6 K^{-1} were used respectively [9, 31].

Metzger (2014) has implemented thermal and irradiation induced swelling models for the U_3Si_2 type fuel [25]. I will not be adding any new U_3Si_2 material models as there is a very limited selection of literature available and her work is directly related to implementing a creep model into BISON for U_3Si_2.

3.2 Irradiation Swelling Model

Irradiation swelling in the UN and UC fuels is projected to be higher than in oxide fuels. Literature gives burnup dependent models for both fuels for specific temperatures. For the UC fuel, Preusser's model for Carbide swelling that was also implemented into URANUS was used. A swelling rate of $\frac{\Delta V}{V}(vol\%/\%Bu) = 1.5vol\%/\%Bu$ was implemented for use of the UC fuel below 700°C. This is temperature independent and only relies on burnup. After 700°C, Preusser's model becomes temperature dependent:

$$\frac{\Delta V}{V}(vol\%/\%Bu) = 1.5 + \left(6.412 - 0.0198T + 0.152\cdot 10^{-4}T^2\right)\cdot\left(\frac{Bu}{Bu_0} - a\right) \tag{3.5}$$

Where T is in °C, Bu is burnup in MWd/kg, Bu_0 is a constant at 10MWd/kg, and a is a constant value of 2. This model is valid for high theoretical density UC fuel. A

higher swelling rate should be expected out of this model due to the inclusion of solid and gaseous swelling terms.

For the UN fuel, a rate of $\frac{\Delta V}{V}(vol\%/\%Bu) = 0.9vol\%/\%Bu$ for temperatures T$\leq$1200°C was implemented based on Feng's article [9]. For temperatures above 1200°C, an equation taken from Ross that includes the effects of solid and gaseous swelling is given as:

$$\frac{\Delta V}{V}_{\%} = 4.7 \cdot 10^{-11} T_{avg(K)}^{3.12} B_{\%} \rho_{\%TD}^{0.5} \tag{3.6}$$

Where $\frac{\Delta V}{V}$ is the total volumetric swelling in % strain, T is temperature in K, B is burnup in %FIMA, and ρ is fuel theoretical density in %TD. This is noted to be the most widely accepted burnup dependent rate for nitride fuel of $\geq$94% theoretical density and fits experimental data accurately.

3.3 Fission Gas Release Model

A fission gas release model based upon the ForMas model that is already implemented into BISON was chosen as a template for the models for UC and UN [14]. Since fission gas release contains an enormous amount of uncertainties in its nature of measurement, a model that would predict fission gas release within a deviation between calculated and measured by a factor of two or greater would be acceptable as concluded by Pastore (2015) [28].

For the UN fuel, a model for the fission gas diffusion coefficient based on porosity, thermal conductivity, temperature, fission rate density, and burnup is used [9]. The equation in the FRAPCON-EP code uses a fitting factor which was removed for use in BISON [13]. The diffusion equation for UN is ultimately input as:

$$D = F_P \cdot \left[8.22 \times 10^{-31} \cdot F_B \cdot f + 2.37 \times 10^{-10} \cdot e^{\frac{-18800}{T}} + 10^{-18} \cdot \frac{f}{K^2 T^2} \cdot e^{\frac{-18400}{T}} \right] \tag{3.7}$$

where F_P is a porosity dependent exponential factor given by:

$$F_P = e^{-\frac{\rho - 80}{3.4}} \tag{3.8}$$

and a burnup fitting factor, F_B given by:

$$F_B = 30 + Bu \tag{3.9}$$

with Bu in MWd/kgU, f is the fission rate density in fissions/cm^{3}s, K is the thermal conductivity in W/m K, T is the temperature in K, and D is the fission gas diffusion coefficient for UN fuel in cm^2/s.

For the UC fuel, a model taken from Matzke suggests a combination of a temperature and irradiation dependent diffusion coefficient for UC material. The model for UC was input into BISON as:

$$D = 0.30282 \cdot e^{\frac{-41773.8}{T}} + 2.5 \cdot 10^{-30} \cdot f \cdot (Bu + 8) \tag{3.10}$$

with Bu in MWd/kgU, f in fissions/cm^3, T in K, and D is the fission gas diffusion coefficient for the UC fuel in cm^2/s.

3.4 Creep Model

Since there is literature for both the UC and UN fuels on the irradiation and thermal creep, models coded similarly to the existing MOX creep model in BISON were implemented. All sources indicate that due to a high thermal conductivity and melting point in these fuels, thermal creep will be negligable for LWR conditions. For the creep of UC, Preusser (1981) gives an abundance of models that are available, but the one chosen is taken from Freund and Steiner's work based off of validity of the model. A combined irradiation and thermal creep model was implemented as:

$$\dot{\epsilon} = \left[1.45 \cdot 10^{10} \sigma^{2.44} e^{\frac{-63000}{T}}\right] + \left[3.6 \cdot 10^{-22} f\sigma\right] \tag{3.11}$$

Where σ is the gap pressure in MPa, f is the fission density rate in Fissions/cm^{3}s, T is temperature in K, and $\dot{\epsilon}$ is the total creep rate in h^{-1} [31].

Feng (2011) suggests a model for irradiation and thermal creep for UN based on the porosity, temperature, stress, and fission density rate as:

$$\dot{\epsilon} = \left[2.054 \cdot 10^{-3} \sigma^{4.5} e^{\frac{-39369.5}{T}} \cdot \frac{0.987 e^{(-8.65 \cdot P)}}{(1-P)^{27.6}}\right] + \left[1.81 \cdot 10^{-26} \left(1 + 1250 P^2\right) \sigma f\right] \quad (3.12)$$

Where σ is the gap pressure in MPa, T is the temperature in K, P is fractional porosity, f is fission rate density in fissions/cm^{3}s, and $\dot{\epsilon}$ is the total creep rate in s^{-1} [9].

3.5 Verification and Validation of Models

To make sure these models are working properly, analysis needed to be done to ensure that errors weren't made while inputting it into the code and that it also agrees with the supplied test data.

One of the first assumptions that has been made while modeling these advanced fuels is that the fuels do not crack because of their lowered temperature gradients. Hallman (2013) gives an equation that calculates the maximum allowable thermal stresses the pellet can handle before cracking [15].

$$\sigma_{t,max} = \frac{\alpha E q'}{8\pi(1-\nu)\lambda} \quad (3.13)$$

Where $\sigma_{t,max}$ is the max thermal stress in MPa, α is the thermal expansion coefficient in K^{-1}, E is the Youngs modulus in MPa, q' is the linear heat generation rate in W/m, ν is Poisson's ratio, and λ is the thermal conductivity in W/mK. Evaluating this with the respected properties for 95% TD UO_2, U_3Si_2, UN, and UC values for the max thermal stresses to crack the fuel can be seen in Table 3.1.

A comparison of the respected fuels, their thermal stresses, and fracture points if applicable are plotted as a function of the linear heat generation rate in the rod can be seen in Figure 3.1. This shows that it takes a much higher q' to cause enough thermal stresses in the fuel to cause them to crack. Therefore, modeling the pellets as solid, uncracked pellets is deemed acceptable for LHGR's of 20kW/m. UO_2 is the only

Table 3.1: Estimated LHGR in order to crack.

	UO_2	U_3Si_2	UN	UC
Youngs Modulus (GPa)	200	80	191.5	215
Thermal Conductivity (W/mK)	3.0	25.0	20.0	20.0
Poisson's ratio (/)	0.31	0.17	0.272	0.288
Thermal Expansion Coeff. (10^{-6}/K)	10.0	15.0	8.0	11.2
Fracture Strength (MPa)	130	200	370	200
LHGR to crack (kW/m)	3.38	86.91	78.71	33.37

one of the fuels that would experience the cracking and relocation phenomena. The low cracking LHGR for the UO_2 fuel agrees well with the data taken by Oguma where he notes that the UO_2 pellet is expected to crack at LHGR's $\leq$5kW/m [26]. The empirical relocation model taken from ESCORE does currently work, but only changes the diameter of the pellet and not stressess in the pellet. The smeared cracking model is still a work in progress at INL and should be implemented, if available, to help provide a more accurate representation of fuel creep for UO_2 type fuel.

Using a simplistic model based solely off of burnup for the UN and UC fuels is acceptable given the amount of literature based on these fuel's histories with LWR conditions tests. The UN and UC fuels have widely been looked at as candidates for LMFBR reactor fuels which run at much higher temperatures and different flux profiles. Most data taken for these fuels is at temperatures above 1200°C, where as centerline temperatures for the runs modeling simplistic LWR conditions at 20 kW/m never exceed 810°C. Using swelling models for temperatures $\geq$400°C below where most data points are valid is not correct. A simplified swelling model only dependent

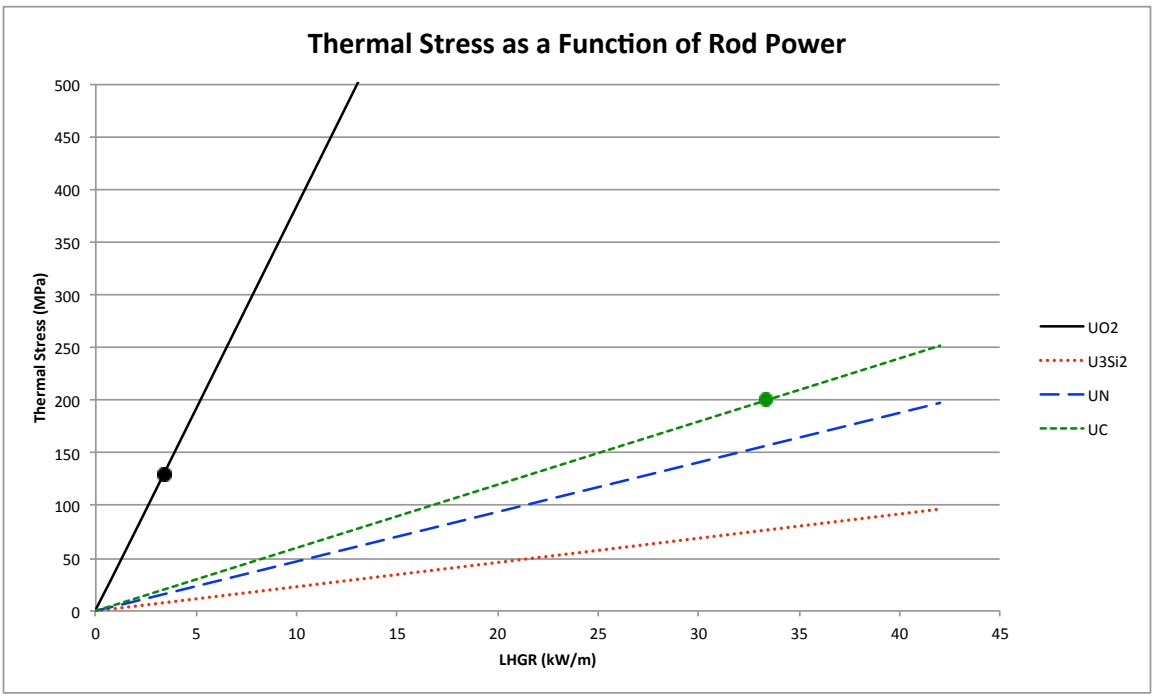

Figure 3.1: Comparison of fuels thermal stresses to LHGR

on burnup is acceptable for this study.

A look into the BISON UN swelling model shows that it is under good agreement with data points provided [3, 9]. For LWR applications, centerline temperatures shouldn't reach any higher than around 900 K. Therefore the only swelling regime should be a purely dependent on burnup of the fuel.

The UC fuel swelling model is based on the model found in the URANUS code. This modified model is shown in Figure 3.3 and relies heavily on temperature if above 700°C. A suggested limit on the swelling rate for UC is said to be 4.558 which includes the effects of gaseous and solid swelling.

Checking the fission gas diffusion coefficient for UN and UC against UO_2 provided to be very useful. The lack of literature on fission gas migration in the presence of temperature and radiation is scarce so getting a relative rate to a known value is the best means of validation present. For the UO_2, UC, and UN fuels a normalized radiation enhanced diffusion coefficient is given as $1 : 0.2 : 0.14$ for the given fuels

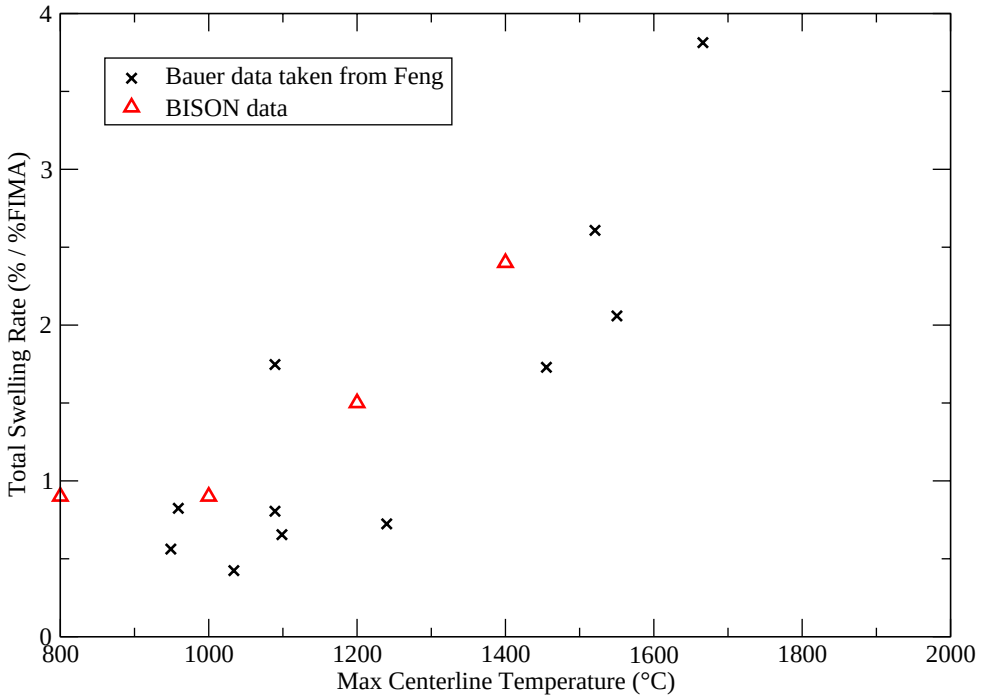

Figure 3.2: BISON UN swelling rate comparison

respectively [23]. Data from Feng's work suggests that the diffusion coefficient for UN should be lowered to more accurately fit fission gas release data. This directly influences the total fission gas released in the ForMas model as it is strictly a diffusion controlled fission gas release model. A comparison of the diffusion coefficients can be seen in Figure 3.4.

Using the given diffusion coefficients for the advanced fuels should yield little to no fission gas released into the plenum for the given amount of time spent in the reactor. According to Zimmerman's predictions for UC in Preusser's article, fuel with a central temperature below 1000°C, practically no fission gas is released from the fuel. This is in line with other sources as well, saying that the UC fuel releases little fission gas especially at low temperatures which attributes to an increased swelling rate in the

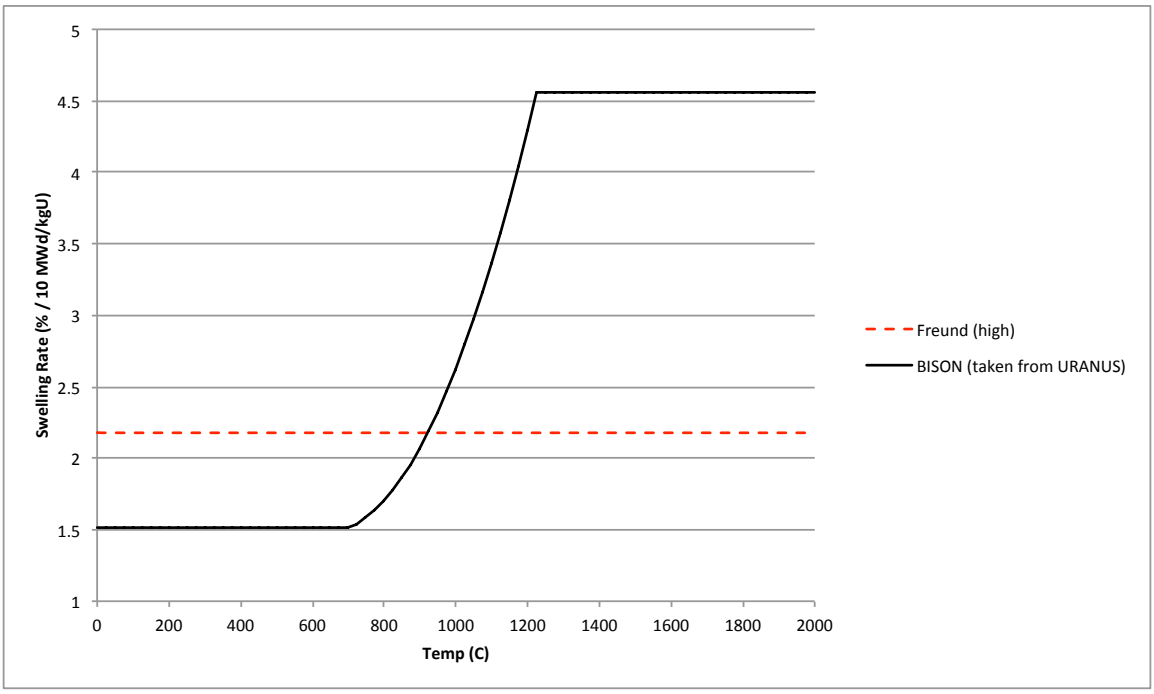

Figure 3.3: Comparison of swelling models available for UC

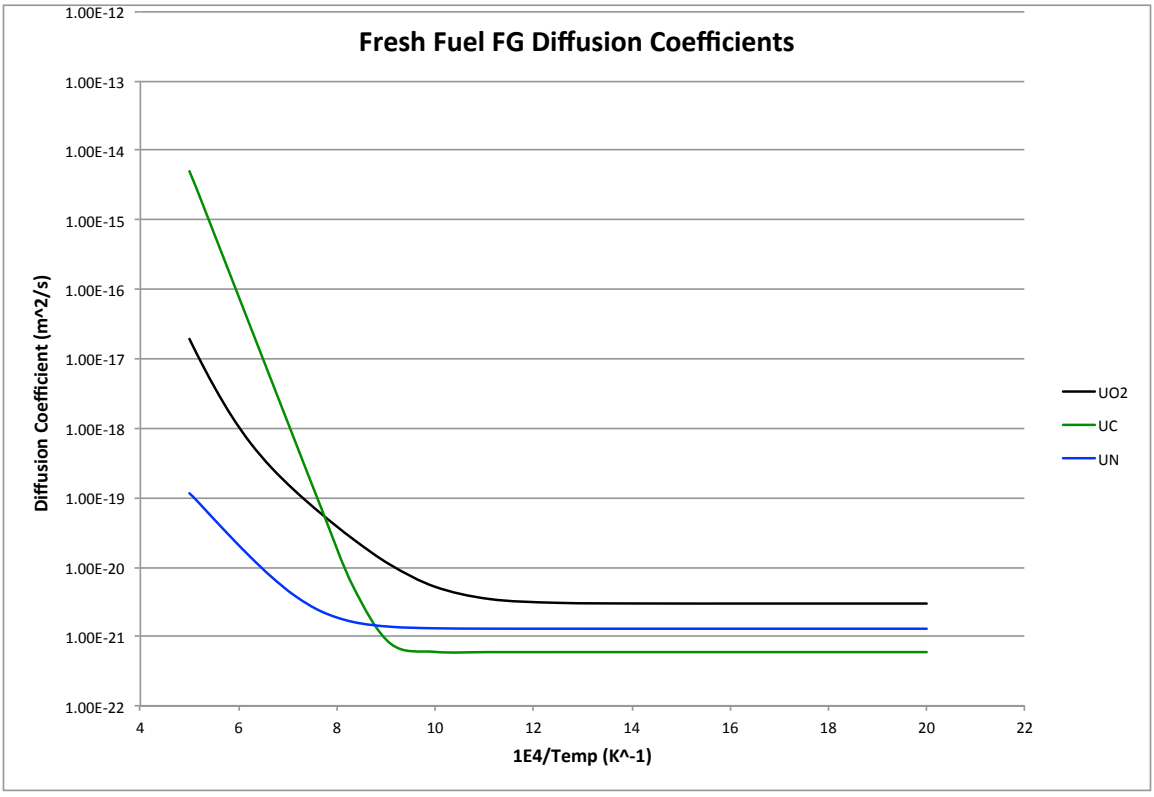

Figure 3.4: Fission gas diffusion coefficient comparison for unirradiated fuels [9, 14, 23]

fuel [8, 35].

For the UN fuel type, similar experimental results suggest that at low temperatures, little fission gas is released. From data reported from 95 UN and 39 (U,Pu)N fuel experimental results Storms proposed an empirical equation for fission gas release rate as a function of fuel temperature, burnup, and density was statistically derived [2].

$$R = 100/\left(exp[0.0025(90D^{0.77}/Bu^{0.09} - T)] + 1\right) \tag{3.14}$$

Where R is the FP gas release rate (%), D the fuel pellets density (% TD), Bu the burnup (% FIMA), and T the temperature of the fuel (K). Using the fuel average temperature, average burnup, and a theoretical density of 95%, this approximation yields a fission gas release rate of 0.472%/% FIMA. For the test case where the fuel is run at 20 kW/m for $8*10^7$ seconds, a typical BISON test case, expected rod average burnup is around 6.33% FIMA. This multiplied by the fission gas release rate predicts 4.67% total fission gas released into the plenum space. My model implemented into BISON gives a value of 2.98%, giving an error of 12% when compared to Storms' FG rate equation.

For the fuel creep model, comparison to literature is a little more difficult as it is hard to seperate out the effects of mechanisms by which the fuel undergoes volumetric changes. Testing to make sure the BISON code was actually giving me the correct values for the variable that were implemented just involved printing out the variables that made up the creep equation at each iteration and performing a hand calculation. This method provides a way to verify that my code is calculating my creep equation is working mathmatically. Checking to see whether fuel stresses and, concurrently, cladding stresses, are relieved by running the same simulation with and without creep will help give insight into how useful modeling with fuel creep models can be.

A comparison of secondary creep rates for the UC, UN, UO_2, and MOX fuels can be seen in Figure 3.5. This agrees with literature in that the UO_2 fuel is expected to

show a creep rate of 10X that of the UN and UC fuels [9, 31]. MOX fuel analysis is not being included in this study, but is shown here just as reference.

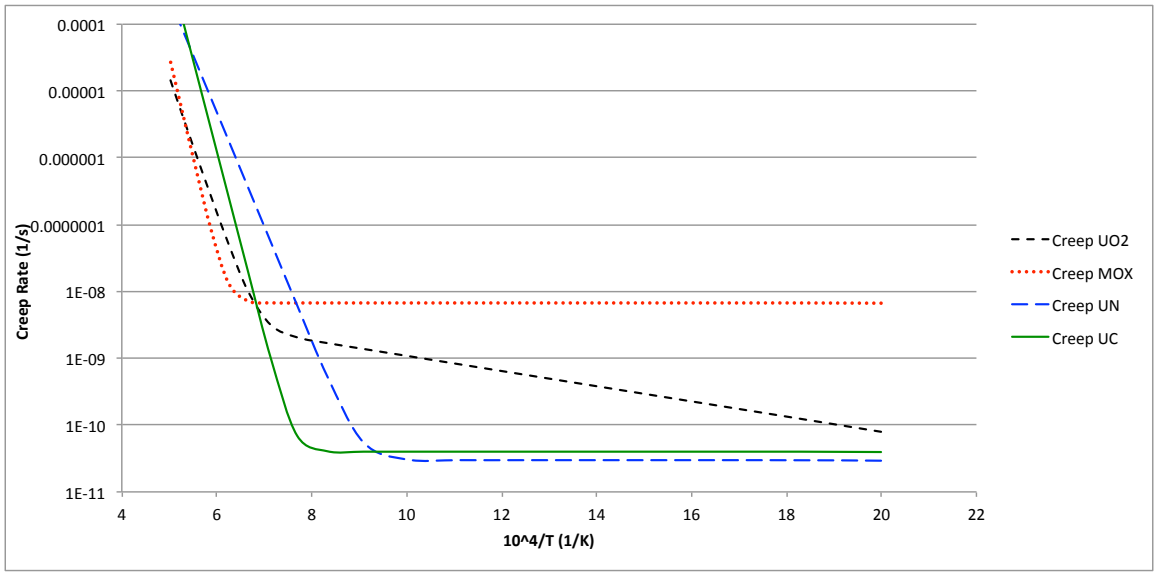

Figure 3.5: Creep rate comparison of fuels in BISON at a fission density rate of 10^19 fissions/m^3s and effective stress of 40 MPa

3.6 Max Hoop Stress Calcluation for BISON

Since BISON does not inherently have an easy method to calculate a hoop stress over a prescribed area similar to FRAPCON and FEMAXI, a method for calculating this was needed. The way that was chosen to do this was to find the area of highest stress in the cladding based off the axial peaking factors was chosen for the case. The mesh was then modified so that there is another block inside of the cladding block that is called 'max_section' where the most cladding hoop stress is predicted to be. By doing this, a postprocessor could be created that averages the hoop stress values only over the block, 'max_section', and not over the entire cladding. This eliminates the posibility that the average might be considered low as the top of the cladding may be in a compressive state while the area containing fuel may be in a tensile state. Averaging the entirity of the cladding may lead to an underestimate of when cladding

failure may occur. Figure 3.6 shows the region that was chosen for calculating the maximum hoop stress in the cladding. Figure 3.7 shows the BISON postprocessor that was used to average the hoop stress values over the 'max_section' block of the cladding.

With the FRAPCON and FEMAXI codes, hoop stress is calculated at each axial node the user desires. By choosing the nodes corresponding to the regions with the highest axial peaking factor associated, all three codes are calculating the same cladding hoop stress value over the same region. This ultimately leads to a more accurate inter-code analysis of cladding hoop stress.

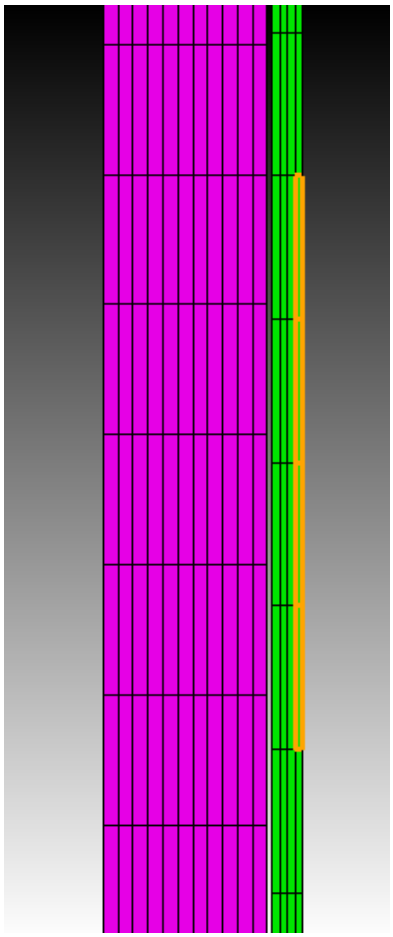

Figure 3.6: Chosen region in cladding for calculating the maximum hoop stress

```
[./max_hoop_stress]
   type = ElementAverageValue
   variable = hoop
   block = max_section
[../]
```

Figure 3.7: Postprocessor block that outputs average value of the hoop stress over the area of the max_section block

3.7 Implementation of SiC into FEMAXI

As additional means of further adding value to this study of advanced fuels and cladding types, The SiC type cladding has been implemented into the Japanese fuel performance code FEMAXI. This is not a major focus of this study, but it allows for another view on the UO_2/SiC fuel system. The added value in implementing this in FEMAXI is that UO_2 fuel creep is a default option that is built into the code.

To add the SiC cladding type in, the following properties of the cladding are given through literature sources [6, 7]:

Table 3.2: FEMAXI properties changed for addition of SiC cladding type

Flag	**Cladding Property**	**Value**	**Units**
CHCAP	Specific Heat	1100	J/kg-K
CPOIR	Poisson Ratio	0.21	-
CTHCON	Thermal Conductivity	0.036	W/cm-K
CDTHEX	Diametral Thermal Expansion	3.0E-6	-
CATHEX	Axial Thermal Expansion	3.0E-6	-
CYIE	0.2% Yield Stress	2.66E+4*T_{clad} + 2.0E+8	Pa
CDKDT	d(CYIE)/dT	2.66E+4	Pa/K
CRN	Strain Hardening Exponent	0.0	-
CDNDT	d(CRN)/dT	0.0	1/K
CELMOD	Elastic Modulus	1.62E+11 - 4.0E+7*T_{clad}	Pa
CDEDT	d(CELMOD)/dT	-4.0E+7	Pa/K

Implementation of these model gives an idea of where the FEMAXI code lies in relation to BISON and FRAPCON for UO_2 fuel inside of the SiC type cladding. The SiC cladding has currently been implemented into the FEMAXI source code as

a modification of one of the Zry cladding options. Future work might be useful in creating a new cladding material option which has its own seperate user flag for the SiC cladding option along with all the other Zry based claddings.

Chapter 4

Results and Discussion

4.1 UO_2/Zry Cases

To get a base line comparison on how each code predicts against the other, a s!imulation in which all of the codes are validated is needed. The UO_2/Zry system provides a means for this comparison. BISON, FRAPCON and FEMAXI are all validated for the use of this fuel/cladding combination based on multiple test cases such as the FUMEX-III datatbase [1]. By using geometries that are similar to what current industry fuel is currently using, one can get a good idea of how each code compares in terms of centerline temperatures, fission gas release, plenum pressure, cladding hoop stress, and fuel outer surface displacement to help extend the codes on to using a SiC based cladding.

To help reduce the increased computational cost needed when adding another dimension to the model, the BISON 2D case, the rod is modeled as a 20 pellet rodlet. This will provide a sufficient fuel region to capture all the necessary physics that occurs during the simulation. In addition to shortening the rod length, the power is run at a constant 20kW/m to help separate the effects due to changing neutron flux. Below in Table 4.1 is a summary of the rod geometries that are used for the UO_2/Zry cases suggested by non-proprietary Westinghouse geometries in all three of the fuel performance codes [4, 6]. Table 4.2 summarizes the run conditions which are used for all three of the codes as well. With the BISON code, a ramp to power was needed which is done in a linearly way which can be seen in Figure 4.1. This only

shows the first 10^6 seconds of the power history, the rest of which is held at 20 kW/m consistantly.

Table 4.1: Pellet and rod geometry for Zry cladding

Rod height (m)	0.22008
Active fuel height (m)	0.196
Pellet height (m)	0.0098
Pellet diameter (m)	0.008192
Dish depth - BISON only (m)	0.0003
Chamfer height - BISON only (m)	0.0005
Chamfer width - BISON only (m)	0.00016
Cladding thickness (μm)	572
Radial gap width (μm)	82

Table 4.2: PWR based run conditions

Rod Average Burnup (GWd/MtU)	60.0
LHGR (kW/m)	20
Initial fill gas pressure (MPa)	2.0
Initial fill gas composition	Helium
System pressure (MPa)	15.5
U235 enrichment (%)	5
Fuel density (% TD)	95

Once all the cases were set up, they were run with and without the use of the fuel creep model. The BISON and FRAPCON codes have both been validated without the presence of fuel creep. This is not an inaccurate assumption as when the fuel comes into contact with the Zry cladding, the cladding will creep much faster than the fuel. The FEMAXI code has the MATPRO-09 and MATPRO-11 fuel creep models available as well as a zero fuel creep model.

Figures 4.2 - 4.12 will serve as the basis for comparison for all future extensions to the code. From looking at the centerline temperatures in Figure 4.2 and Figre 4.3 show that while FRAPCON and FEMAXI do not predict a centerline temperature difference when fuel creep is added to the mixture, BISON shows that a 15 K reduction in centerline temperatures at EOL with an added fuel creep model. Since it is known that

contact has been made at around 25MWd/kgU, the explaaination for the reduction in centerline temperature could be attributed to the lack of radial displacement which can be seen in Figrure 4.4. The further the heat has to be transmitted through a material to get to the heat sink, the coolant, the hotter the temperature should be expected.

The fission gas release comparison graphs show that the FRAPCON code predicts nearly 4% more total fission gas released into the plenum than the BISON or FEMAXI codes. Figures 4.5 and 4.6 show that the FRAPCON model has a 'knee' point around 38MWd/kgU where the gas release begins to accelerate. From looking into the code, this can be attributed to account for the high burnup structure model. According to the FRAPCON code, at 40MWd/kgU, if the total gas released at a radial node is less than 5%, an additional 1% gas release is accumulated for every 10MWd/kgU above 40MWd/kgU. This in effect allows for a rapid release of fission gas, creating a sharp knee-point in the fission gas release graph.

From Figures 4.7 and 4.8, we can see that plenum pressures never exceed 5MPa. System pressure of 15.5MPa is never matched by the rod internal pressure, therefore there is little to no risk of seeing cladding lift-off, where the cladding is forced off of the fuel due to extremely high internal rod pressures. This could be seen in cases where the rod internal pressure exceeds the system pressure of 15.5MPa

Figures 4.11 and 4.12 show the radial component of the fuel's displacement as predicted by each of the codes. As seen in Figure 4.4, BISON predicts a 38μm difference in radial fuel displacement when using the creep model. BISON may be slightly overestimating the amount of fuel creep in UO_2 fuel from comparing with FRAPCON's difference prediction of 19μm and FEMAXI's 23μm and the knowledge that the model is only truely valid when used in combination with a smeared cracking model. See section 2.7 for an explaination of smeared fuel cracking.

Taking all of these results goes to show that for the most part fuel creep does not

play a very big role in changing any results with the UO_2/Zry fuel system. BISON predicts that the fuel will experience heavy fuel creep due to the 15.5 MPa system pressure once in contact with the cladding. This prediction is likely erroneous and will need to be addressed in future works. Furthermore one can also note that none of these codes align in an absolute sense so it should be noted that further comparisons with UO_2/SiC and the advanced fuels/SiC be examined according to how each code compares to itself with and without the effects of creep and not against the other codes. This is also a weakness that may need to be addressed in future work as well. Having codes that predict nearly identical results for the same given case would be beneficial to comparison work.

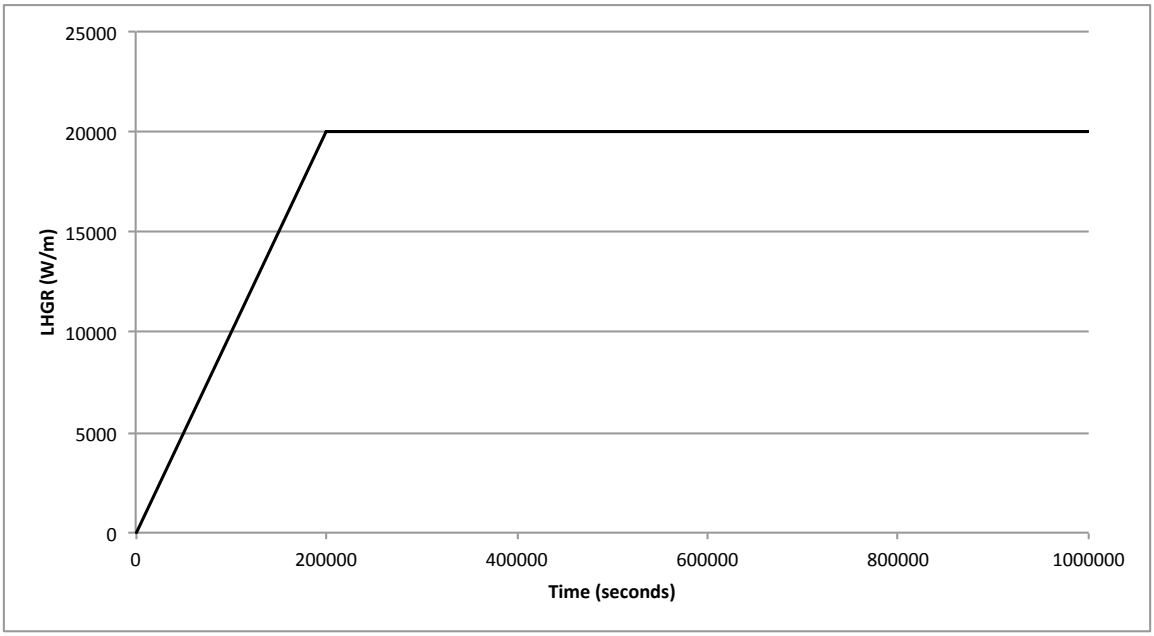

Figure 4.1: BISON linear heat rate ramp up to 10^6 seconds

4.2 UO_2/SiC Cases

The UO_2/SiC system was modeled in the BISON and FRAPCON codes. This fuel and advanced cladding is currently being considered as the intermediate step between the UO_2/Zry system and the advanced fuel/SiC system. As noted before, one of

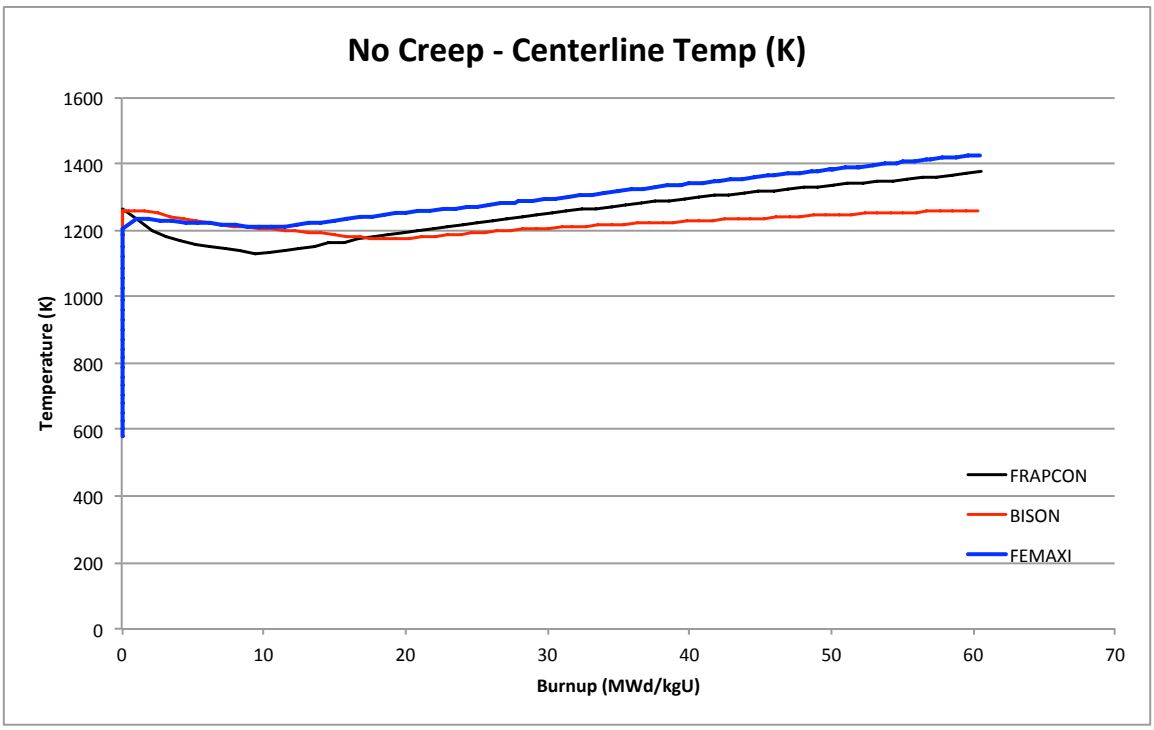

Figure 4.2: Centerline temperature for UO_2/Zry at 20kW/m without creep

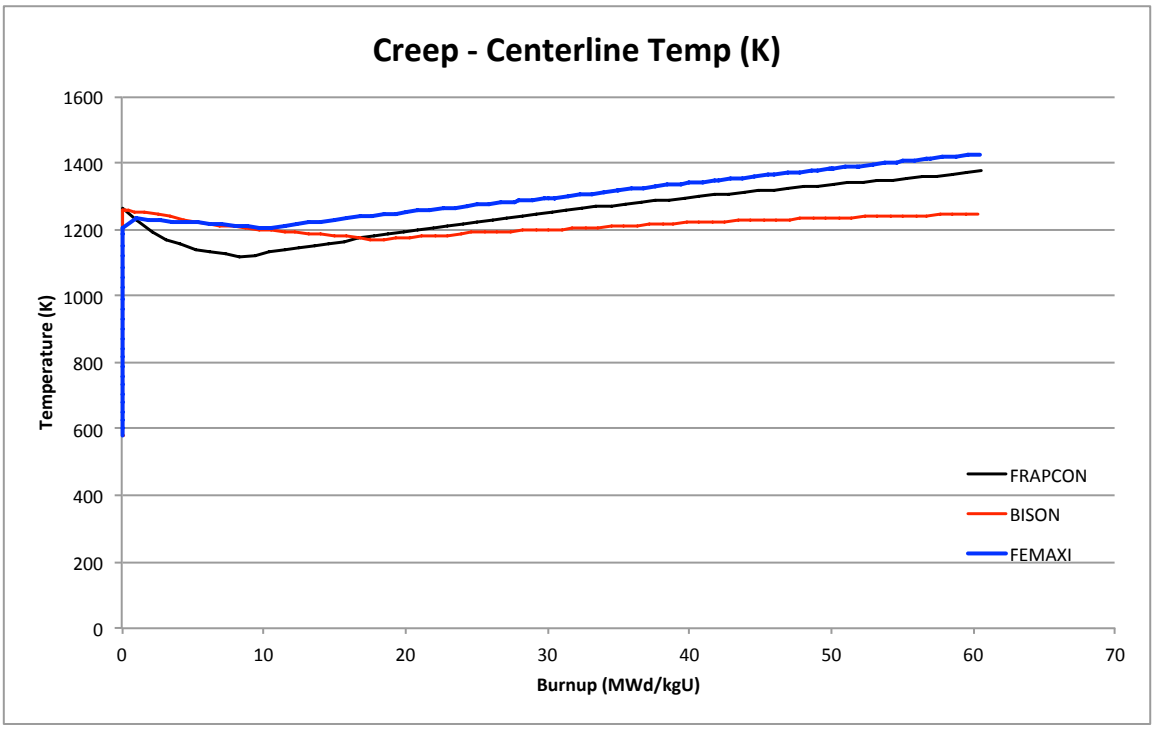

Figure 4.3: Centerline temperature for UO_2/Zry at 20kW/m with creep

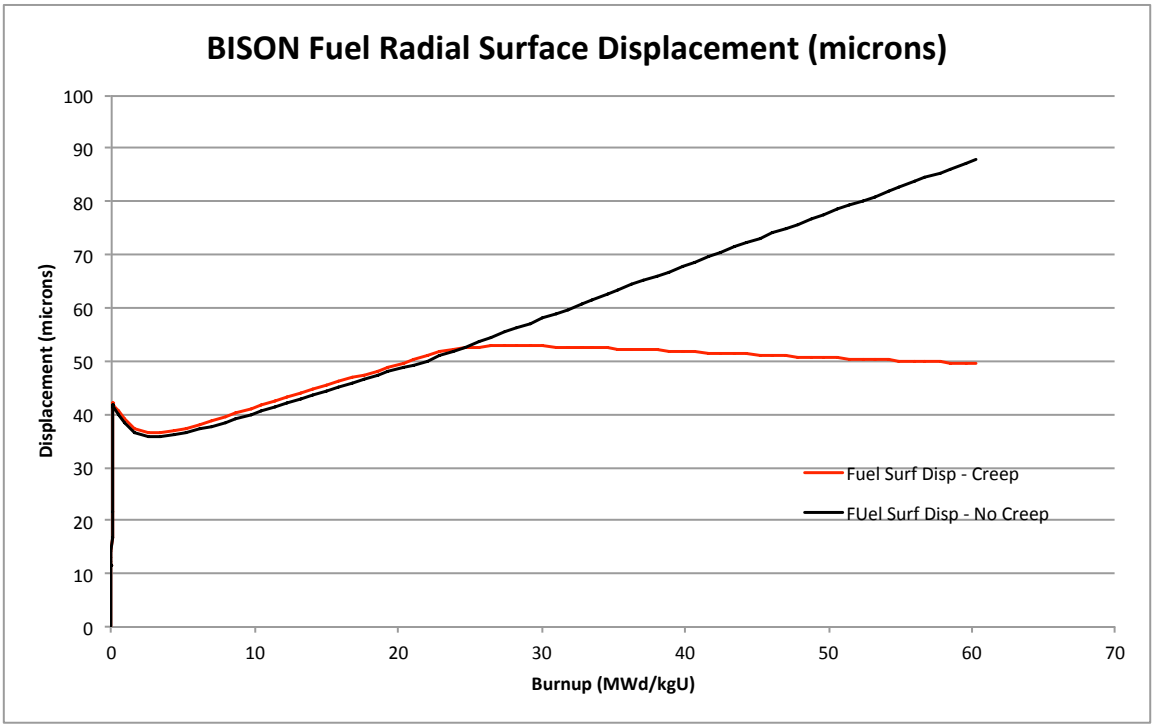

Figure 4.4: Displacement of the radial component of the fuel for UO_2/Zry predicted by BISON at 20kW/m

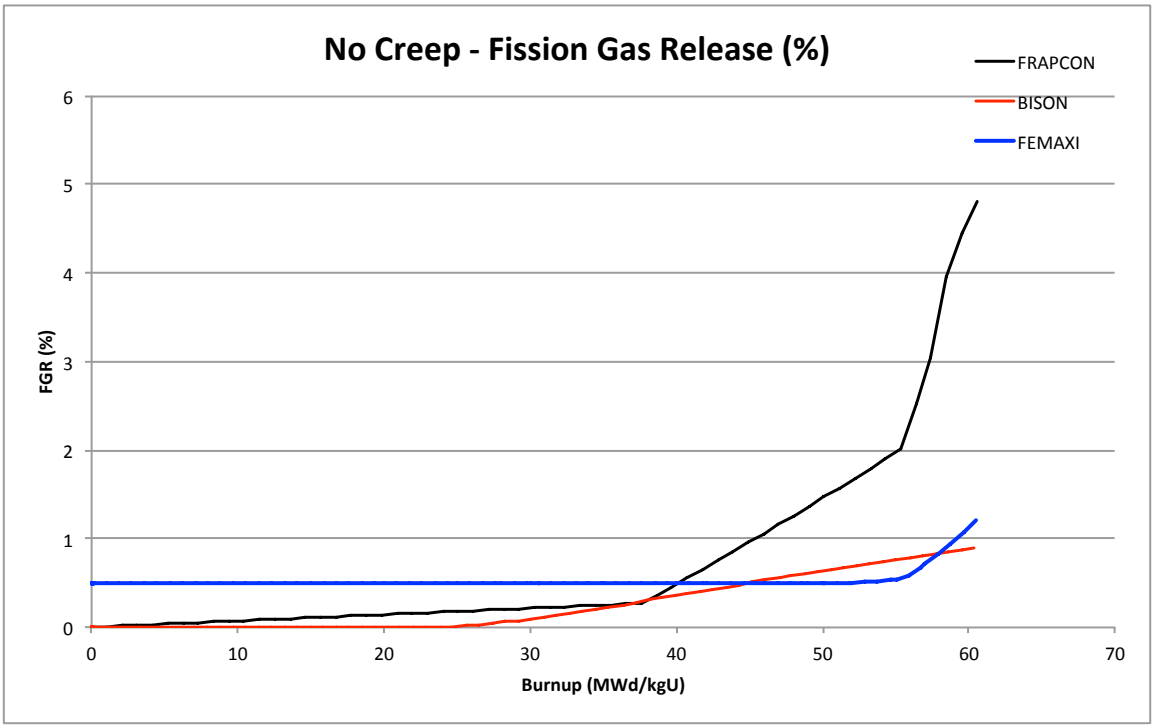

Figure 4.5: Fission gas release for UO_2/Zry at 20kW/m without creep

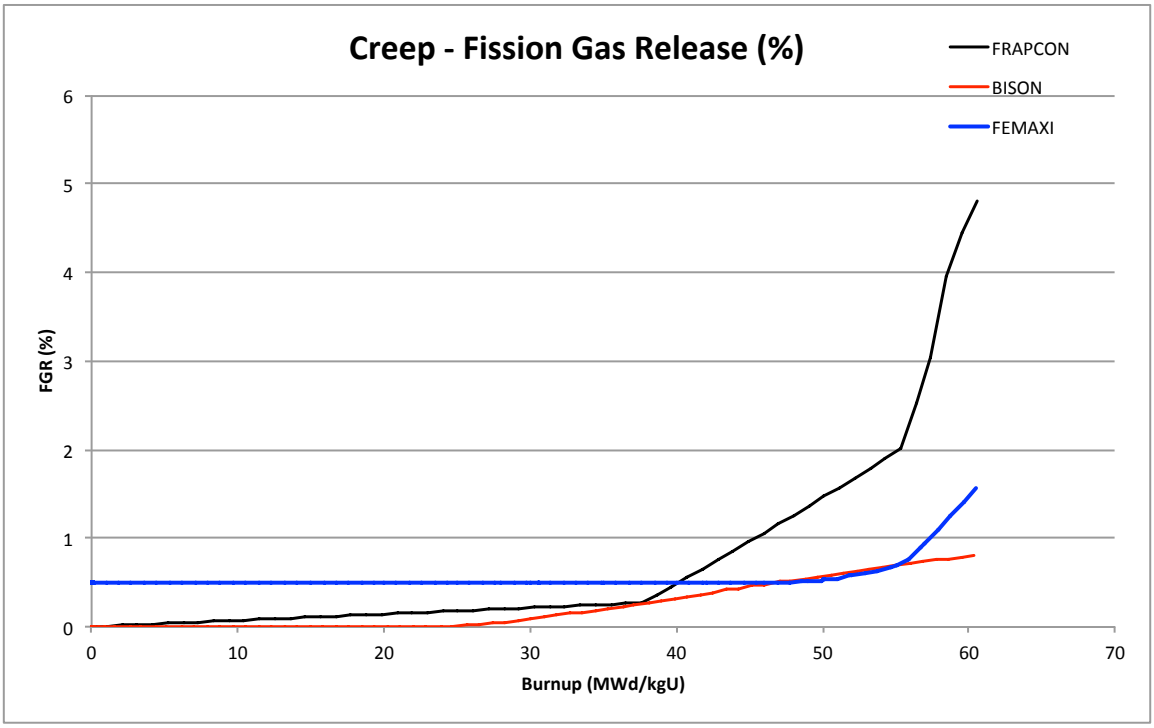

Figure 4.6: Fission gas release for UO_2/Zry at 20kW/m with creep

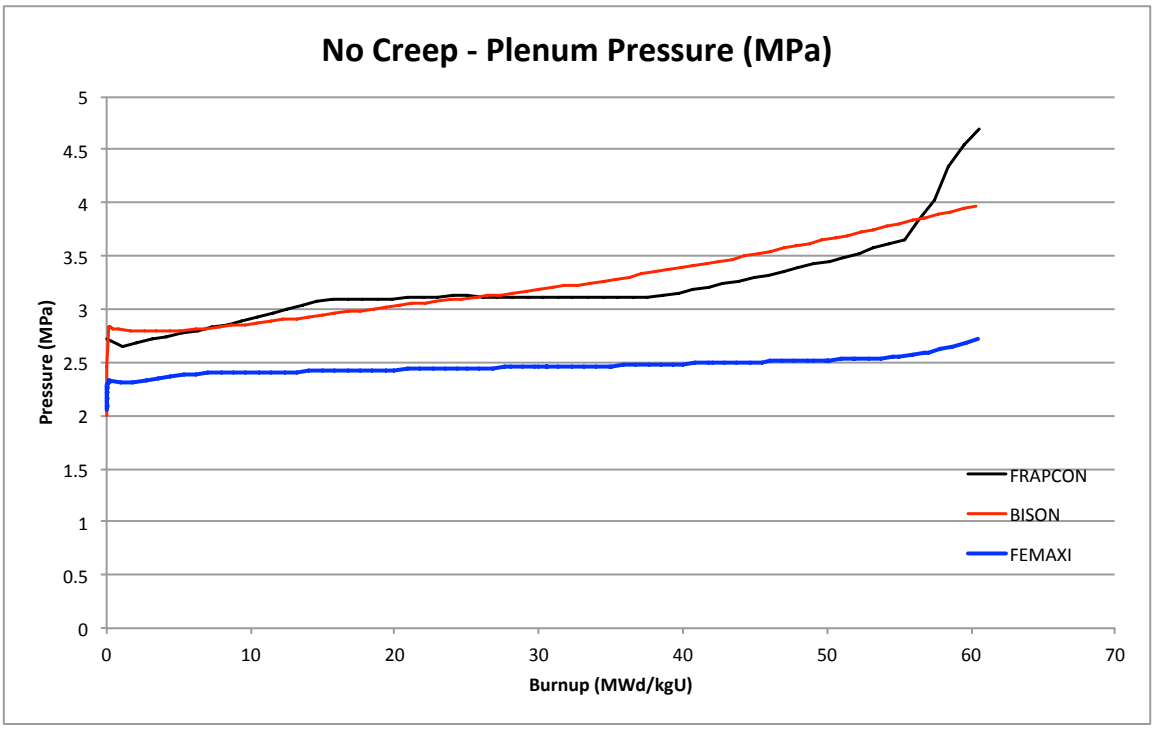

Figure 4.7: Plenum pressure for UO_2/Zry at 20kW/m without creep

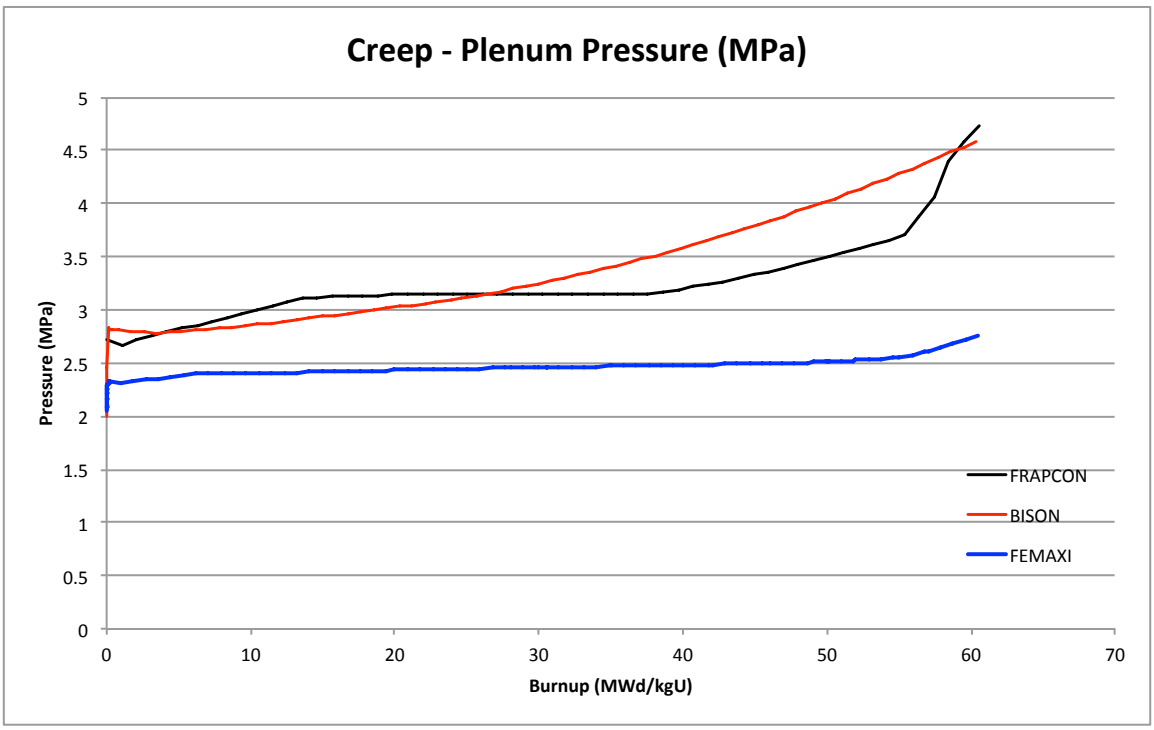

Figure 4.8: Plenum pressure for UO_2/Zry at 20kW/m with creep

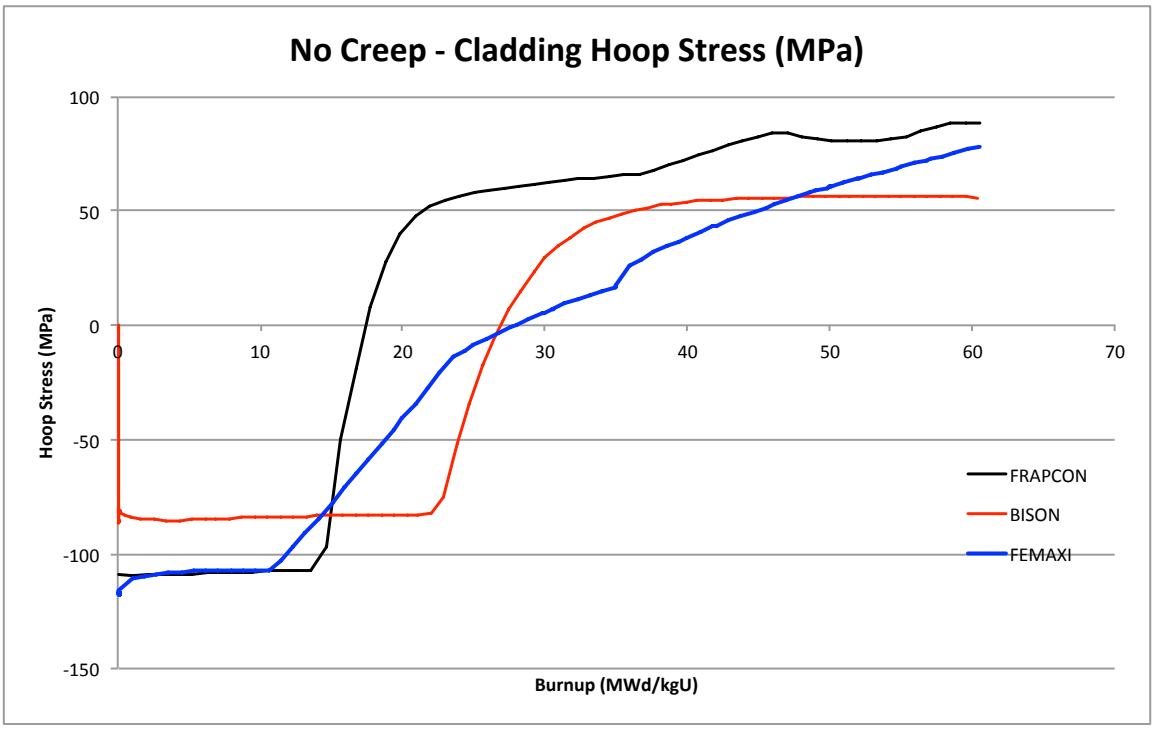

Figure 4.9: Cladding hoop stress for UO_2/Zry at 20kW/m without creep

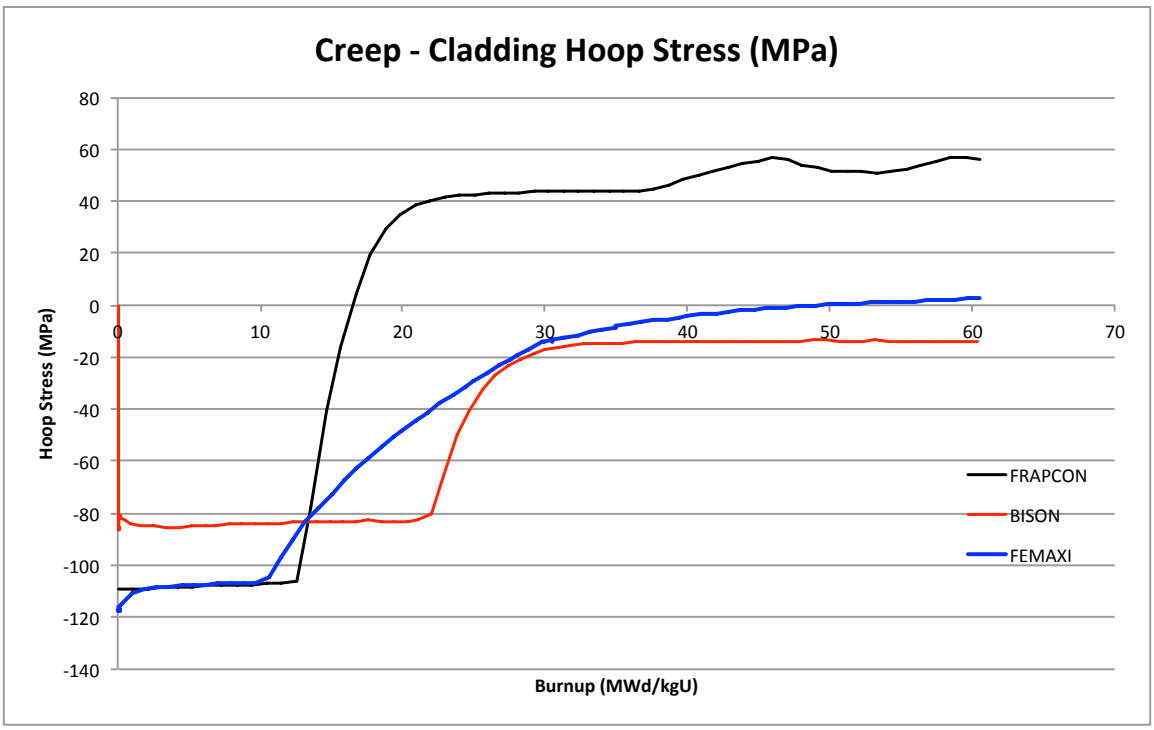

Figure 4.10: Cladding hoop stress for UO_2/Zry at 20kW/m with creep

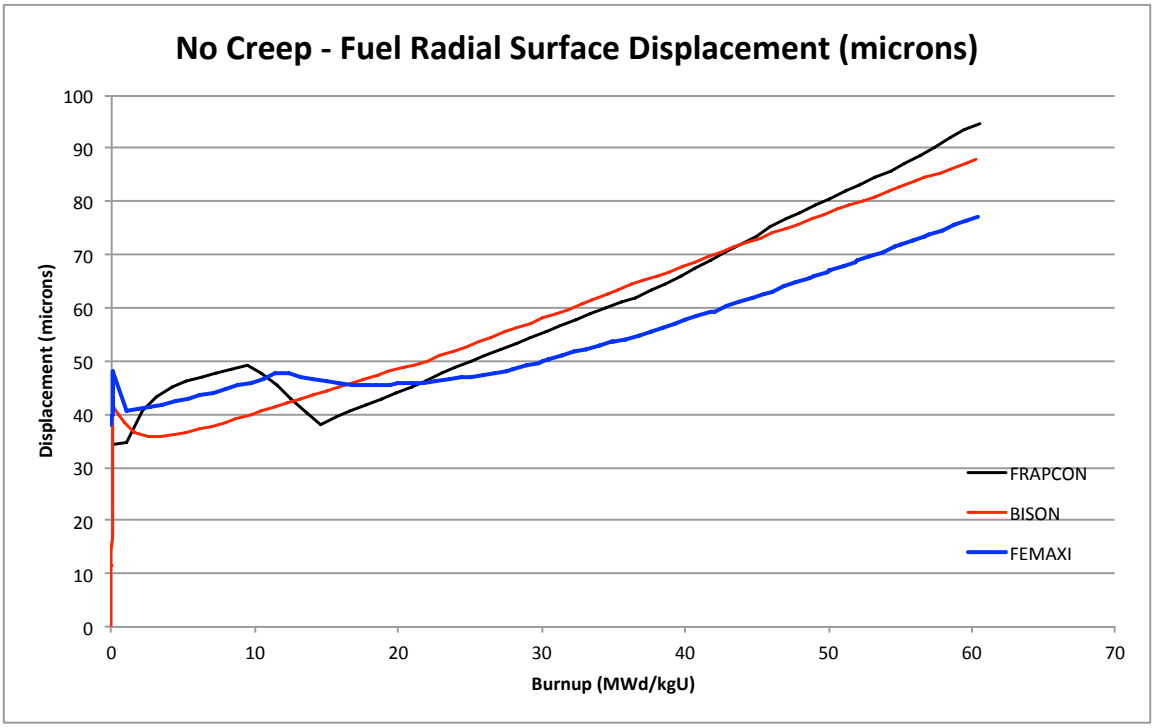

Figure 4.11: Displacement for radial componenet of fuel for UO_2/Zry at 20kW/m without creep

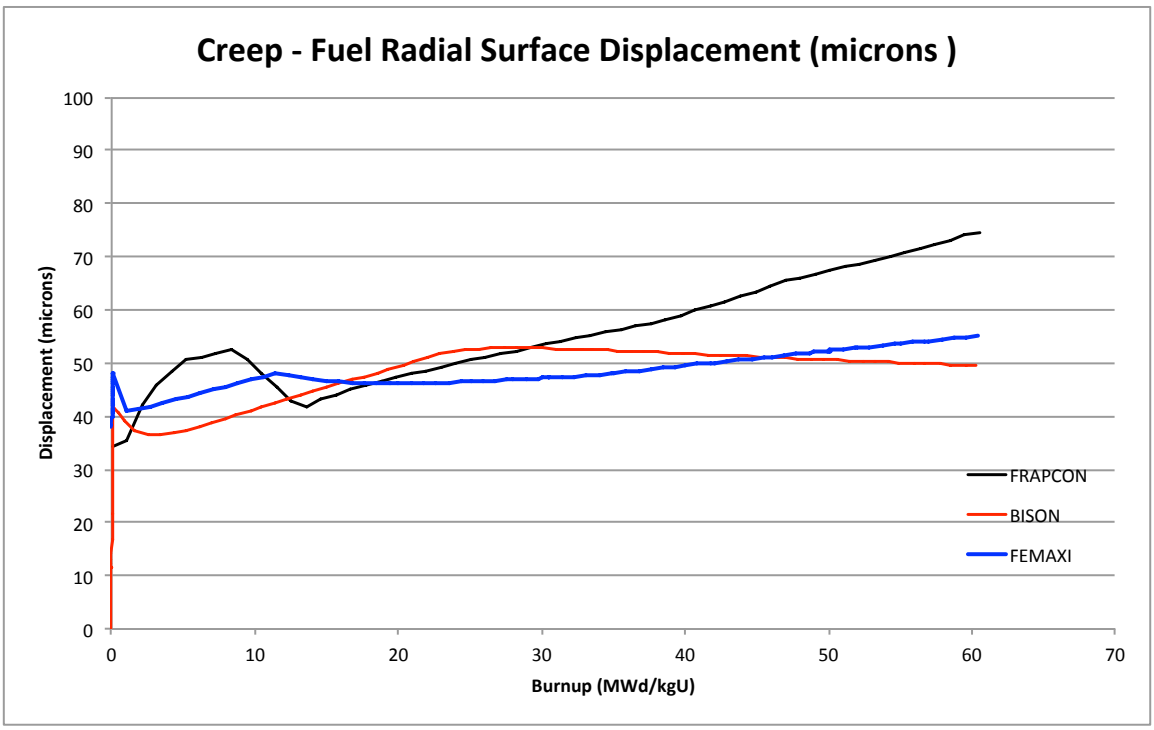

Figure 4.12: Displacement for radial componenet of fuel for UO_2/Zry at 20kW/m with creep

the major current issues with using SiC as a cladding type is allowing enough of a radial gap between the fuel and cladding to avoid PCMI. The SiC cladding is brittle and unyielding which leads to nearly immediate fracture levels of hoop stress upon contact. In order to allow for equivalent burnups to that of the UO_2/Zry cases, an increased radial gap and thicker cladding walls have been used. This design is one that Westinghouse suggests for use with their SiC claddings. Table 4.3 summarizes the cladding and fuel geometry used for all the codes using the SiC cladding. The sytem run parameters will be kept the same, see Table 4.2 for all the values used.

Using the code to compare results should give insight into how interfacial pressure between the cladding and fuel can be relieved by the addition of fuel creep. From what previous research shows, this can be integral in helping relieve cladding hoop stress and may ultimately lead to the fuel being able to stay in contact for longer than anticipated [7].

Rod height (m)	0.22008
Active fuel height (m)	0.196
Pellet height (m)	0.0098
Pellet diameter (m)	0.0082
Dish depth - BISON only (m)	0.0003
Chamfer height - BISON only (m)	0.0005
Chamfer width - BISON only (m)	0.00016
Cladding thickness (μm)	750
Radial gap width (μm)	120

Table 4.3: Pellet and rod geometry for SiC cladding

In Figures 4.13 and 4.14, centerline temperatures are shown for the UO_2/SiC cases without and with the addition of fuel creep. The first thing that we can note is that temperatures are much higher than the UO_2 cases using the Zry based cladding. With the SiC type cladding, there is no creep down due to system pressure, therefore the radial gap is only being closed by the volumetric expansion, largely due to swelling, of the fuel. In addition to the increased gap width, the cladding itself has a much lower thermal conductivity creating a larger temperature gradient between the inner and outer cladding wall. This in turn leads to higher fuel temperatures due to the combination of the above factors.

From looking at the differences in centerline temperatures, we can see that from Figures 4.13 and 4.14 that the BISON and FRAPCON codes predict that the centerline temperatures are lowered with the addition of fuel creep while the FEMAXI code code predicts that the centerline temperature is increased with the addition of fuel creep. This may be due to the combination that the BISON and FRAPCON codes predict a more rapid gap closure with the addition of the creep model and the the prediction that the FEMAXI code releases 35% more fission gas with the addition of the MATPRO-09 fuel creep model as seen from Figures 4.15 and 4.16.

One of the immediate differences that is shown with Figures 4.15 and 4.16, is that the total fission gas released between the BISON and FRAPCON code is much better aligned that Figures 4.5 and 4.6 predictions. A study on the temperature sensitivity

of the UO_2 fuel is shown later in this chapter to help get an idea of how sensitive each code's fission gas release model is to temperature.

Figures 4.17 and 4.18 show that the rod internal pressure for all three cases does not exceed system pressure of 15.5 MPa. This ensures that cladding lift-off will not be an issue.

Since it is determined that the threshold for cladding failure for the SiC cladding is to be 261 MPa of hoop stress, any line that crosses that threshold on Figures 4.19 and 4.20 is considered failed. For the case with no fuel creep, the only code to predict failure is the FRAPCON code. At 56 MWd/kgU, the failure threshold is reached. With the FRAPCON case that uses a fuel creep model, none of the codes predict failure and for FRAPCON enough cladding stress is relieved from the creeping of the fuel so that failure is not reached within the 60 MWd/kgU EOL criteria. This equates to an EOL cladding hoop stress reduction of 78% for the FRAPCON case with creep.

As mentioned before, the addition of fuel creep models for the BISON and FRAPCON codes cause the gap width to close more quickly. Figures 4.21 and 4.22 show the two codes radial displacements. Only the FRAPCON code shows the fuel coming into contact with the cladding, therefore the radial displacements of the other codes' fuels do not differ much.

The first importance of this study is to show that for the specified amount of burnup, 60 MWd/kgU, most of the codes predict that the cladding will not fail during that time period due to PCMI. Only the FRAPCON code with no fuel creep shows that the cladding will reach the failure threshold during this time period.

4.3 UO_2/SiC Temperature Sensitivity

To help understand the effects of temperature, in particular fuel temperature, on other phenomena, specifically fission gas release, two separate cases were run in all three codes. An increase of 50% in power, 30kW/m, and a decrease of 50% in power,

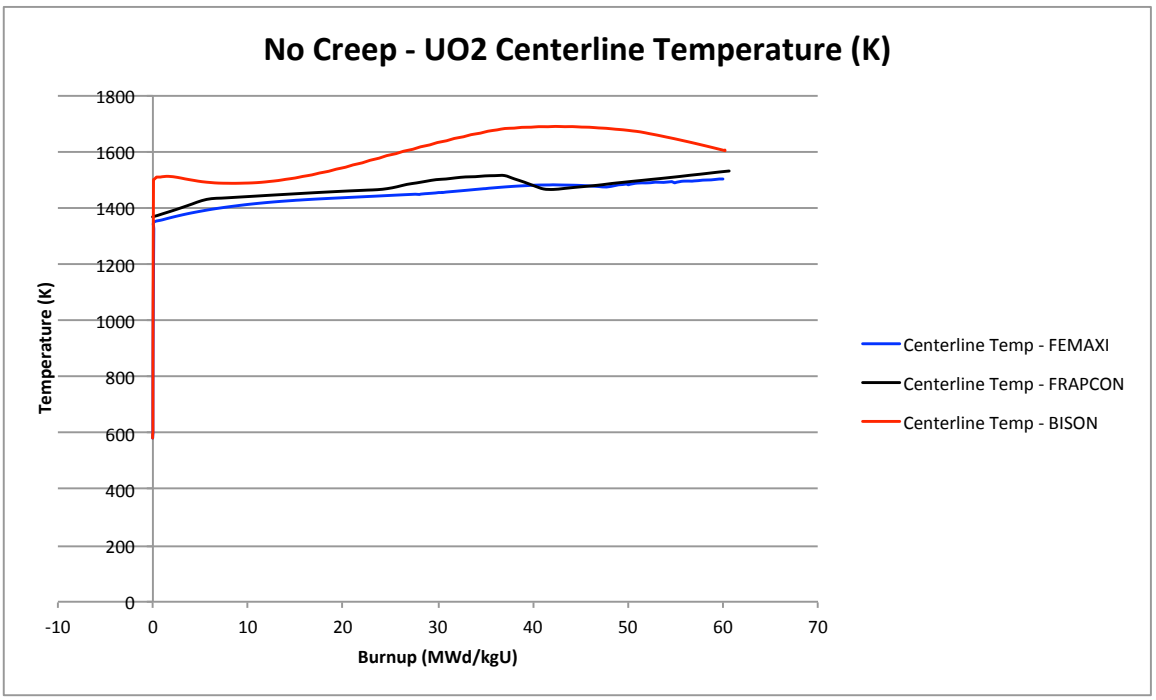

Figure 4.13: Centerline temperature for UO_2/SiC at 20kW/m without creep

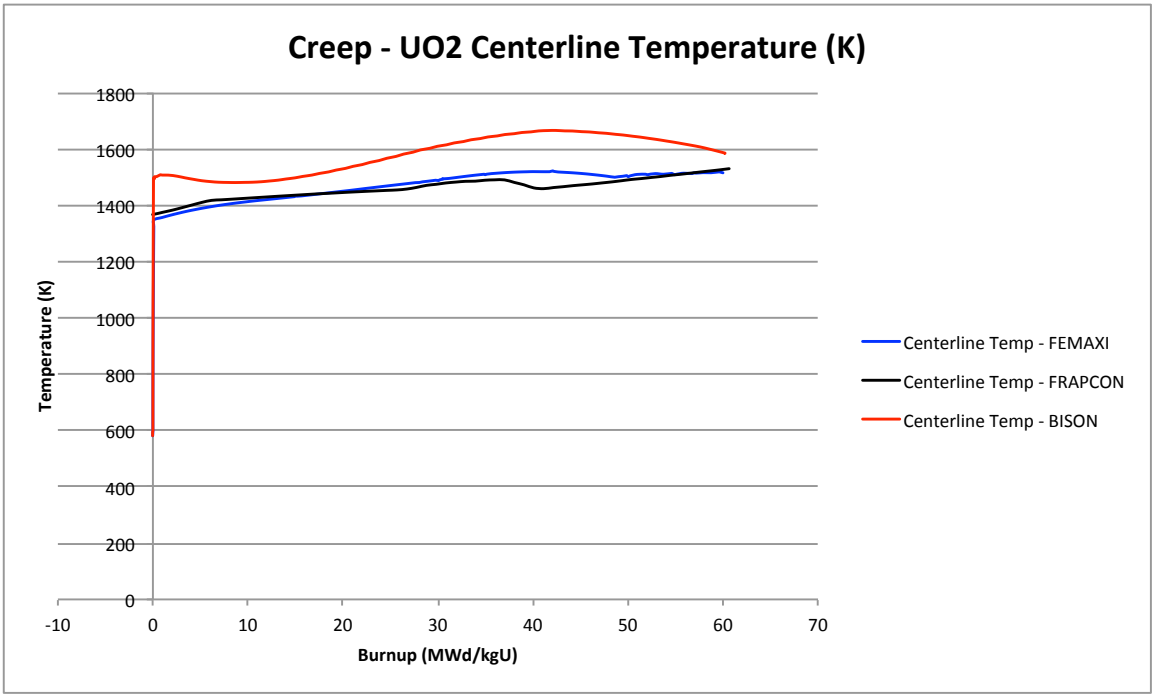

Figure 4.14: Centerline temperature for UO_2/SiC at 20kW/m with creep

10kW/m, to possibly give insight into how sensitive each code's fission gas release model and displacment model are to temperature. To help seperate out effects of

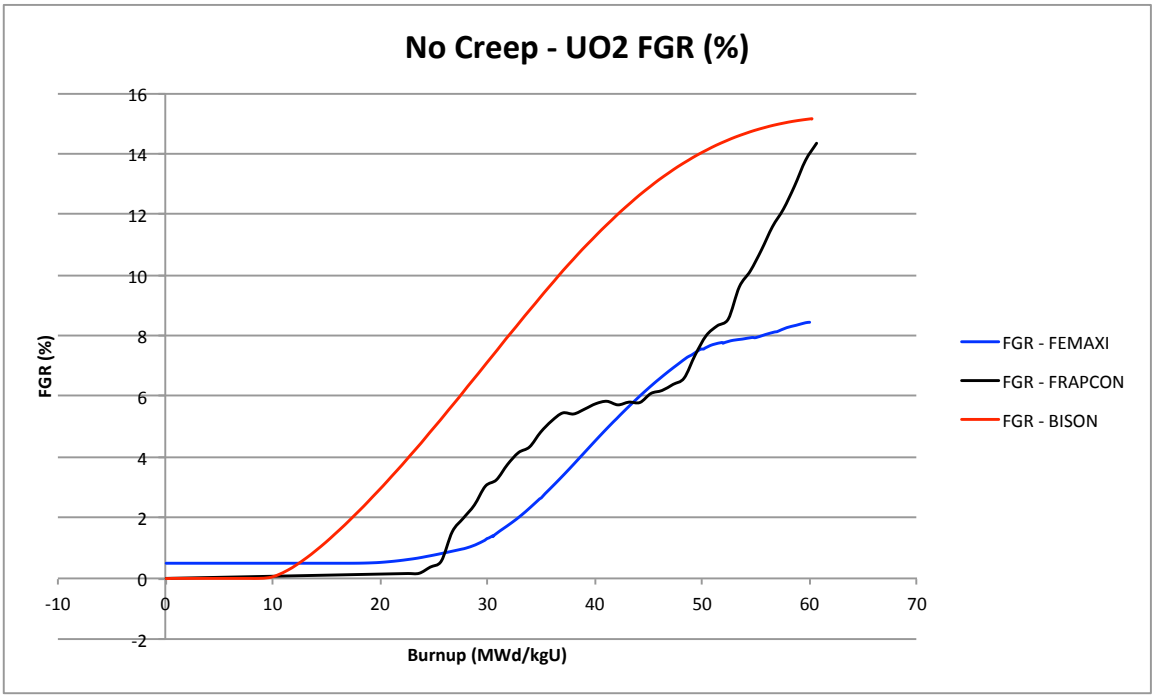

Figure 4.15: Fission gas release for UO_2/SiC at 20kW/m without creep

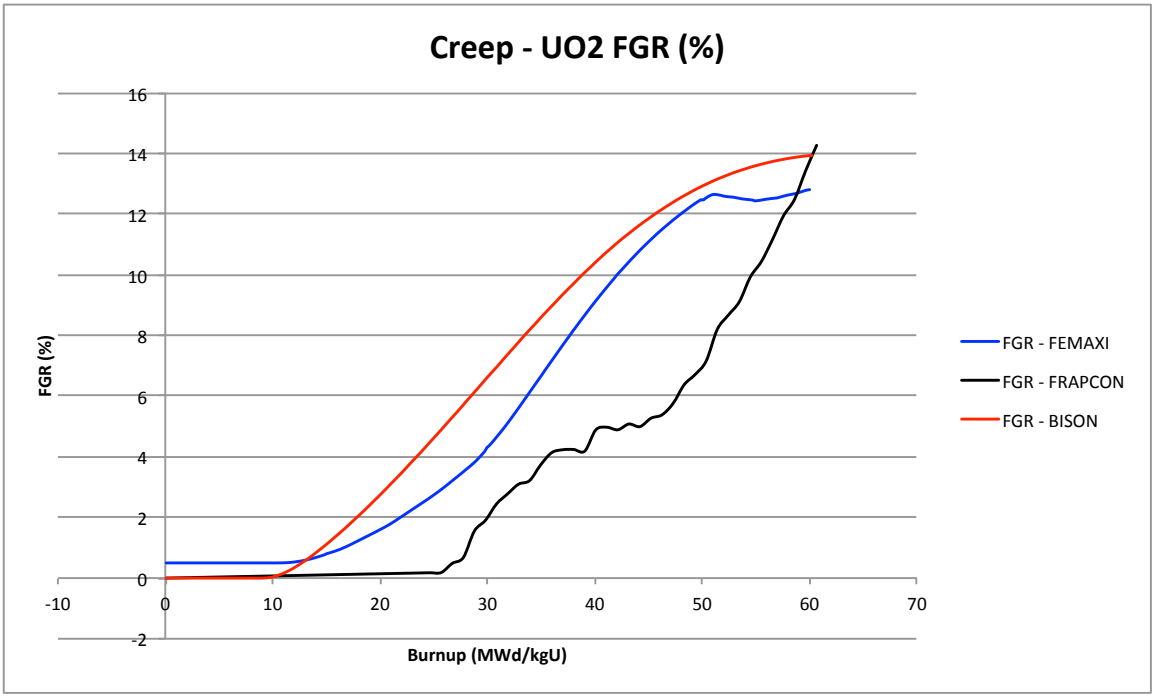

Figure 4.16: Fission gas release for UO_2/SiC at 20kW/m with creep

neutron flux, the UO_2/Zry case provides a way to do so. This provides a quick way to examine the fuel at a lower temperature with a constant neutron flux, which is related

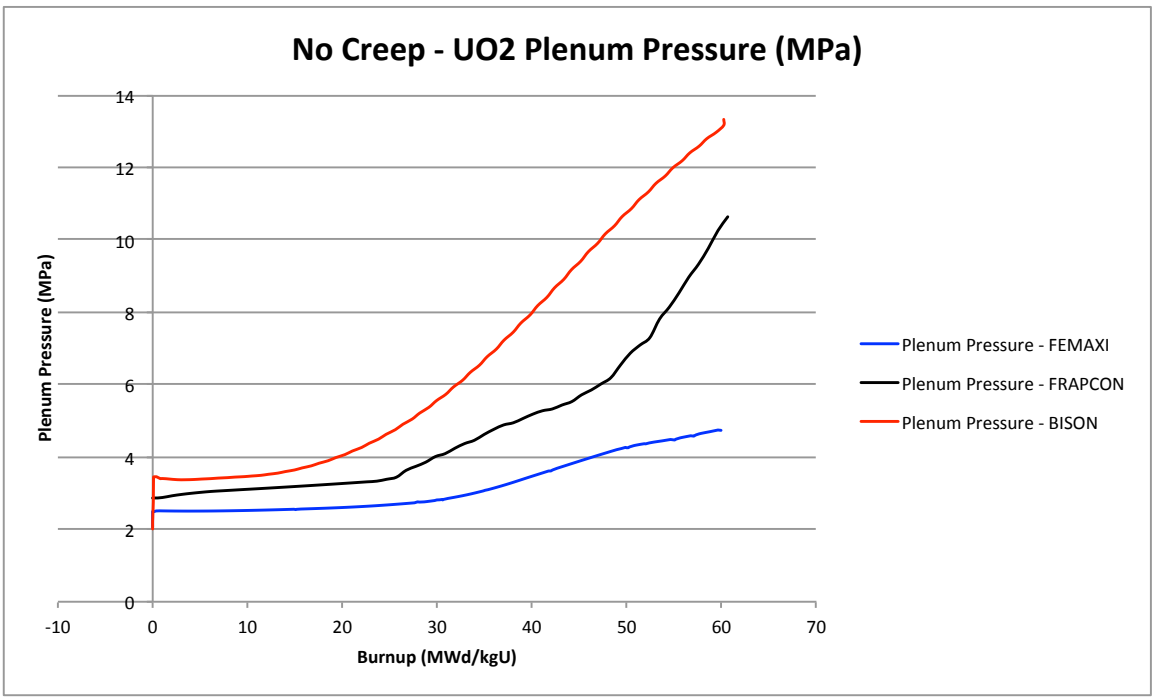

Figure 4.17: Plenum pressure for UO_2/SiC at 20kW/m without creep

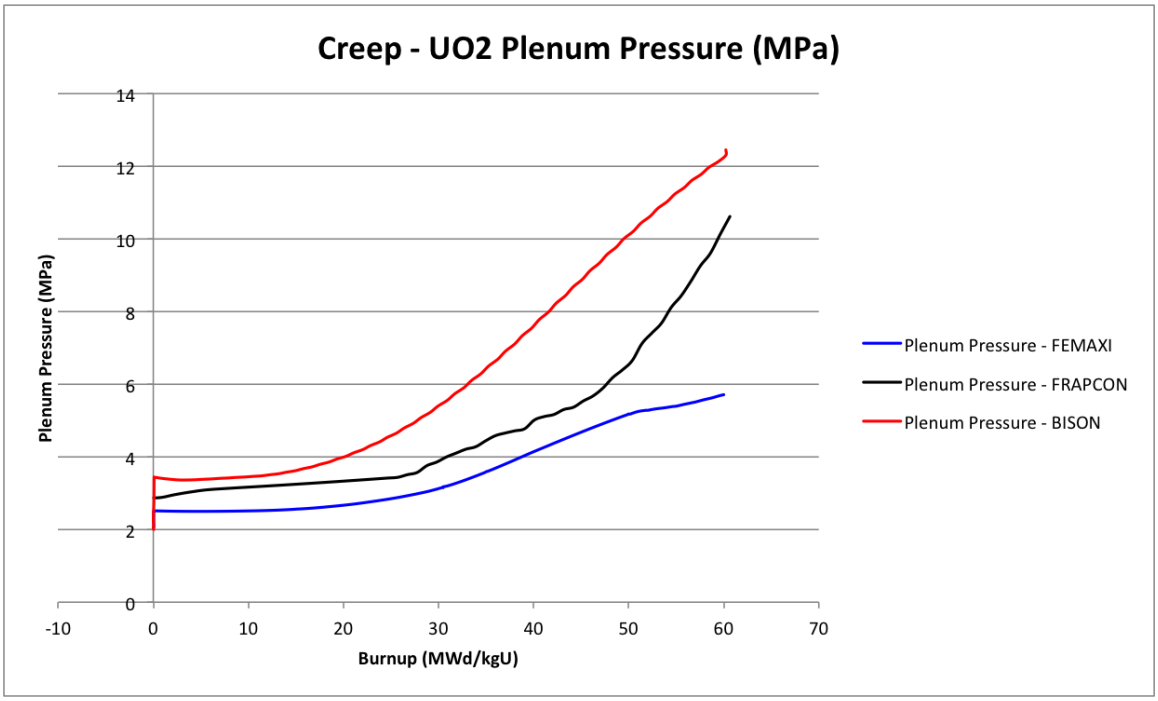

Figure 4.18: Plenum pressure for UO_2/SiC at 20kW/m with creep

to the user supplied LHGR. Doing this for each code should provide understanding to the previous UO_2/SiC's results comparison with the UO_2/Zry system.

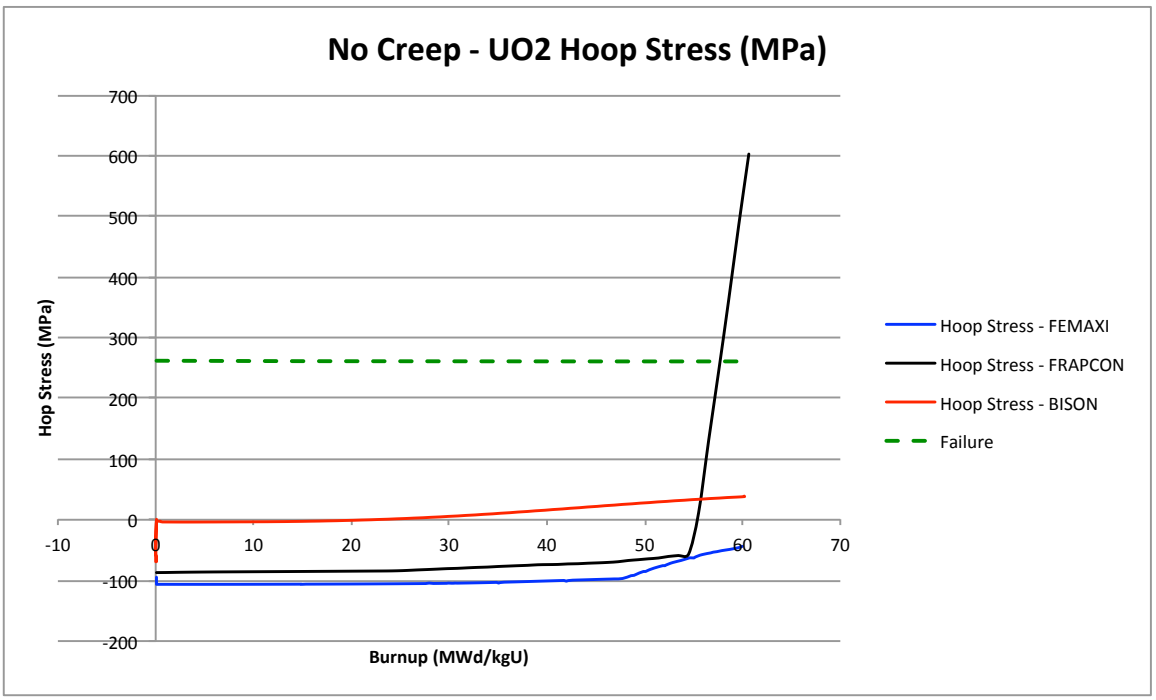

Figure 4.19: Cladding hoop stress for UO_2/SiC at 20kW/m without creep

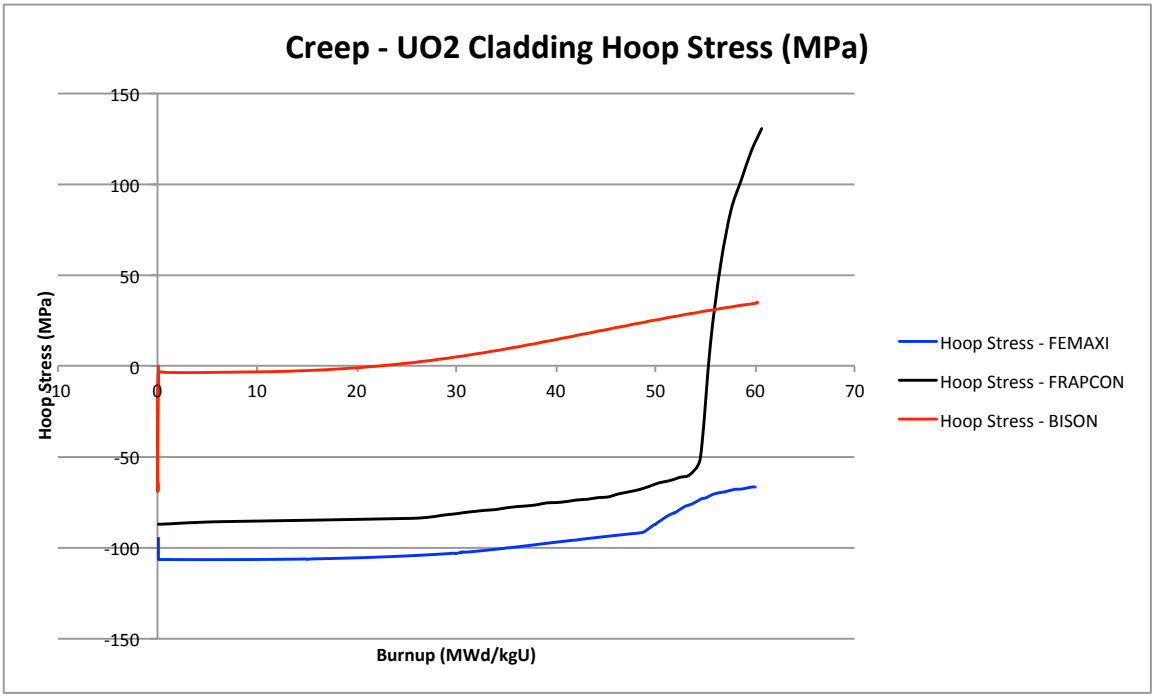

Figure 4.20: Cladding hoop stress for UO_2/SiC at 20kW/m with creep

In this study the only parameter that gets changed is the LHGR. Having a higher LHGR will require less time to reach the same burnup and vice-versa for a lower

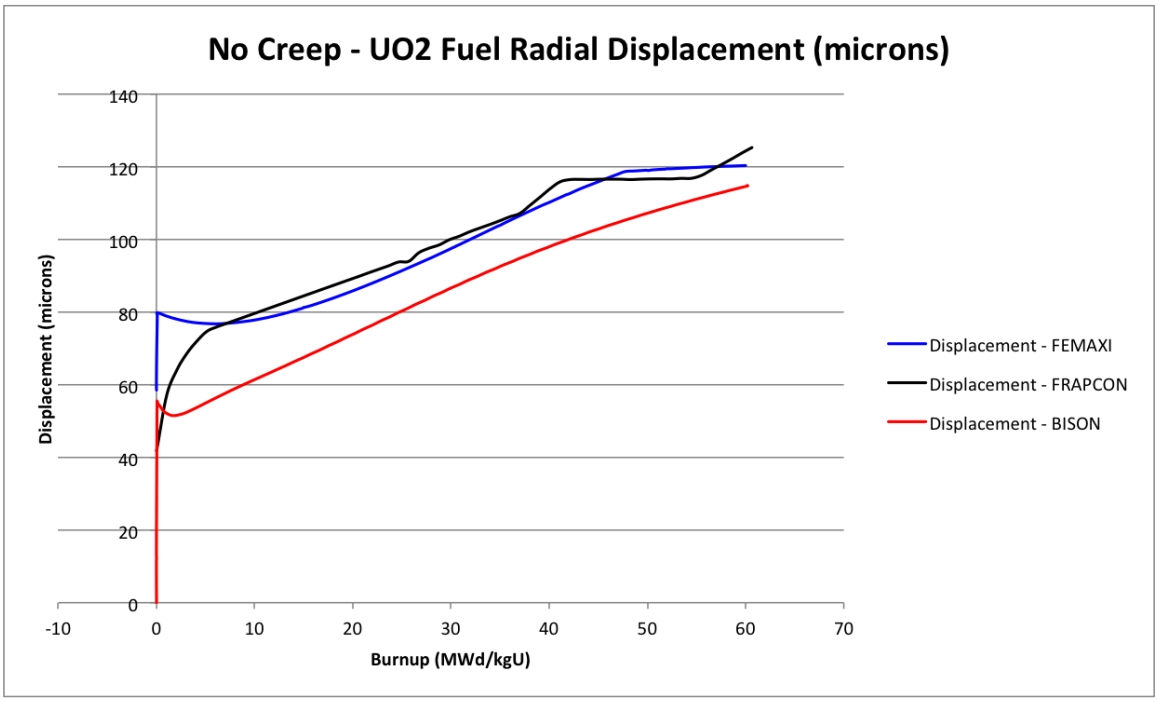

Figure 4.21: Fuel surface radial displacement for UO_2/SiC at 20kW/m without creep

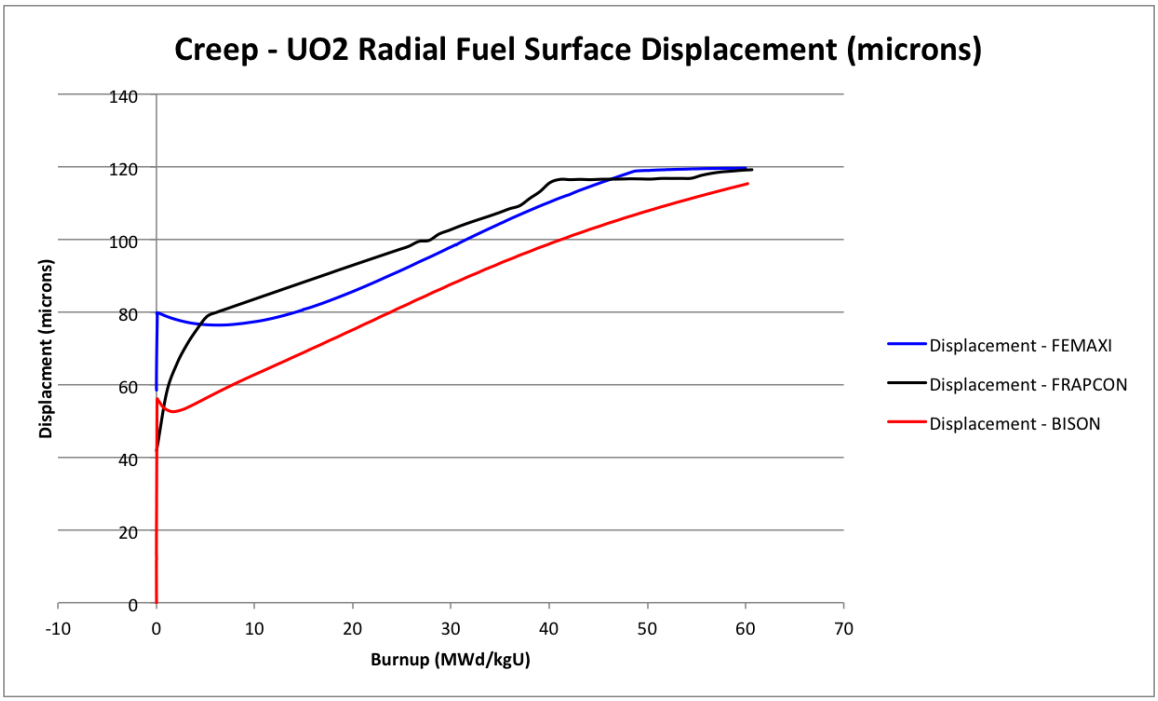

Figure 4.22: Fuel surface radial displacement for UO_2/SiC at 20kW/m with creep

LHGR. With the changing of the LHGR, temperature changes are also brought on. Since so many of the models are temperature dependent, this is a way to examine how

dependent each model is upon temperature. This study will mainly focus on the effects of temperature on fission gas release for each of the codes to try and clear up some discrepency between the UO_2/Zry fission gas release amounts between FRAPCON and BISON. Figures 4.23, 4.24, and 4.25 show the code's prediction for centerline temperatures at the given power.

Taking a look at the BISON centerline temperatures at EOL as seen in Figure 4.23, it can be seen that the temperature difference between the 30kW/m case and the 20kW/m case is 300 K and 530 K between the 20kW/m case and the 10kW/m case. The FRAPCON case seen in Figure 4.24 shows that the temperature difference between the 30kW/m case and the 20kW/m case is 589 K and 496 K between the 20kW/m and the 10kW/m cases. The FEMAXI code seen in Figure 4.25 predicts a major difference in the 30kW/m case for the run with fuel creep and without fuel creep. Between the 10kW/m and the 20kW/m case there is a temperature delta of 490 K. The temperature difference between the 20kW/m case and the 30kW/m case without creep is 493 K, and 685 K for the 30kW/m case with creep.

Figures 4.26, 4.27, and 4.28 show the corresponding cumulative fission gas release for each power level. While all are undoubtly affected by the increasing power levels, the FRAPCON and FEMAXI codes predict much higher total gas release values at 30kW/m. This leads one to believe that fuel centerline temperatures over 1500 K in the FRAPCON and FEMAXI codes leads to exponental gas release rates by these codes. Since the advanced fuels have much higher thermal conductivities than UO_2, one should not expect that this would be an issue.

The only code that shows a major difference in using a fuel creep model is the FEMAXI code run at 30kW/m as shown in Figure 4.25. With using the MATPRO-09 creep model in FEMAXI there is 200 K degree increase in centerline temperature. This can be explained somewhat by looking at the radial and axial displacement comparison graphs seen in Figure 4.31 and 4.32. These figures show that by adding a

creep model, the fuel does not expand radially as quickly as without using a creep model. At 30kW/m, the centerline temperature is highly dependant on gap width especially with a low thermally conductive cladding, such as SiC.

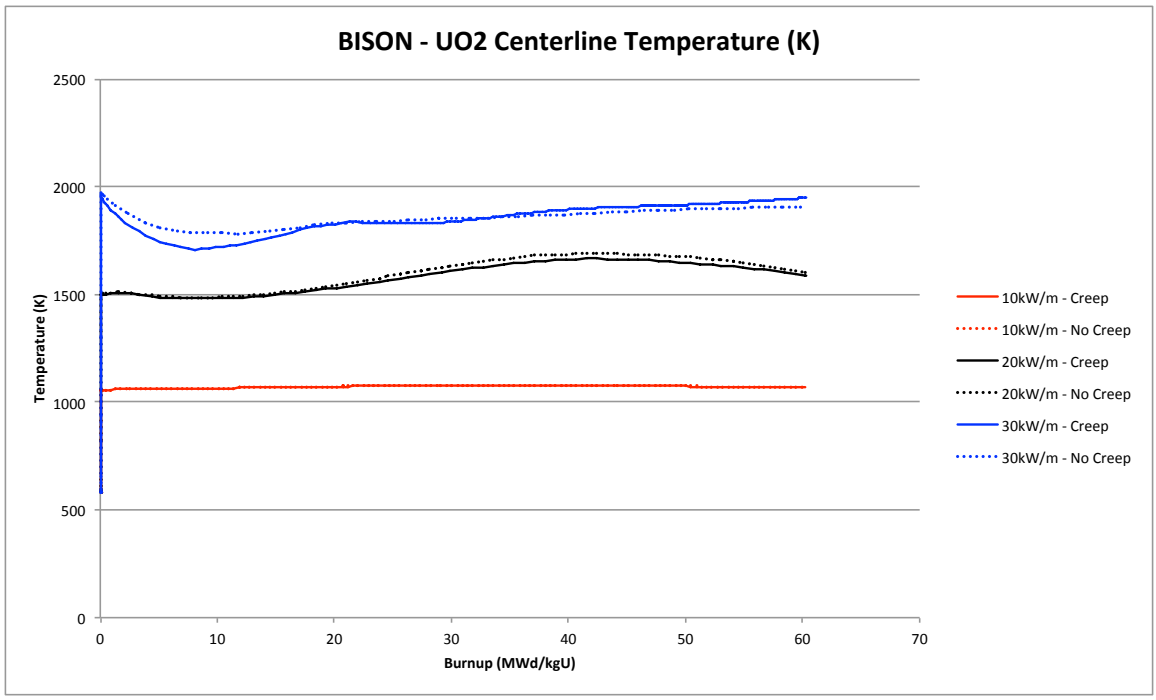

Figure 4.23: Centerline temperatures for fuel modeled by BISON at three different LHGR's

4.4 UN/SiC Cases

By looking at the figures below, one of the first things to note is that for the UN type fuel, PCMI is nearly avoided with the use of this specified geometry for the given run parameters. Cladding hoop stress can be seen in Figures 4.39 and 4.40. The FRAPCON code predicts that the cladding will stay in a compressive hoop stress regime for the entirity of the run where the BISON code predicts that after 45 MWd/kgU, the cladding will be in a tensile hoop stress regime. This is an indication that the BISON code predicts that there is a slight bit of contact, but in both codes the maximum cladding hoop stress of 261 MPa is nowhere near being reached.

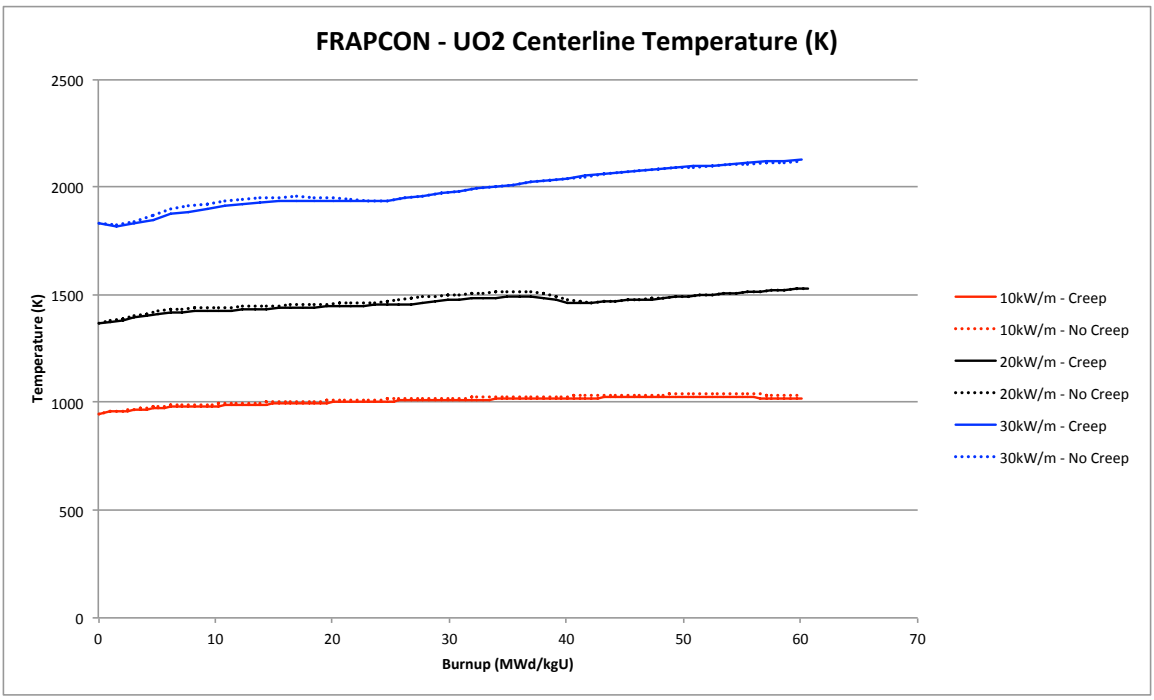

Figure 4.24: Centerline temperatures for fuel modeled by FRAPCON at three different LHGR's

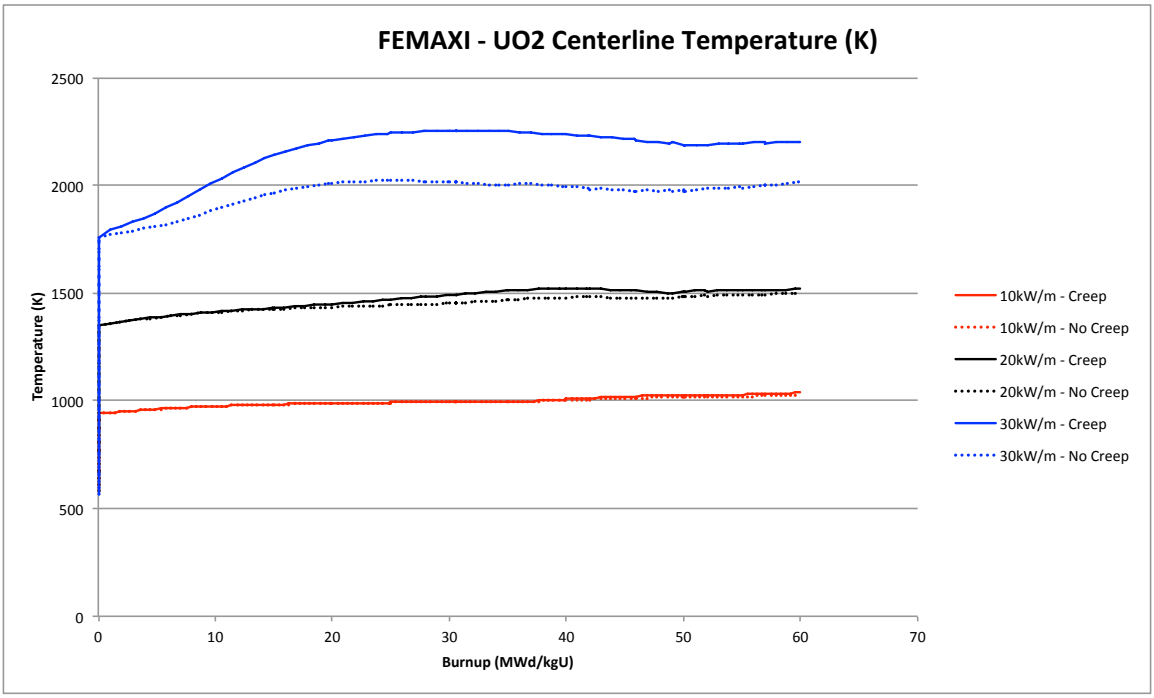

Figure 4.25: Centerline temperatures for fuel modeled by FEMAXI at three different LHGR's

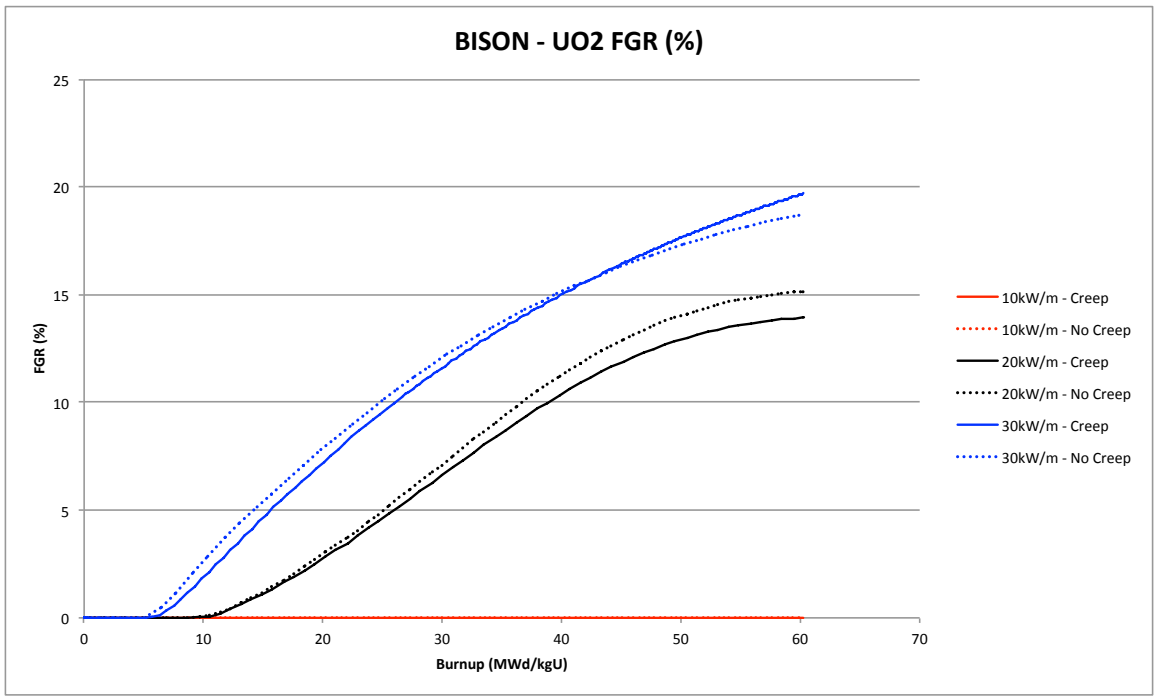

Figure 4.26: Fission gas released for fuel modeled by BISON at three different LHGR's

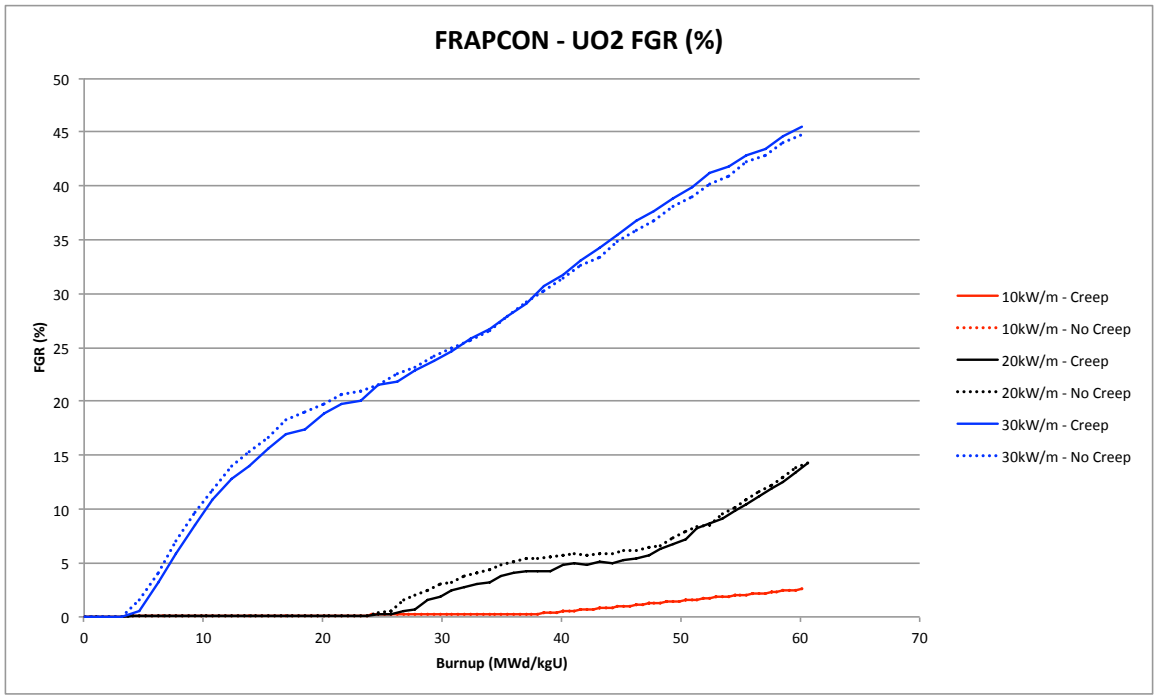

Figure 4.27: Fission gas released for fuel modeled by FRAPCON at three different LHGR's

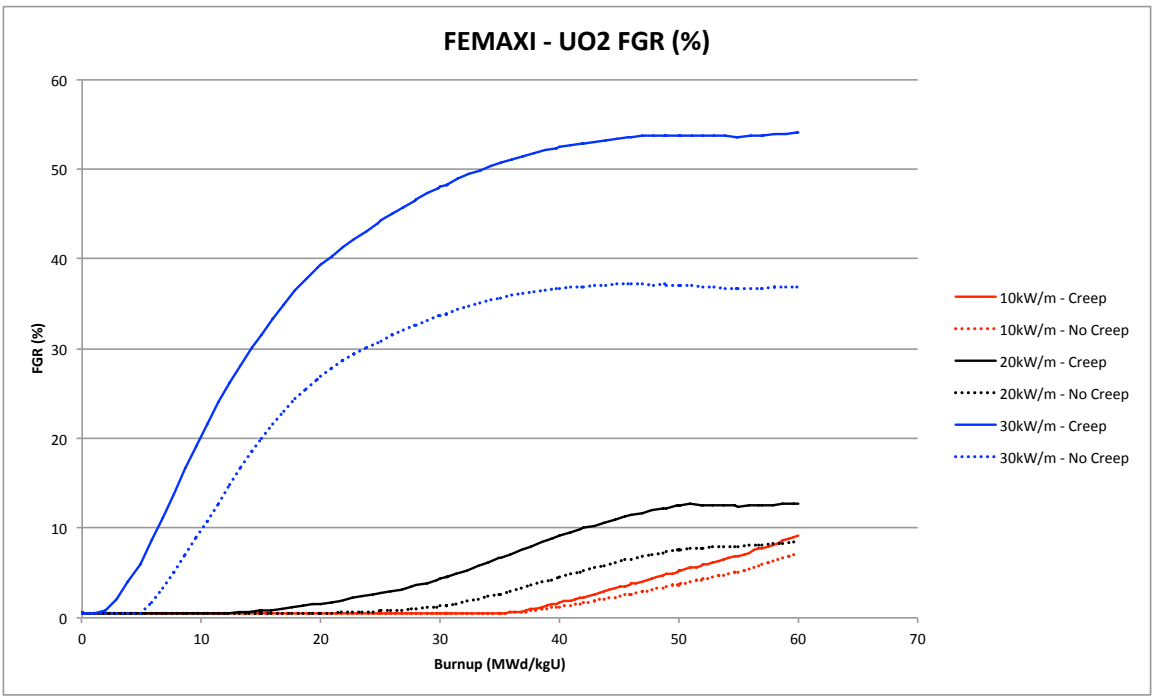

Figure 4.28: Fission gas released for fuel modeled by FEMAXI at three different LHGR's

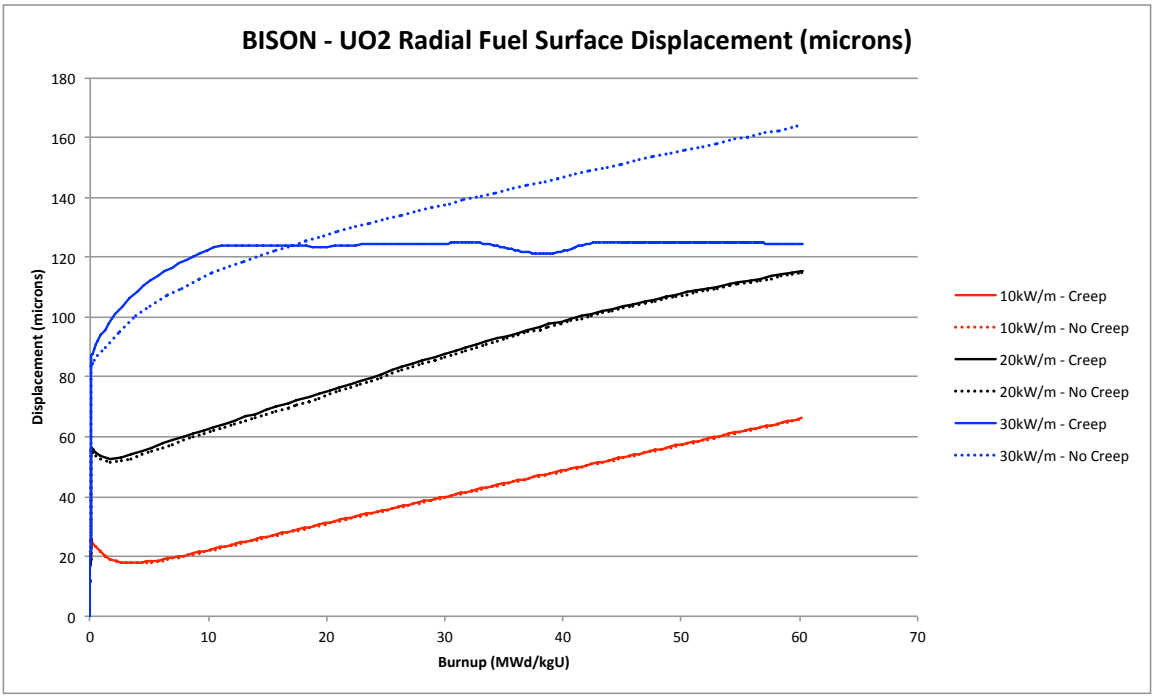

Figure 4.29: Fuel surface radial displacement for UO_2/SiC using the BISON code at three different power levels

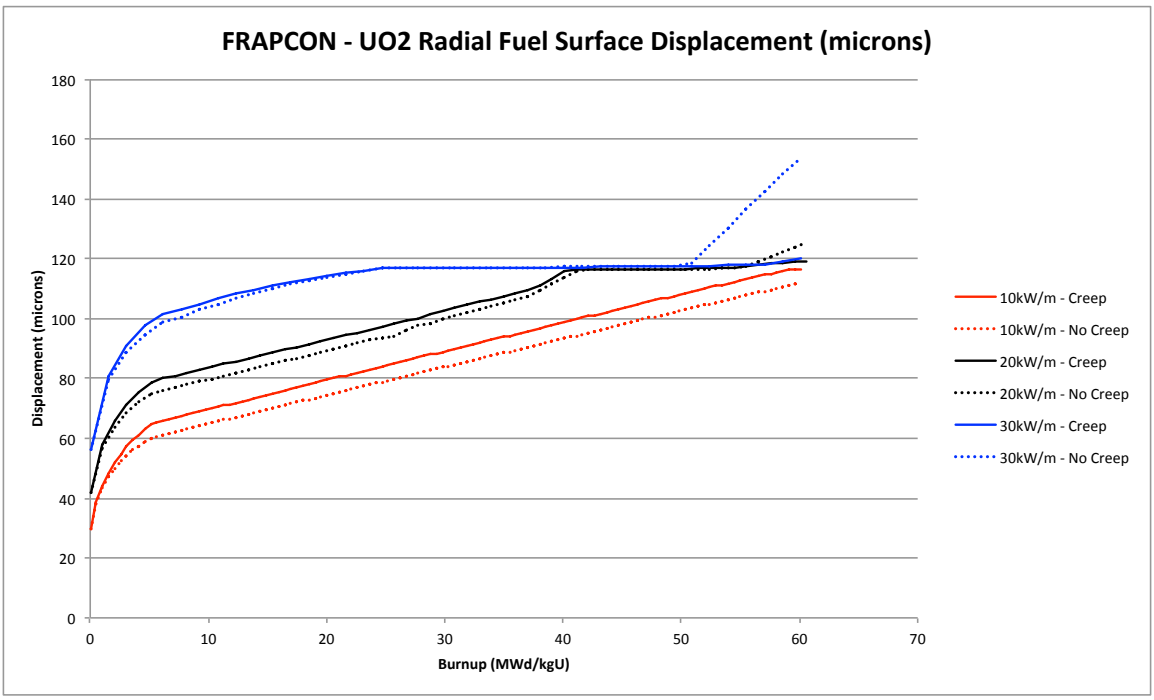

Figure 4.30: Fuel surface radial displacement for UO_2/SiC using the FRAPCON code at three different power levels

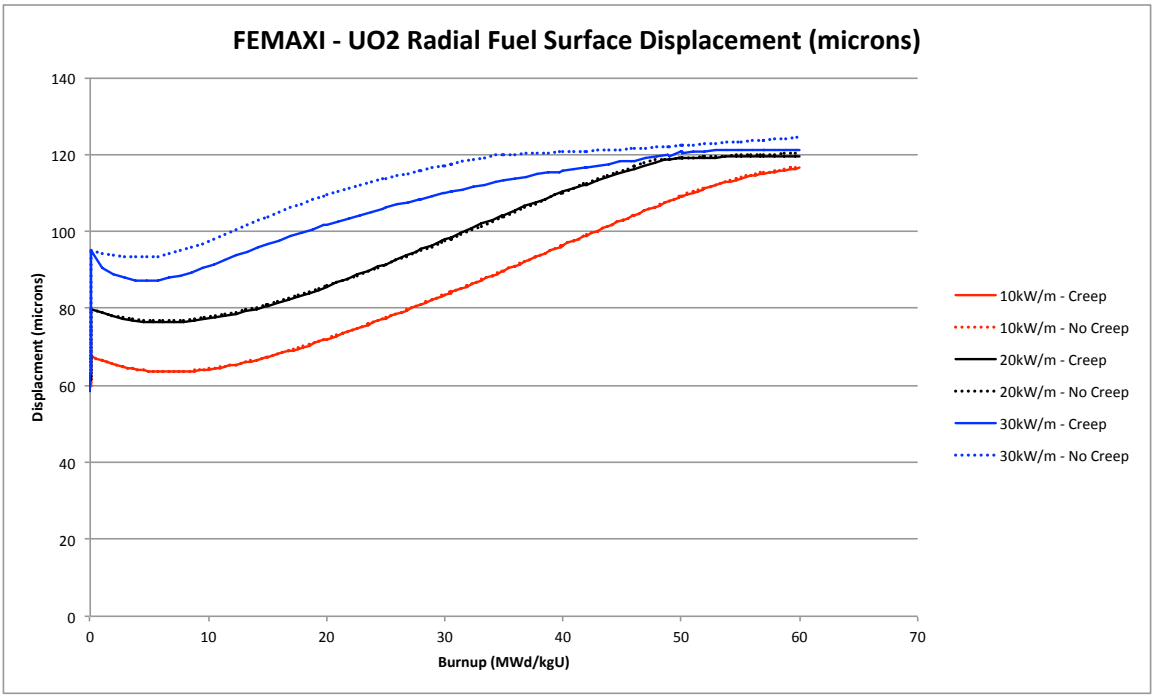

Figure 4.31: Fuel surface radial displacement for UO_2/SiC using the FEMAXI code at three different power levels

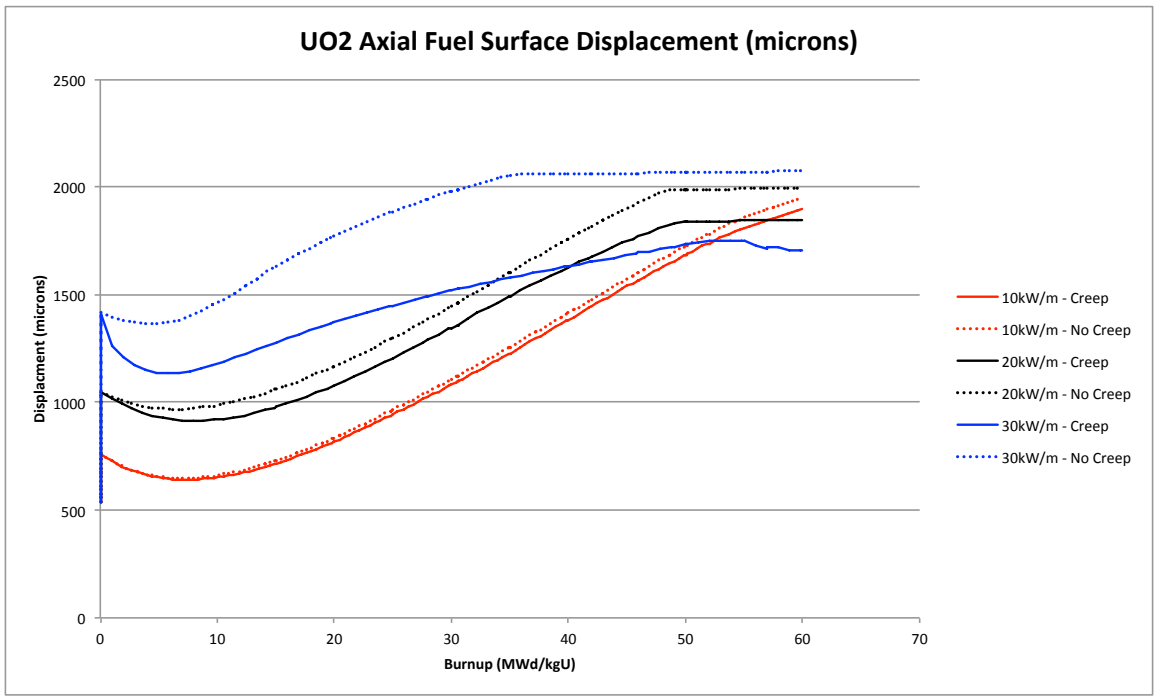

Figure 4.32: Fuel surface axial displacement for UO_2/SiC using the FEMAXI code at three different power levels

From Figures 4.33 and 4.34 one can see that there is a slight discrepancy in the temperatures at the beginning of life. There is a 50 K difference in centerline temperatures which might be best attributed to the increased fission gas added to gap size differences. The BISON code predicts that there is not as much immediate radial displacement as what FRAPCON predicts. This could be attributed to a slight difference in the thermal expansion models between the two codes where BISON would predict that the fuel expands less than FRAPCON.

There is also a bump in the centerline temperature for BISON at 45 MWd/kgU where centerline temperatures level off and then lead on to increase. This could be attributed to the addition of fission gas to the plenum causing a degredation of radial gap heat transfer to be happening. This addition of fission gas can be seen in Figures 4.35 and 4.36. At 45 MWd/kgU the fission gas predicted by BISON surpasses the prediction of FRAPCON, causing a larger difference in centerline temperatures. This additional fission gas released in combination with a larger radial gap present

due to slight differences in the thermal expansion models causes this temperature discrepancy.

Since PCMI does not occur during the timeframe of this specific run, there is not much of a conclusion that can be drawn on whether fuel creep is useful in UN in relieving cladding hoop stress. This is discussed in further detail in Section 4.6.

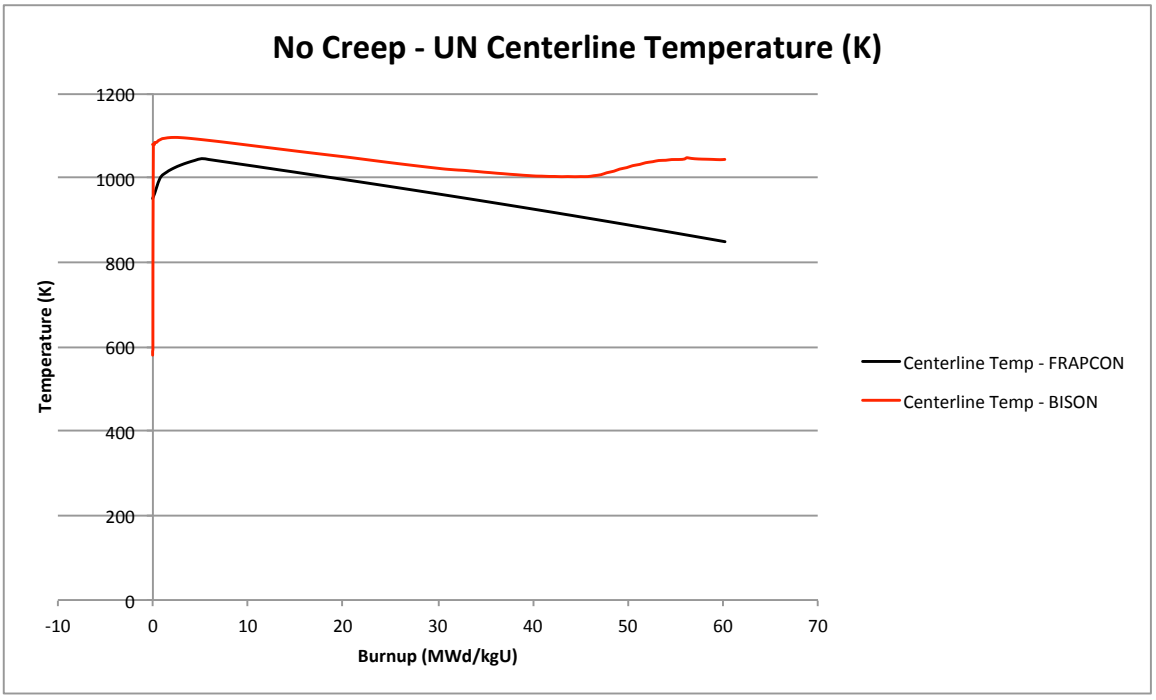

Figure 4.33: Centerline temperature for UN/SiC at 20kW/m without creep

4.5 UC/SiC Cases

After adding the UC type fuel into the BISON and FRAPCON codes, cases based on the UO_2/SiC geometry as seen in Table 4.3 were run to examine how the UC fuel interacts mechanically with the SiC cladding. Because UC has an extremely high swelling rate, we should expect that PCMI will occur. Immdiately one can see that this fuel/cladding design is not suitable for use at this power level and burnup. Even though from looking at Figures 4.48 and 4.47, the cladding hoop stress is reduced by 34% by the addition of fuel creep, values for cladding hoop stress are too high with

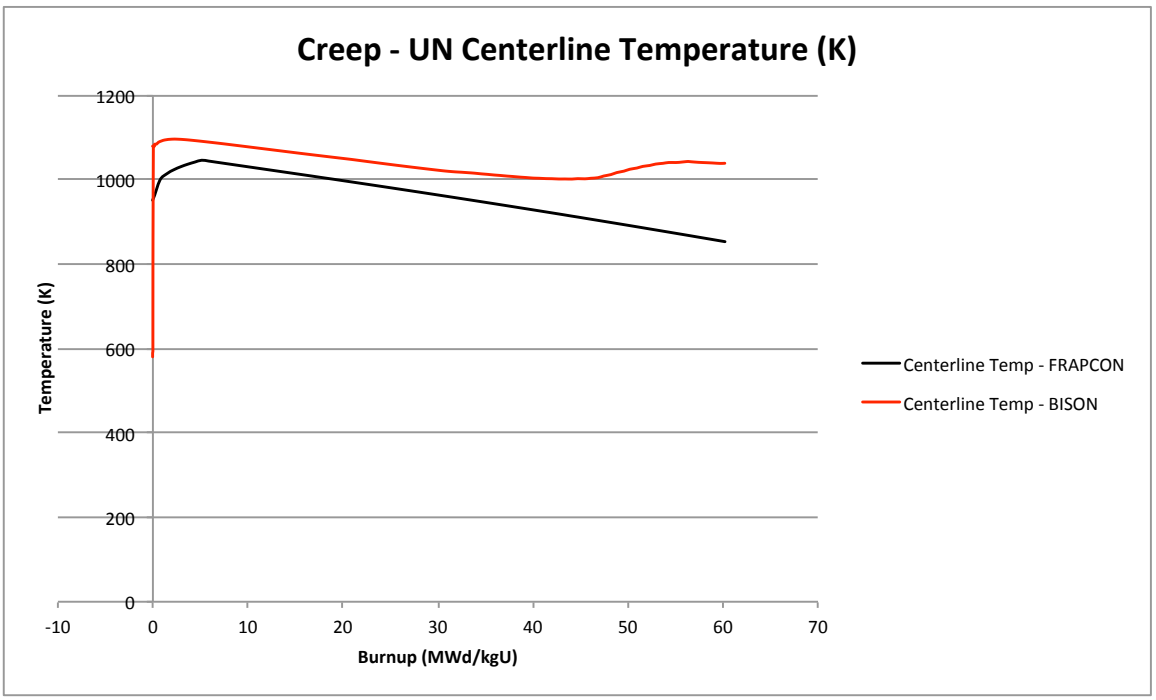

Figure 4.34: Centerline temperature for UN/SiC at 20kW/m with creep

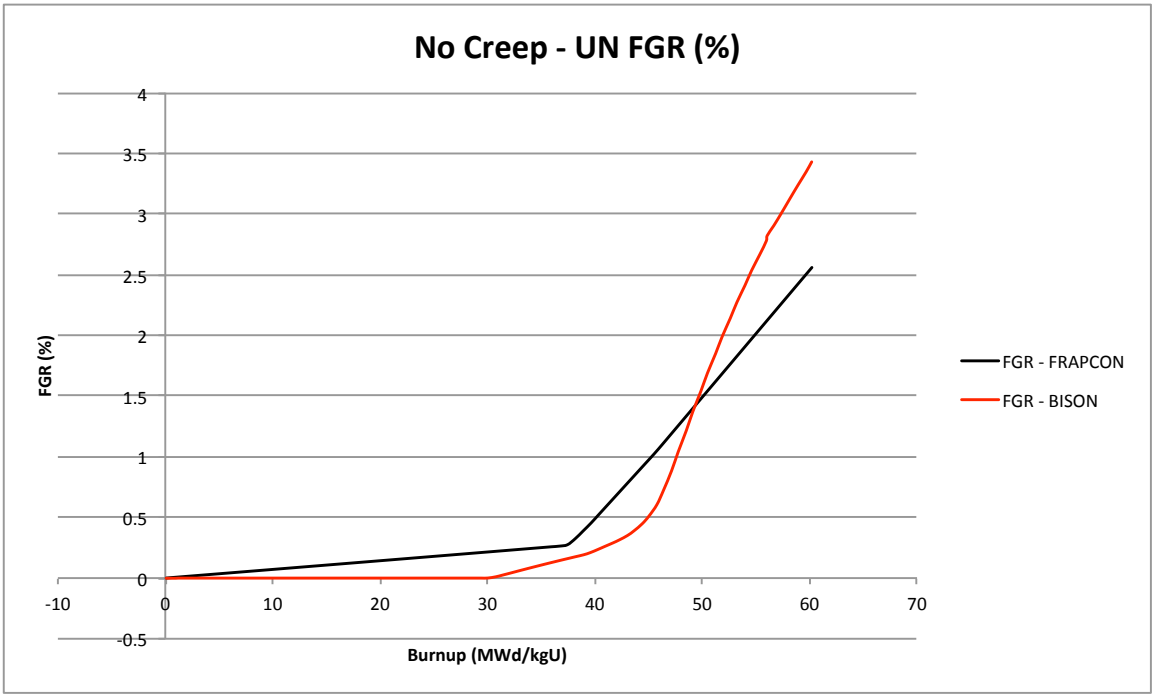

Figure 4.35: Fission gas release for UN/SiC at 20kW/m without creep

and without fuel creep at 904 MPa and 1370 MPa respectively. Figure 4.49 shows the radial gap width between the fuel and cladding. PCMI occurs whenever the gap

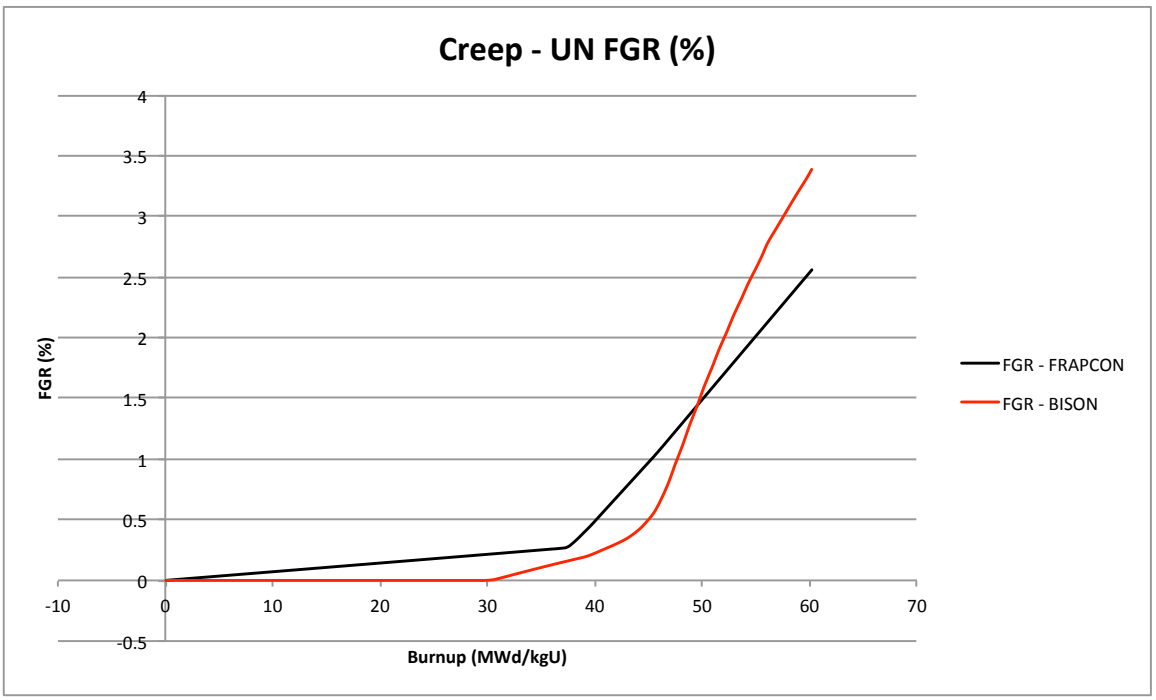

Figure 4.36: Fission gas release for UN/SiC at 20kW/m with creep

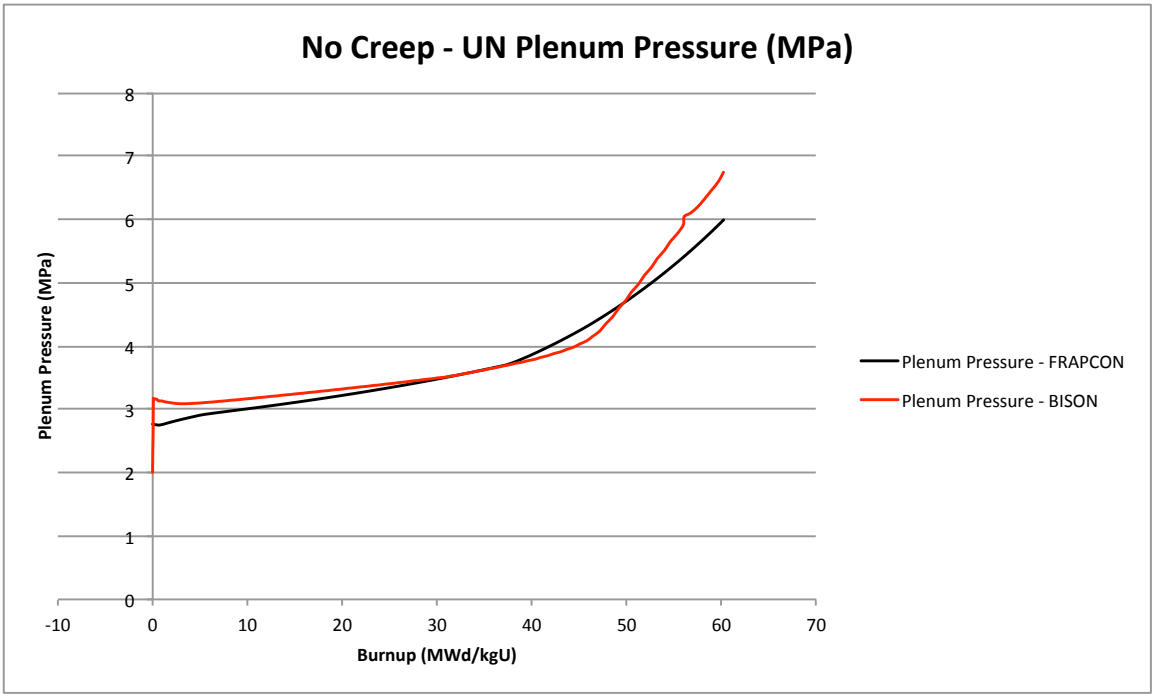

Figure 4.37: Plenum pressure for UN/SiC at 20kW/m without creep

width reaches zero.

For the UC cases in FRAPCON and BISON, the models seem to give very similar

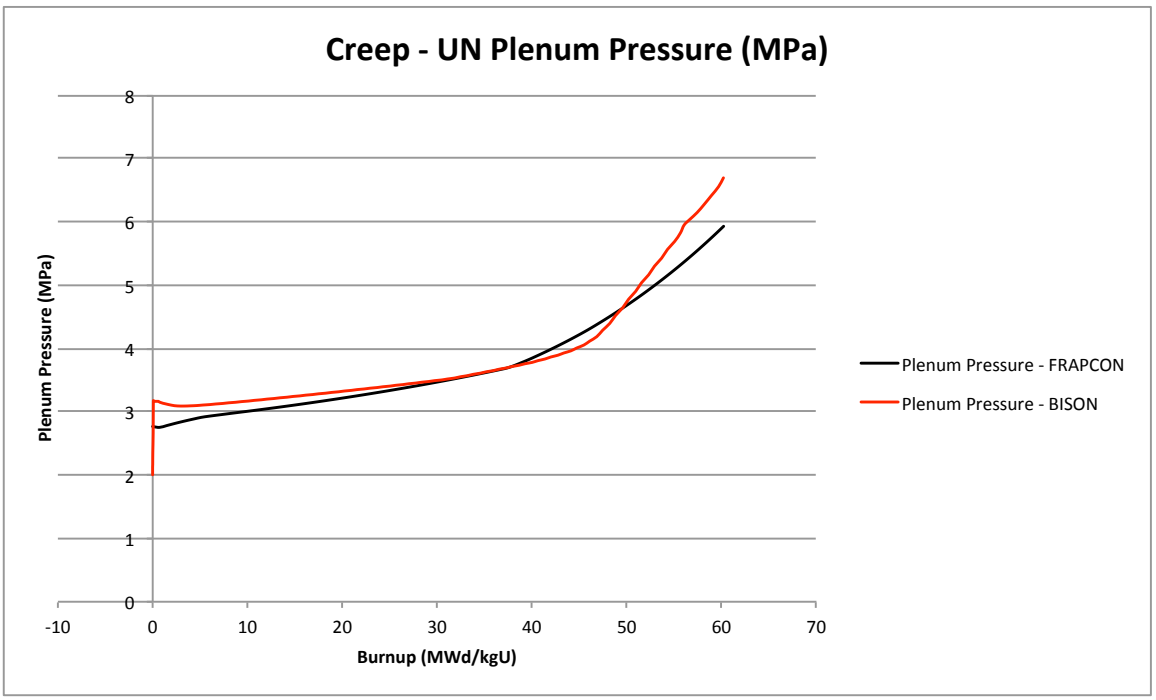

Figure 4.38: Plenum pressure for UN/SiC at 20kW/m with creep

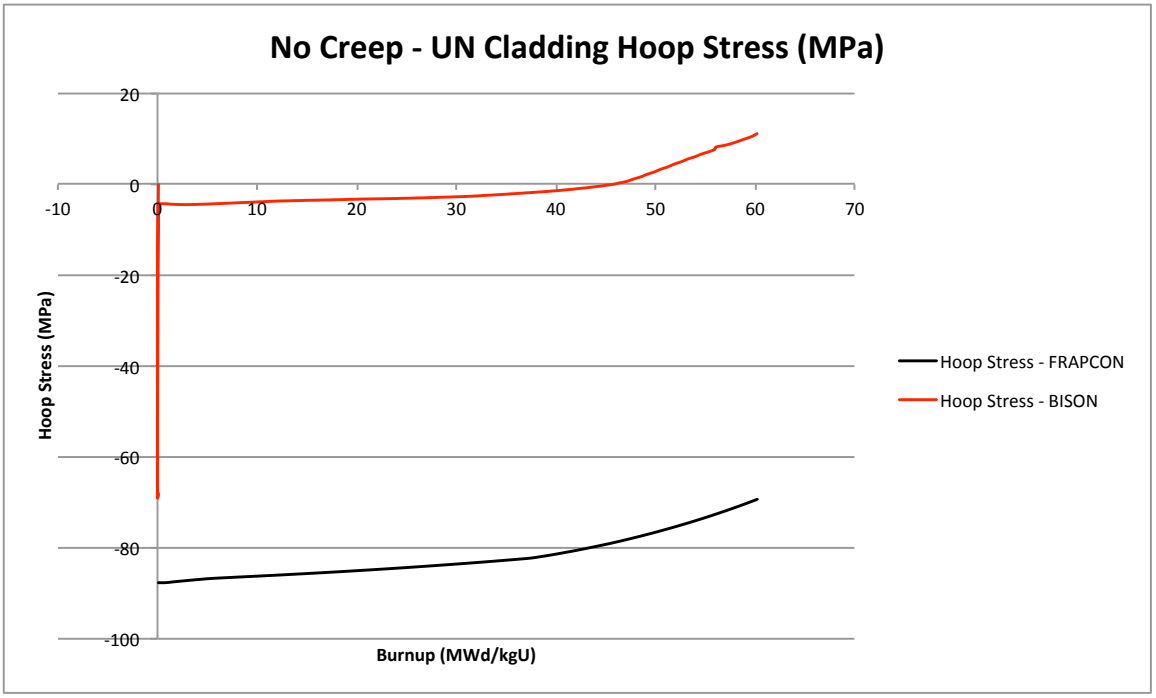

Figure 4.39: Cladding hoop stress for UN/SiC at 20kW/m without creep

results. Centerline temperatures as seen in Figures 4.43 and 4.44 show almost identical results. From Figures 4.45, 4.46, 4.50, and 4.51 we can see a slight difference in initial

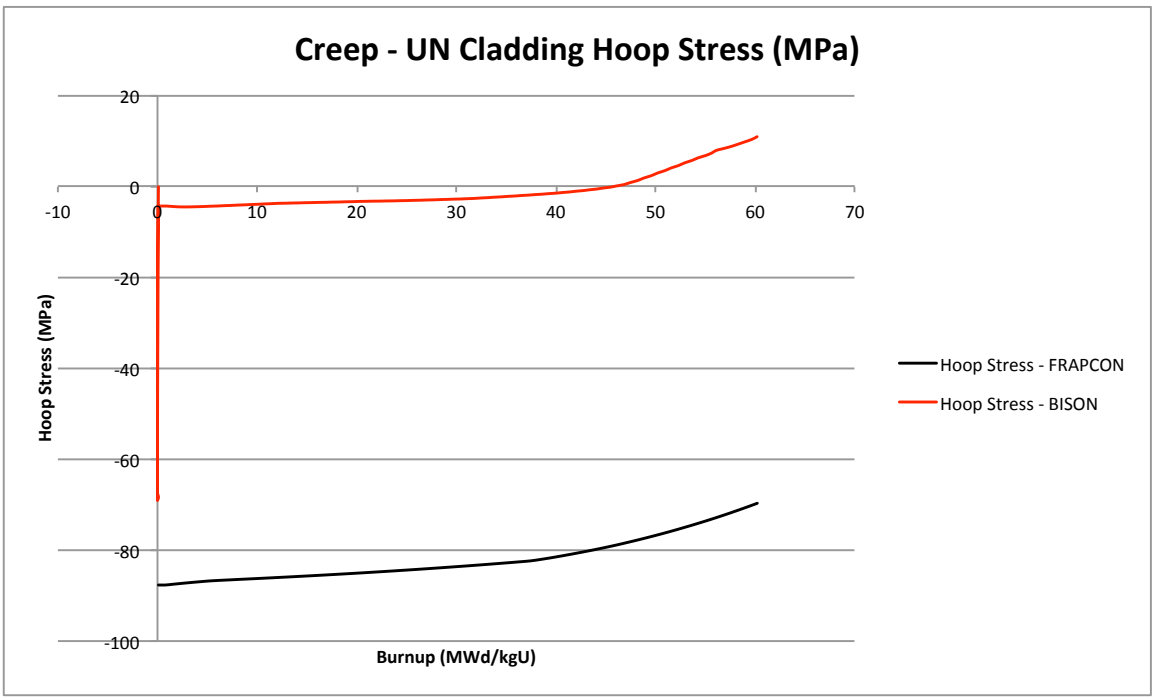

Figure 4.40: Cladding hoop stress for UN/SiC at 20kW/m with creep

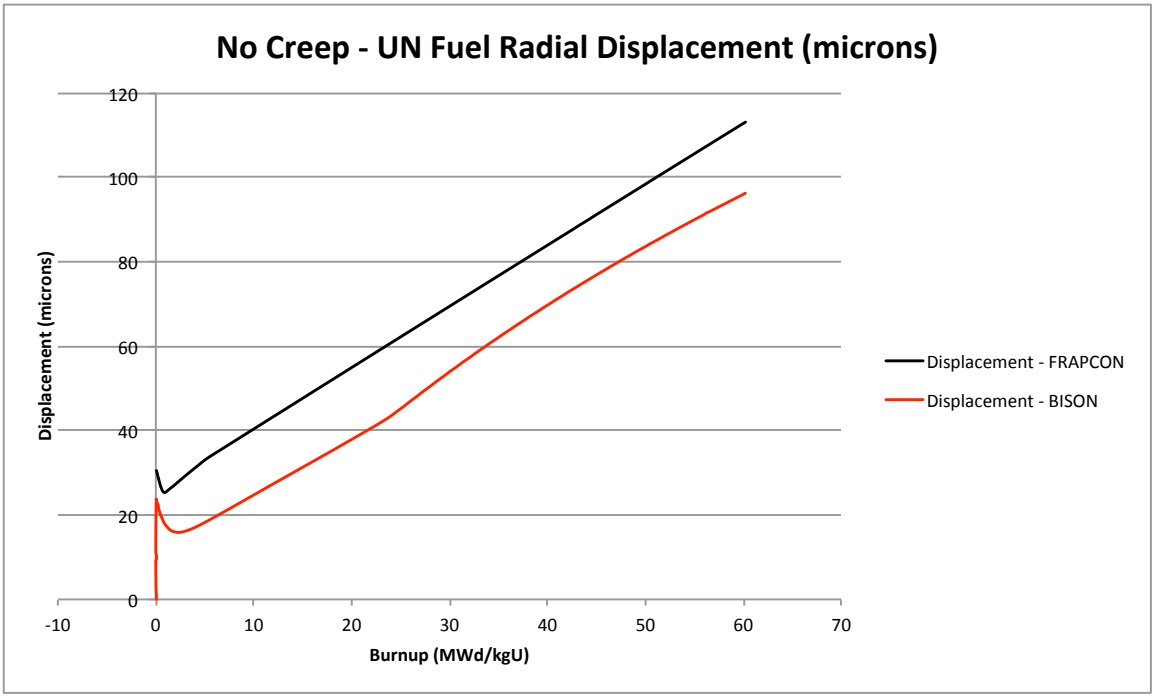

Figure 4.41: Fuel surface radial displacement for UN/SiC at 20kW/m without creep

plenum pressures and radial displacement values. This could be attributed to the BISON model having a slightly higher thermal expansion coefficient causing the fuel

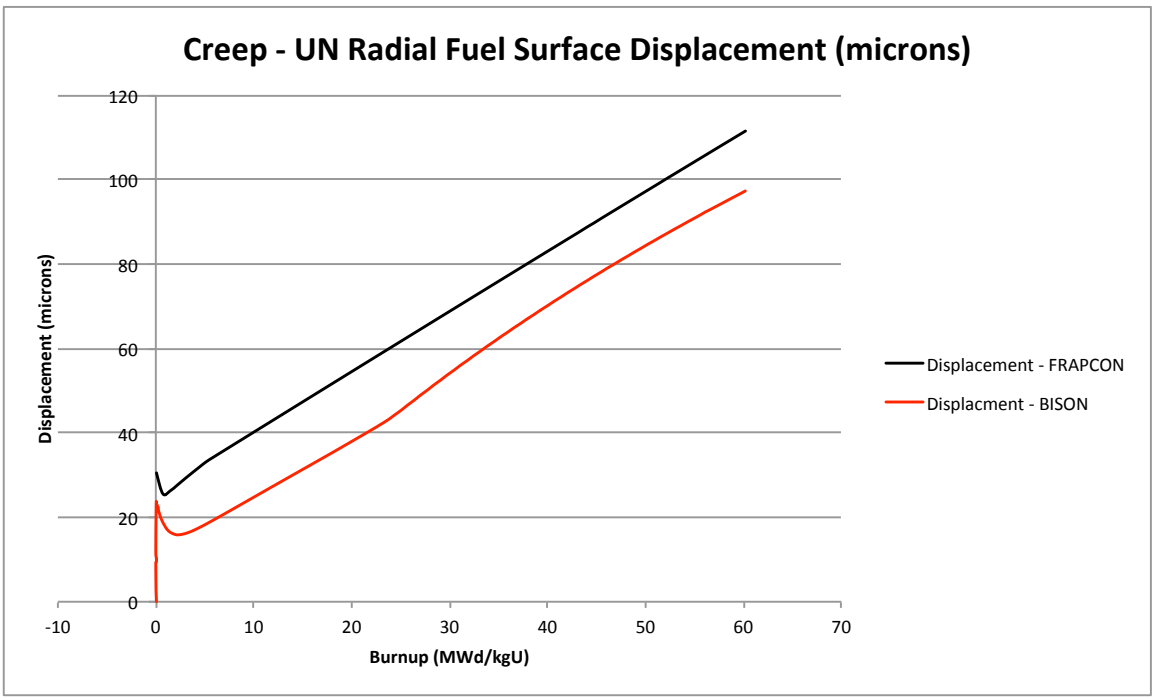

Figure 4.42: Fuel surface radial displacement for UN/SiC at 20kW/m with creep

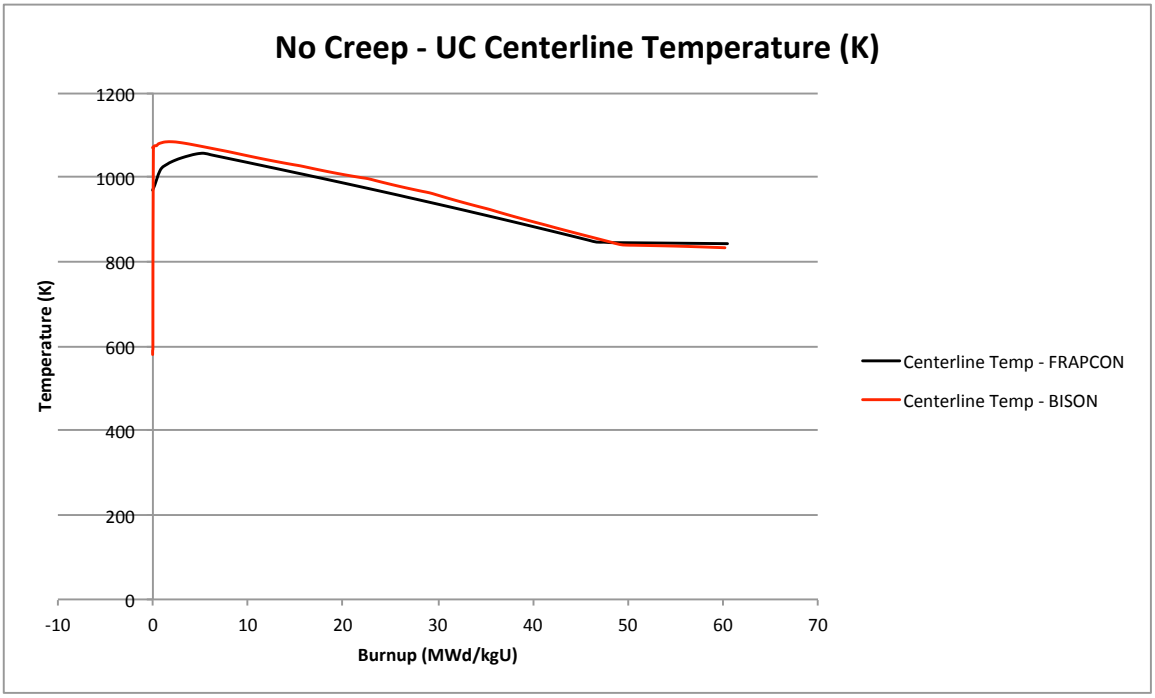

Figure 4.43: Centerline temperature for UC/SiC at 20kW/m without creep

to expand more once up to power. Past this point, the fuel seems to take similar rates for the duration of the run. Since both codes predicted that there was 0% fission gas

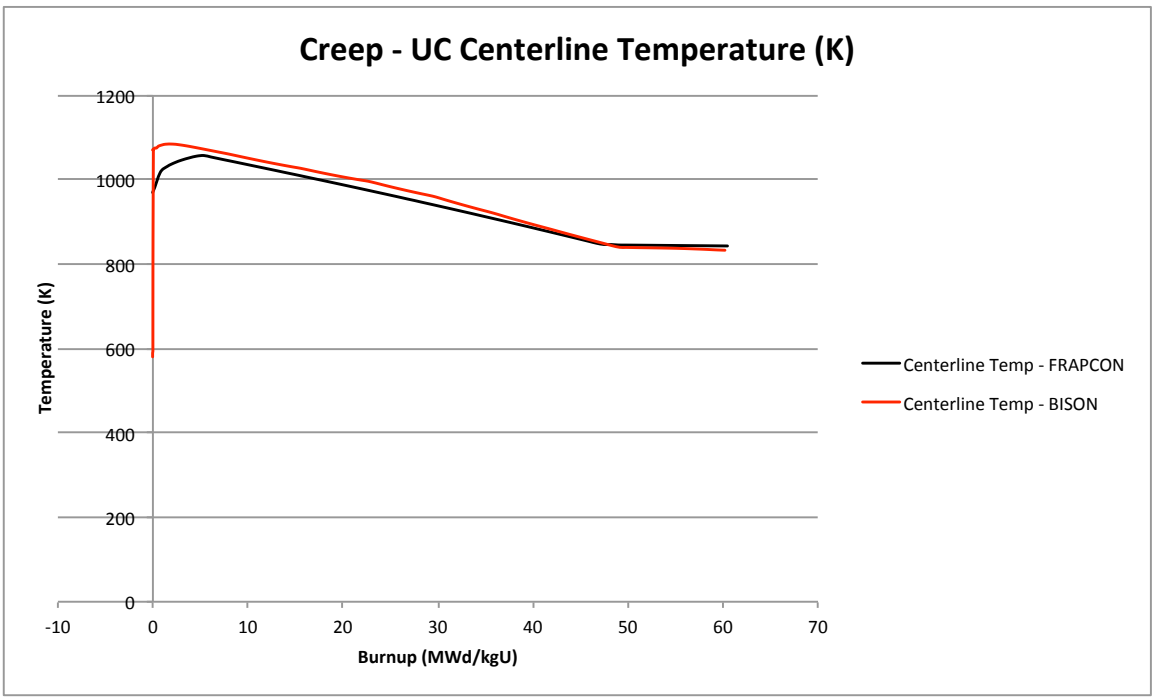

Figure 4.44: Centerline temperature for UC/SiC at 20kW/m with creep

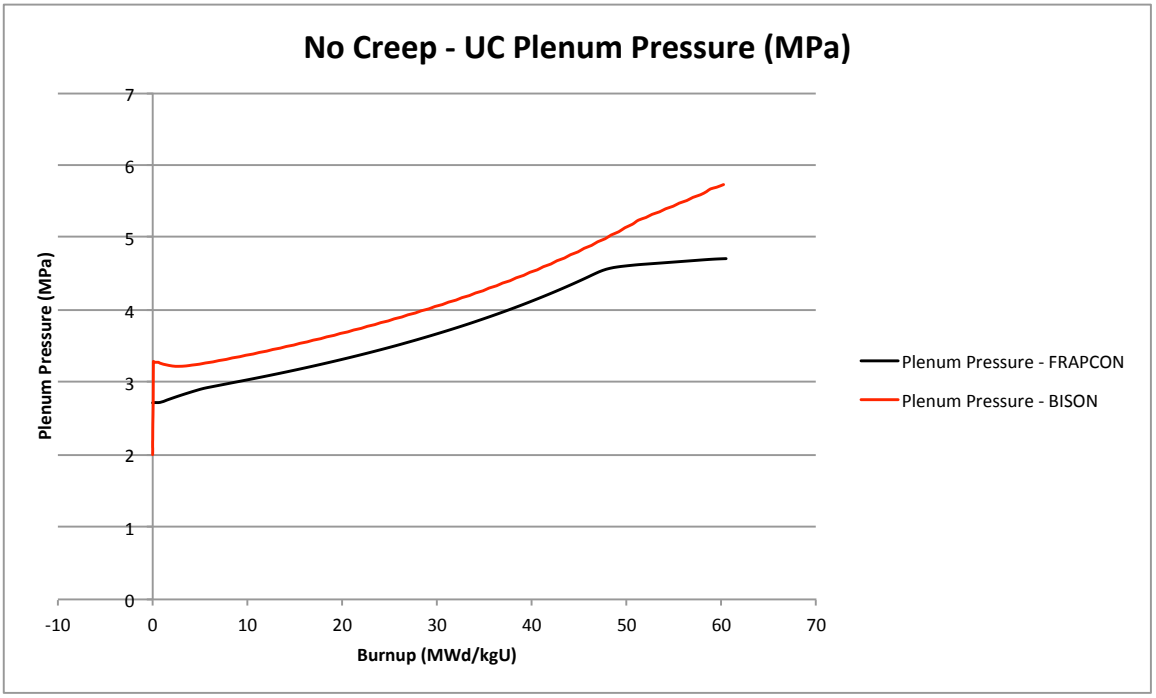

Figure 4.45: Plenum pressure for UC/SiC at 20kW/m without creep

being released to the plenum, graphs were not included for comparison. This agrees with what Zimmerman predicts in Preusser's article noting that there should not be

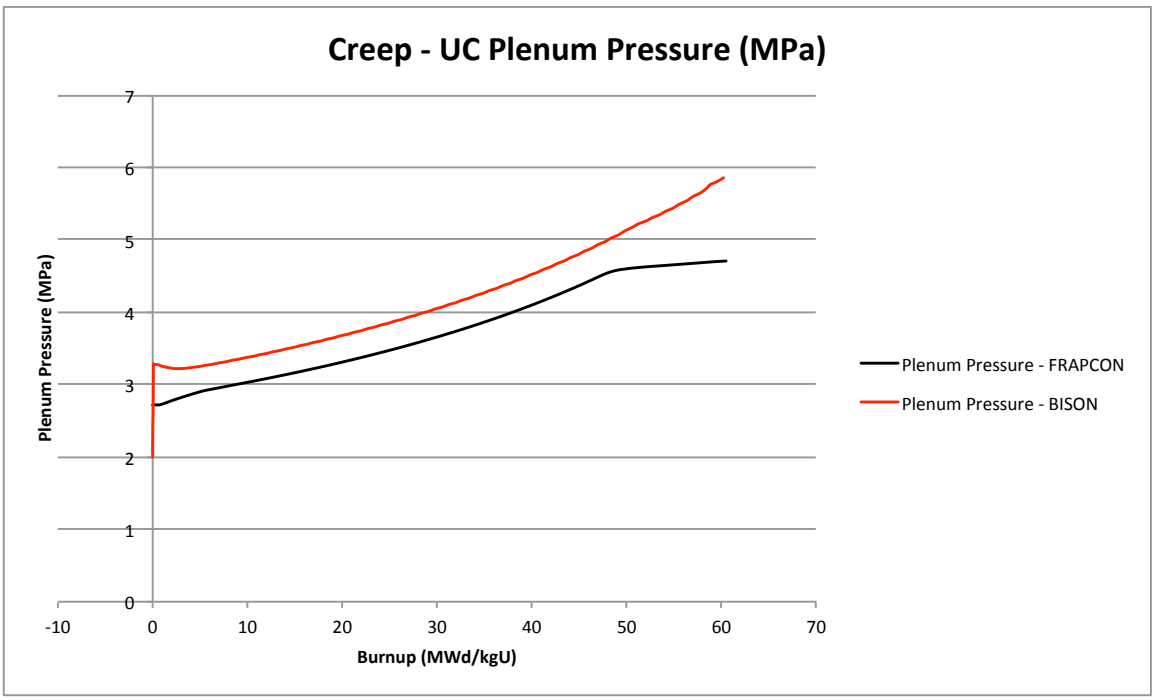

Figure 4.46: Plenum pressure for UC/SiC at 20kW/m with creep

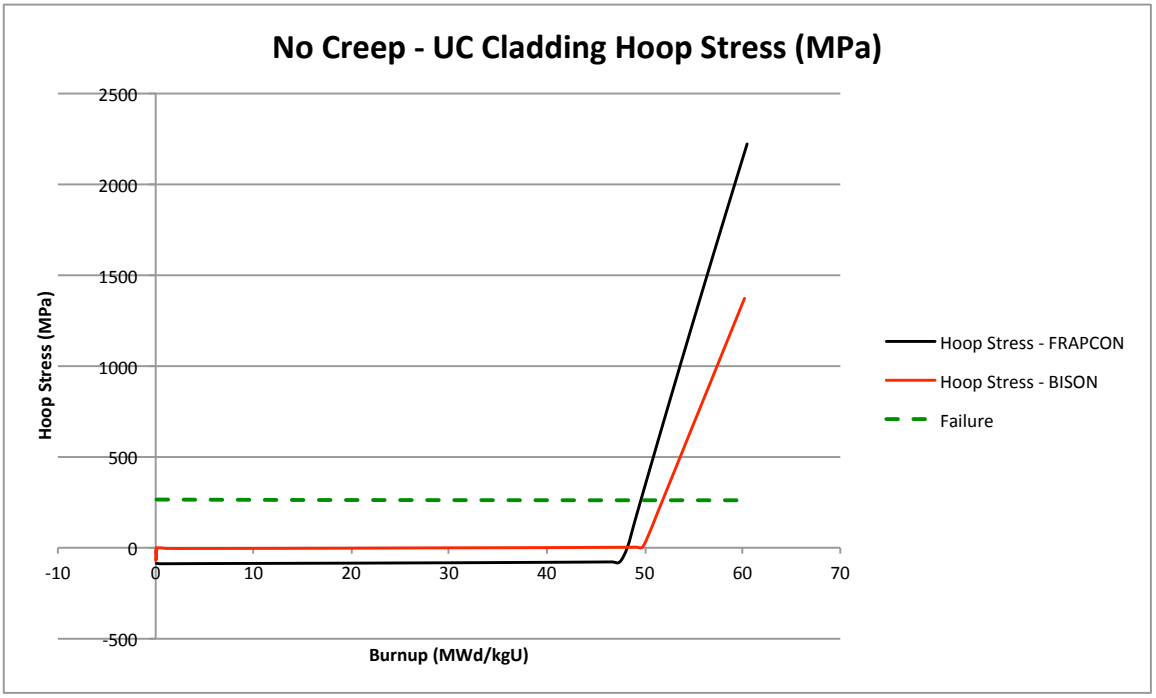

Figure 4.47: Cladding hoop stress for UC/SiC at 20kW/m without creep

any fission gas to be released into the plenum at temperatures below 1000°C [31]. Given that at this power level, the maximum centerline temperature reached by either

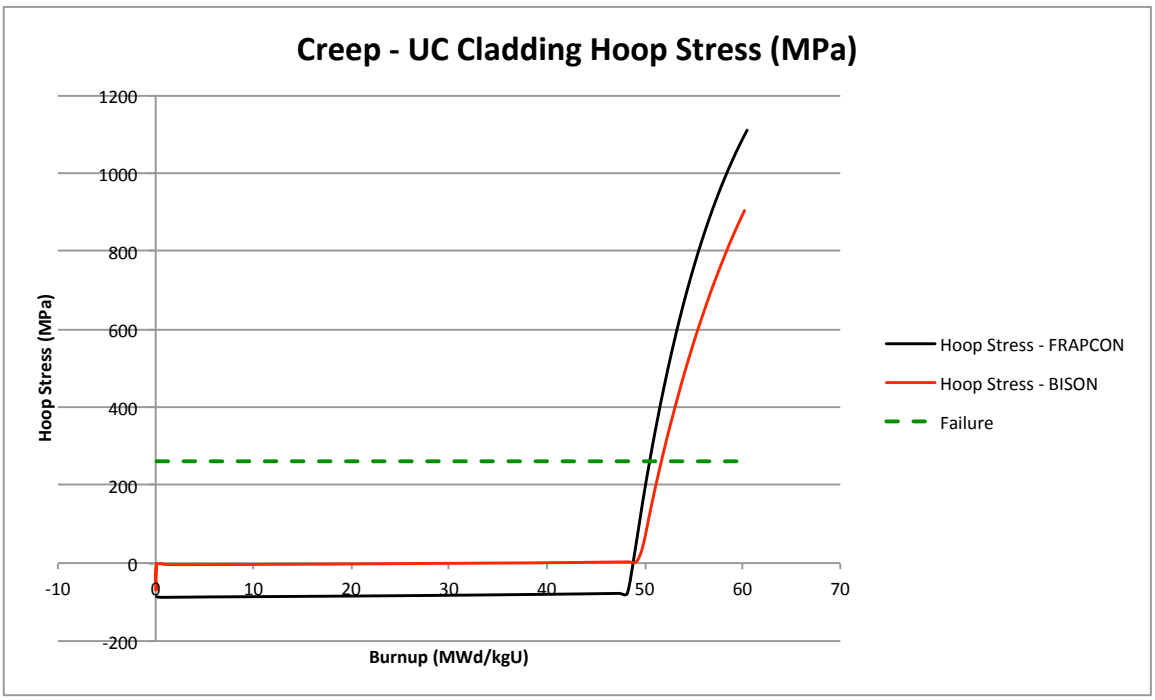

Figure 4.48: Cladding hoop stress for UC/SiC at 20kW/m with creep

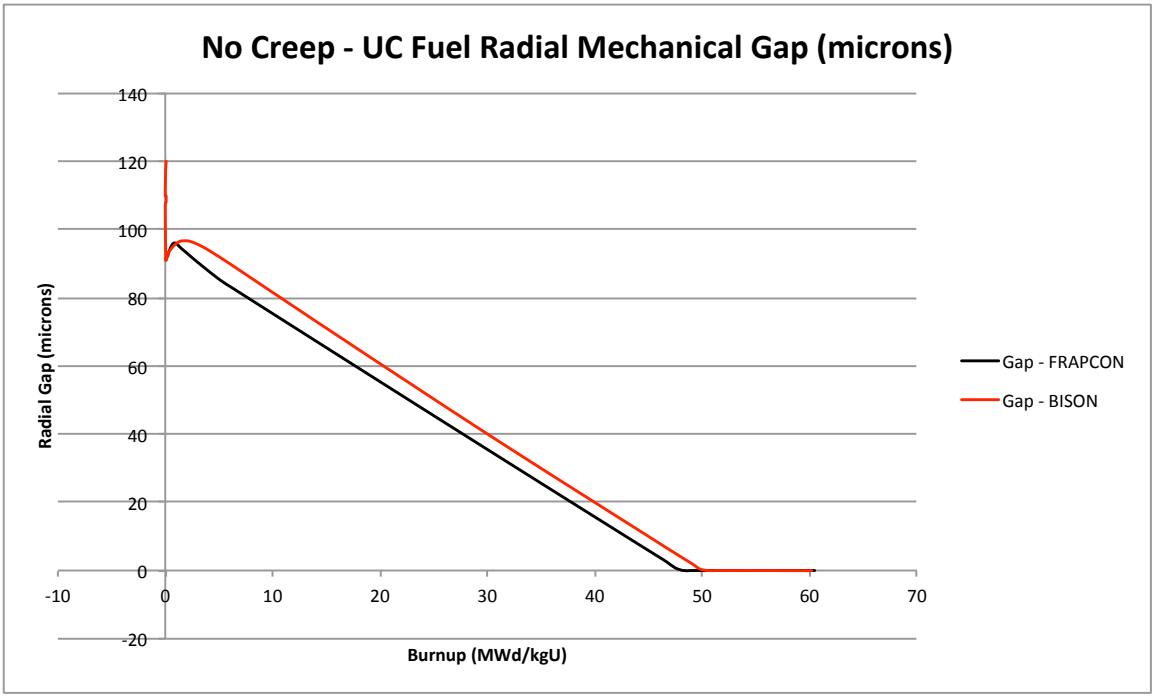

Figure 4.49: Radial gap width for the UC/SiC at 20kW/m without creep

of the codes is 810°C, which is well below this limit.

From a mechanical standpoint solely, it is easy to see that the UC type fuel is not

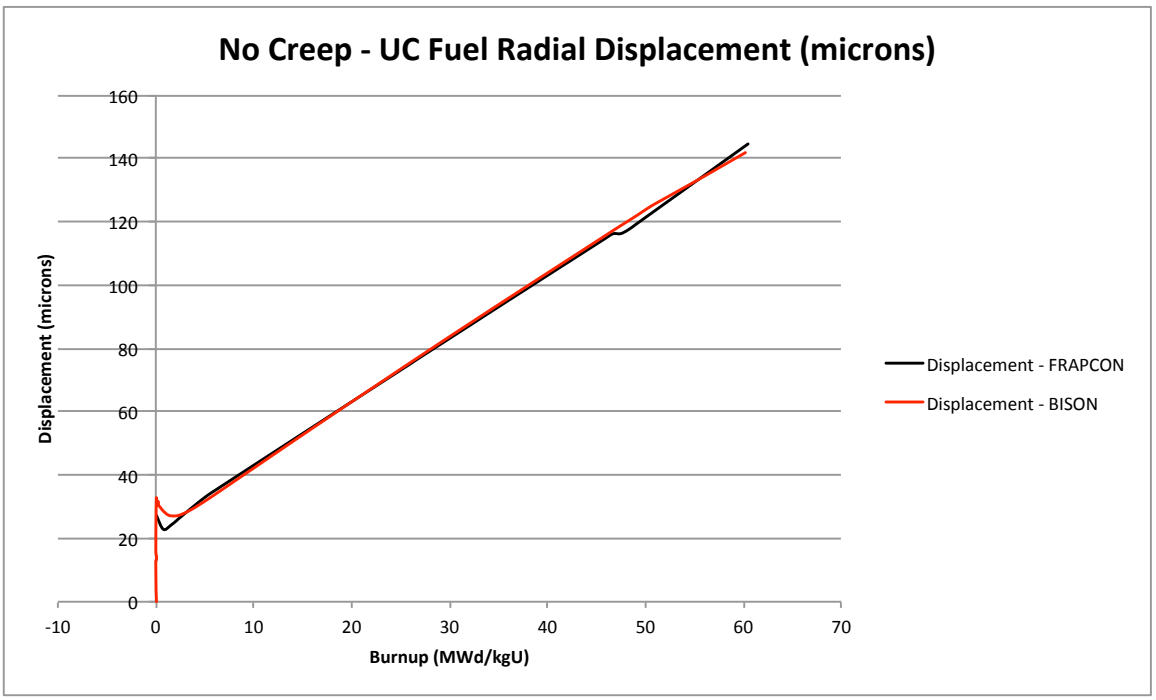

Figure 4.50: Fuel surface radial displacement for UC/SiC at 20kW/m without creep

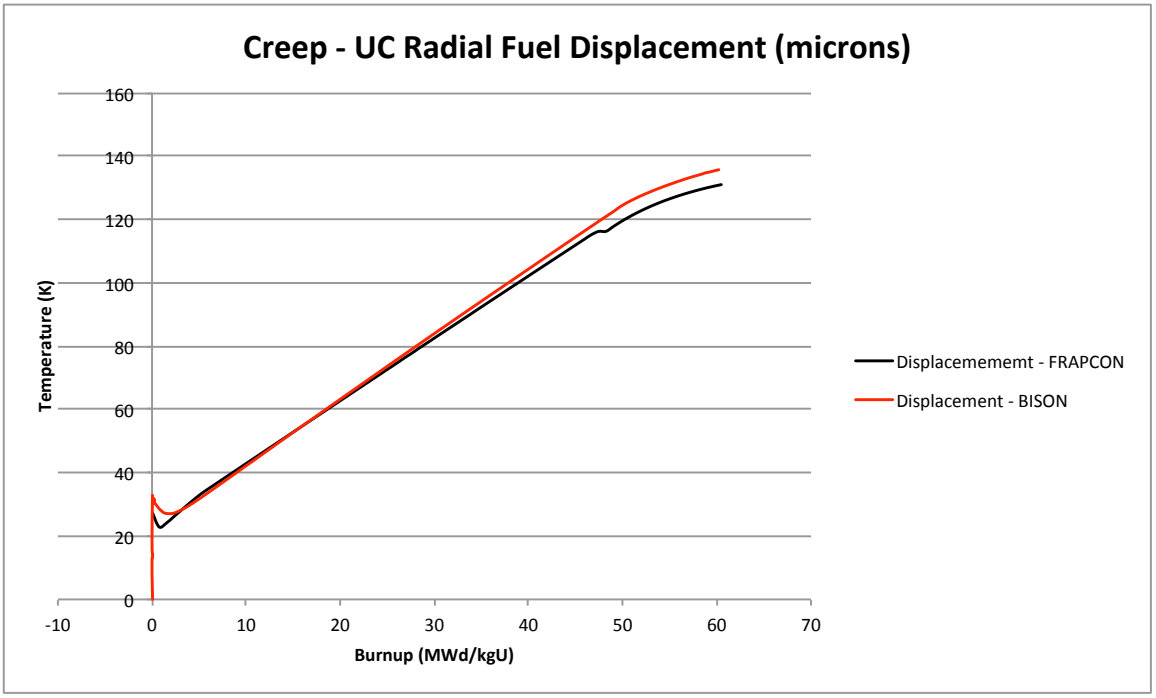

Figure 4.51: Fuel surface radial displacement for UC/SiC at 20kW/m with creep

an acceptable match for this cladding type, given the geometry, power level, and the duration of irradiation period.

4.6 Fuel Cycle Extension

To conclude this work examining fuel creep and how it can affect computational fuel modeling predictions, examining how much burnup it takes for the cladding to fail due to PCMI was studied. Using both fuel models, with and without fuel creep, will help give insight into how different predictions can be. Figures 4.52 and 4.53 all show the extension that the codes predict with the use of a fuel creep model in combination with SiC cladding. All three of the codes are in unison on the fact that cladding stress will be severly relieved due to fuel creep to the point where all of the codes are predicting double the amount of burnup the fuel can achieve before failure due to mechanical contact. The BISON and FRAPCON codes both predict that UO_2 will benefit from the addition of the fuel creep model. Both codes predict a significant increase in the amount of time the fuel can stay under the SiC mechanical failure threshold. The BISON code predicts a 52% increase in burnup allowed and FRAPCON predicts a 54% increase in allowable burnup. Comparing these results to those of Figures 4.54, 4.55, 4.47, and 4.48 we can see that the addition of a fuel creep model to UO_2 affects the fuel much more than it does to the advanced fuels. The combination of the knowledge that the UO_2 fuel operating at higher temperatures and the fact that the UO_2 fuel is expected to creep 10 times faster than UN and UC underpin these findings. In the case of the UN fuel, adding in fuel creep actually does oppisite of what would be expected. Figure 4.54 shows that the fuel actually comes into contact and reaches failure slightly sooner than without fuel creep. This could be explained by the weight of the fuels causing a radial creep within the pellets causing them to expand outward and reach the cladding more quickly.

Fuel creep in the advanced fuels only seems to be noticeable whenever the stresses are extremely high. Due to their lowered operating temperatures and lowered creep rates, the advanced fuels will never be able to relieve as much stress as the UO_2 fuel

will under the same conditions.

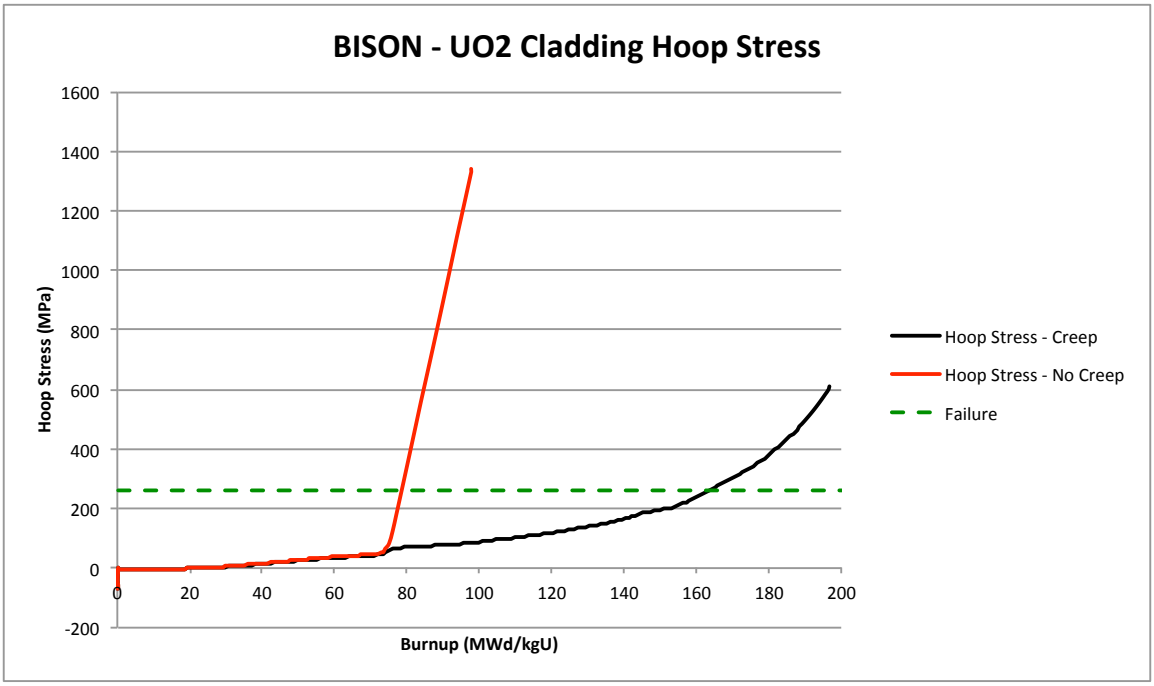

Figure 4.52: Cladding hoop stress for UO_2/SiC in BISON extended out to reach failure

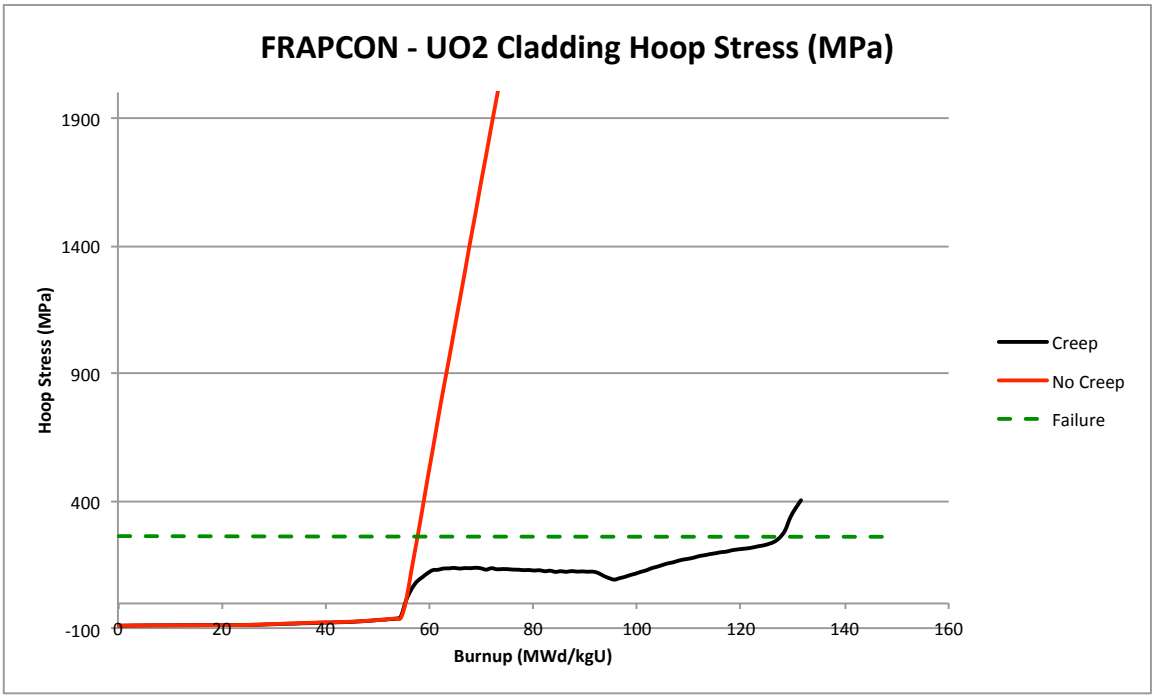

Figure 4.53: Cladding hoop stress for UO_2/SiC extended out to reach failure

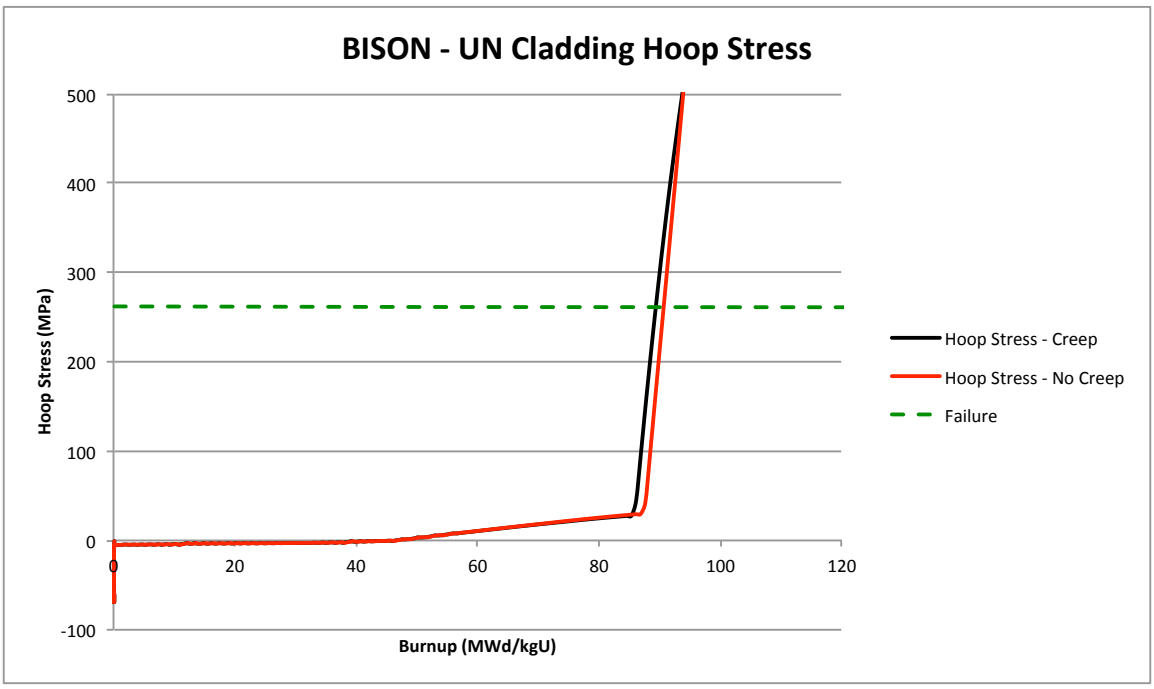

Figure 4.54: Cladding hoop stress for UN/SiC in BISON extended out to reach failure

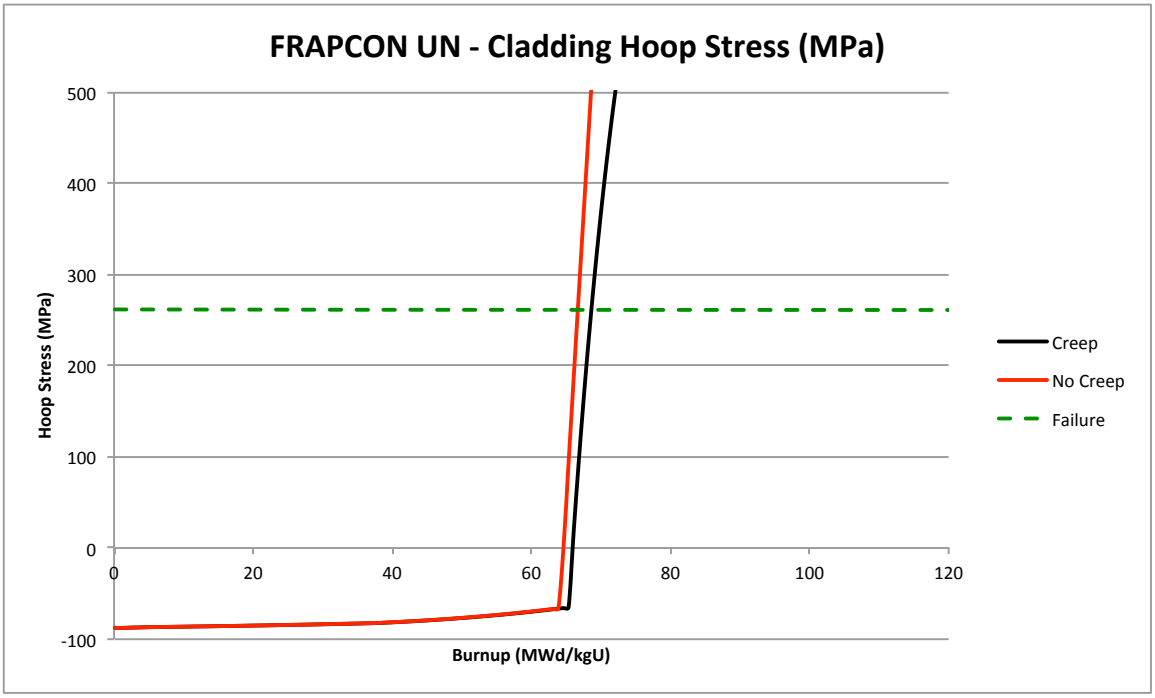

Figure 4.55: Cladding hoop stress for UN/SiC in FRAPCON extended out to reach failure

Chapter 5

Conclusions

5.1 Conclusions

Understanding that the advanced fuels have, on a whole, higher swelling rates than that of UO_2 makes the design process a little more difficult from a mechanical interaction standpoint. The push for SiC type cladding by the ATF campaign also adds to this difficulty as contact between cladding and fuel should be avoided at all cost due to the near immediate failure of the brittle cladding. This may not be so beneficial as in order to accomplish this, fuel diameters will need to be reduced to accomidate the thicker SiC cladding. This in effect negates some of the plant's goals of using a higher uranium density fuel by reducing the total amount of fuel in the core.

One thing to note is that while the codes do not align when comparing against each other for the same run specifications, they follow a trend when comparing the codes to themselves with and without creep. It would be beneficial that the codes predict very similar results for a simple test case such as the one that was chosen. This is one of the slight downfalls that has been run into with this study and may leave room for improvement in future work.

Both the BISON and FRAPCON fuel performance codes show that upon the onset of PCMI, the cladding hoop stress reaches failure criteria almost immediately. Since the advanced fuels models that were implemented in both of these codes are not as well studied and verified as the UO_2 type fuel, and therefore should be investigated more heavily if seriously being considered as an alternative fuel type to UO_2.

Based on results seen in Chapter 4, design changes for UC type fuel would be needed. While UC is not seriously being considered as a viable candidate for monolithic fuel for LWR applications, it is good to see the effects that contact with cladding causes. To allow UC to become viable for LWR use, an increased pellet-cladding gap would need to be implemented to account for the extreme swelling rates seen by this fuel. This would increase time to PCMI and ultimately achieve the goals of becoming a safer fuel alternative.

Another alternative that may prove beneficial for modeling purposes, would be the analysis work done on an annular pellet stack. Allowing the fuel to swell into the annulus might prove useful in reducing cladding stresses, hopefully keeping them below the design limit of 261 MPa. Allowing this to happen in the fuel performance codes as they are currently would require no extra modifications, but a new geometry design would need to be implemented to maximize fuel mass while keeping enough of an annulus to allow for sufficient swelling to occur.

Bibliography

1. International Atomic Energy Agency, *Improvement of Computer Codes Used for Fuel Behaviour Simulation (FUMEX-III)*, IAEA-TECDOC-1697 (2013).

2. Y. Arai, *Nitride Fuel*, 2012, pp. 41–54.

3. A.A. Bauer, *Mixed-Nitride Fuel Irradiation Performance*, Transactions of the American Nuclear Society **14** (1971).

4. David A. Bloore, *Reactor Physics Assessment of Thick Silicon Carbide Clad PWR Fuels*, Massachusetts Institute of Technology (2013).

5. F. Caligara, *TPROF-A A Computer Code for Analysing the Behaviour of the Advanced Fuels*, European Institute for Transuranium Elements (1978).

6. David Carpenter, *Assessment of Innovative Fuel Designs for High Performance Light Water Reactors*, Massachusetts Institute of Technology (2006).

7. Spencer Carroll, *Implementation and Evaluation of Fuel Creep Using Advanced Light-Water Reactor Materials in FRAPCON 3.5*, 2014.

8. W. Dienst, *Swelling, Densification and Creep of (U, Pu)C Fuel Under Irradiation*, Journal of Nuclear Materials **124** (1984), 153–158.

9. Bo Feng, *Steady-State Nitride Fuel Behavior Modeling with FRAPCON-EP and its Application to PWR's*, Proceedings of ICAPP 2011 (2011).

10. M.R. Finlay, *Irradiation behaviour of uranium silicide compounds*, Journal of Nuclear Materials **325** (2004), 118–128.

11. D. Freund, *Auslegung Bestrahlung and Nachuntersuchung der UC- and (U,Pu)C-Brennstabe der Versuchsgruppenm Mol-11/K1 and Mol-11/K2*, Kernforschungszentrum Karlsuhe (1976).

12. B.R.T. Frost, *Materials Science and Technology*, 1994.

13. K.J. Geelhood, *FRAPCON-3.4: A Computer Code for the Calculation of Steady-State Thermal-Mechanical Behavior of Oxide Fuel Rods for High Burnup*, NUREG/CR-7022, Vol.1 (2011).

14. Jason D. Hales, *BISON Theory Manual*, Idaho Nationl Laboratory (2014).

15. Luke Hallman, *Advanced Fuels Modeling: Evaluating the Steady-State Performance of Carbide Fuel in Helium-Cooled Reactors Using FRAPCON 3.4*, University of South Carolina (2013).

16. Jason Harp, *Preliminary Investigation of Candidate Materials for Use in Accident Resistant Fuel*, LWR Fuel Performance Meeting/Top Fuel 2013 (2013).

17. _____, *Uranium Silicide Fabrication for ATF Fuel at INL*, U.S. Department of Energy (2014).

18. Rolf E. Hummel, *Understanding Materials Science*, 2004.

19. IAEA, *Development Status of Metallic, Dispersion, and Non-Oxide Advanced and Alternative Fuels for Power and Research Reactors*, IAEA-TECDOC-1374 (2003).

20. M. A. Kramman, *ESCORE The EPRI Steady-State Core Reload Evaluator Code: General Description*, Combustion Engineering (1987).

21. Bo-Shiuan Li, *Pellet Cladding Mechanical Interactions of Ceramic Claddings*, University of South Carolina (2013).

22. D. Manara, *Thermodynamic and Thermophysical Properties of Actinide Carbides*, 2012, pp. 87–137.

23. H.J. Matzke, *Science of Advanced LMFBR fuels, Solid State Physics, Chemistry and Technology of Carbides, Nitrides, and Carbonitrides of Uranium and Plutonium*, North Holland Physics Publishing (1986).

24. Ken McClellan, *ATF-1 Test of UN-U_3Si_5*, Los Alamos National Laboratory (2014).

25. Kallie Metzger, *Model of U3Si2 Fuel System Using BISON Fuel Code*, ICAPP 2014 (2014).

26. Masaomi Oguma, *Cracking and Relocation Behavior of Nuclear Fuel Pellets During Rise to Power*, Nippon Nuclear Fuel Development Co. (1983).

27. Donald R. Olander, *Fundamental Aspects of Nuclear Reactor Fuel Elements*, 1976.

28. Giovanni Pastore, *Uncertainty and Sensitivity analysis of fission gas behavior in engineering-scale fuel modeling*, Journal of Nuclear Materials **456** (2015), 398–408.

29. Danielle M. Perez, *Assessment of BISON: A Nuclear Fuel Performance Analysis Code*, Idaho National Laboratory (2013).

30. Ian Porter, *RaySystem Analysis with Improved Thermo-Mechanical Fuel Rod Models for Modeling Current and Advanced LWR Materials in Accident Scenarios*, Universiity of South Carolina (2014).

31. Timm Preusser, *Modeling of Carbide Fuel Rods*, Institute of Reactor Technology (1981).

32. B.D. Rogozkin, *Mononitride Fuel For Fast Reactors*, Atomic Energy (2003).

33. Steven B. Ross, *Uranium Nitride Fuel Swelling Correlation*, Institute for Space Nuclear Power Studies (1989).

34. A.G. Samoilov, *Dispersion-Fuel Nuclear Reactor Elements*, Atomizdat (1965).

35. A.K. Sengupta, *Carbide Fuel*, 2012, pp. 55–86.

36. H. Shimizu, *The Properties and Irradiation Behavior of U_3Si_2*, Atomics International **NAA-SR-10621** (1965).

37. Lance Snead, *Handbook of SiC properties for fuel performance modeling*, Journal of Nuclear Materials **371** (2007), 329–377.

38. H. Steiner, *Das Materialverhalten der karbidischen Brennstoffe*, IMF-Bericht (1975).

39. K. Tanaka, *Fission Gas Release and Swelling in Uranium-Plutonium Mixed Nitride Fuels*, Journal of Nuclear Materials (2004).

40. M. Uno, *Thermodynamic and Thermophysical Properties of Actinide Nitrides*, 2012, pp. 61–85.

41. Michael B. Weinstein, *Fission Gas Release Correlation for Uranium Nitride Fuel Pins*, Lewis Research Center (1973).

42. Josh T. White, *Report on Performance of Advanced Ceramic LWR Fuel Candidates*, Los Alamos National Laboratory (2013).